2009

Self-centering bridge pier columns with structural fuses

Mark Christopher Currie
Iowa State University

Self-centering bridge pier columns with structural fuses

by

Mark Christopher Currie

A thesis submitted to the graduate faculty

in partial fulfillment of the requirements for the degree of

MASTER OF SCIENCE

Major: Civil Engineering (Structural Engineering)

Program of Study Committee:
Jon M. Rouse, Major Professor
F. Wayne Klaiber
Kelly Strong

Iowa State University

Ames, Iowa

2009

TABLE OF CONTENTS

LIST OF FIGURES

LIST OF TABLES

ABSTRACT

An innovative structural system for pier columns was investigated through a series of laboratory experiments. The columns and connections examined were comprised of precast concrete segments to accelerate construction. In addition some of the columns employed elastic elements to self-center the columns when subjected to lateral loads and structural fuses to control large lateral deflections, dissipate energy, and expedite repair in the event of a catastrophic loading event.

Six cantilever columns with varying component materials and connection details were subjected to a regimen of vertical dead loads and cyclic, quasi-static lateral loads. One column was designed as a control column to represent the behavior of a conventional reinforced concrete column and provide a basis for comparison with the remaining five jointed columns designed with the proposed structural system. After sustaining significant damage, the self-centering, jointed columns were repaired by replacing the structural fuses and retested to failure to investigate the effectiveness of the repair.

The experiments identified both effective and unsatisfactory details for the jointed system. Two of the jointed columns demonstrated equivalent lateral strength, greater lateral stiffness, and greater lateral deformation capacity than the control column. The self-centering capability of the jointed columns was clearly demonstrated as well, and the repair technique proved effective as demonstrated by nearly identical pre and post repair behavior. The authors believe the proposed system to be a feasible alternative to conventional pier systems and recommend additional research.

1. INTRODUCTION

1.1 Background

1.1.1 Precast columns used in the field for accelerated bridge pier construction

One of the most promising means of accomplishing advances in the field of accelerated bridge construction is the development of effective designs and construction techniques for prefabricated substructures. Precast substructures have been used around the country with varying degrees of success over the past two decades. A concise overview of the existing technology that has been employed in the field is given in "State-of-the-Art Report on Precast Concrete Systems for Rapid Construction of Bridges" (2005) by Hieber et al. Billington et. al also make recommendations for standardizing precast substructure elements in "Alternate Substructure Systems for Standard Highway Bridges" (2001). Current precast practices are stated and a proposed precast segmental substructure system is presented. The elements of the system are discussed, as well as the fabrication and erection of the pieces, the economic impact of using precast elements, and future applications of precast substructure systems.

1.1.2 Precast columns in research

Due to their self-centering capabilities, attempts have been made to develop precast columns that have unbonded post-tensioning. Traditional, bonded post-tensioning requires a non-corrosive grout mix to be injected into the post-tensioning duct after tensioning. This results in the post-tensioning bar or strand experiencing strains equal to those in the concrete. Thus, any localization of strains in the member such as a crack also causes a localization of strains in the post-tensioning bar. If the localized strains are larger than the yield strain of the post-tensioning bar, the bar will sustain a permanent elongation. After yielding of the bar occurs, the column's moment capacity may decrease considerably due to the loss of post-tensioning force. The column will also lose its ability to behave elastically and rebound to its original shape. Yielding of the post-tensioning bar, however, provides a mechanism for dissipating the energy of the applied loads and enhances the member's ductility.

While a grouted post-tensioning bar is bonded to the member along its entire length, unbonded post-tensioning is only connected to the member at its ends. This distributes strain uniformly along the bar's entire length, allowing the bar to remain in its elastic range for much larger deformations. Since the bar is not bonded to the concrete, little or no localization of strain is developed.

One significant structural concern with unbonded post-tensioning is the lack of a mechanism for damping the hysteretic energy of the applied load, which can lead to large deflections and a brittle failure. Damping of hysteretic energy in unbonded structural systems has been the focus of many research topics.

Billington and Yoon discuss one such system in "Cyclic Response of Unbonded Post-tensioned Precast Columns with Ductile Fiber-Reinforced Concrete" (2004), in which unbonded post-tensioning is used to reduce residual displacements, epoxy-grout and match-cast joints are used to connect all segments, and ductile fiber-reinforced cement-based composite (DRFCC) in the precast segments at potential plastic hinging regions is used to dissipate hysteretic energy. The two main variables in the investigation were the material used in the plastic hinging region segment and the depth at which that segment was embedded in the column foundation.

In "Unbonded Post-tensioned Concrete Bridge Piers. I: Monotonic and Cyclic Analysis" (2003), Kwan and Billington present functional- and survival-performance limits to guide the design of a proposed unbonded, post-tensioned concrete bridge pier system. The system used unbonded post-tensioning to reduce residual displacements and bonded internal reinforcement to provide energy dissipation. Adjustments could be made to the ratio of bonded reinforcement to unbonded post-tensioning according to the emphasis placed on the control of the maximum displacement versus the control of residual displacement. This system adopted similar concepts of reinforcement combinations as presented by Ikeda (1998) and Ito et al. (1997).

Stephan, Restrepo, and Seible presented "Seismic Behavior of Bridge Columns Built Incorporating MMFX Steel" (2003). They compared the results of columns using conventional reinforcement with columns containing MMFX steel. This corrosion resistant, high strength steel was used in an attempt to increase the capacity of the column and reduce

residual displacements. Results revealed that these columns, which were representative of the Oakland Touchdown Substructure of the San Francisco Oakland Bay Bridge, could be designed to form ductile, flexural plastic hinges at their bases. A maximum lateral drift of approximately 4% could be obtained by the columns before failure.
While some research has explored damping of hysteretic energy, no system to date has been developed that can simultaneously reduce residual displacements to negligible levels, sustain large (~10% drift) deformation, and be repaired cost-effectively.

1.2 Objectives

1.2.1 Accelerated bridge pier construction

The primary objective of this research was to accelerate bridge pier construction through the use of precast columns in order to reduce construction costs, decrease traffic delays, improve work zone safety, and minimize environmental impacts. By prefabricating all elements of the system offsite and early in the project schedule, column erection can take place with more speed and efficiency. Connections aimed at minimizing cure time for grouting, temporary shoring requirements, and restrictive construction/fabrication tolerances were investigated. Ultimately, contractors' savings gained through enhanced constructability can be passed on to transportation agencies and the traveling public. Future standardized details for the precast substructures will also help the streamline construction for the proposed structural system investigated in this project.

1.2.2 Improved structural performance

This research also aimed to develop a pier system that could endure an extreme loading event such as a vehicle or ship impact, severe wind storm, flood, blast, or earthquake, better than a conventional pier. Structural benefits associated with the system include improved durability associated with precast concrete, improved stability and reduced repair costs should a structure ever be subjected to an extreme load, and improved public safety gained through small residual deformations that would allow bridges to remain in service after an extreme load event. The system also allows a wide range of architectural options to improve bridge aesthetics and highlight attractive structural features.

1.2.3 Repairability

An additional objective of this research was to develop a bridge pier system that can be repaired cost-effectively after an extreme loading event. This system incorporates a design that minimizes damage to precast column segments by localizing damage to sacrificial structural fuse plates that joint the segments. These external plates required minimal labor to replace, and this repair technique was shown through testing to effectively restore the column's initial structural integrity.

1.3 Proposed Structural System

1.3.1. System elements

The system that was investigated in this research is illustrated in Figures 1-4. Key features of the system included steel collars at the ends of segments (Figure 2), external reinforcement of segment joints (i.e. structural fuse plates) with bolted connections (Figure 3), elastic elements (e.g. unbonded post-tensioning) to self-center the columns, and bearing plates between segments to avoid labor-intensive grouting procedures (Figure 4).

The steel collar assembly at the ends of each column segment, as illustrated in Figure 2, served three purposes: (1) reinforcement of the segment ends to prevent damage during shipping and erection, (2) confinement of the concrete at the ends of the segments to provide additional concrete strength and ductility, and (3) a convenient means for attaching exterior structural fuse plates. A single column segment is illustrated in Figure 3 with steel collars at each end. Shown in Figure 4 is the foundation connection, as well as the first joint connection. The first (lowest) column segment fits into a socket formed in a cast-in-place pile cap, precast pile cap, or spread footing. A flowable epoxy grout fills the annular space in the socket surrounding the first column segment.

This system, when subjected to lateral loads, is designed to concentrate deformation at the segment joints. Such behavior is achieved by designing the replaceable external plates as structural fuse plates which are intended to yield preferentially while leaving the remainder of the structure relatively undamaged and elastic. When a sufficient lateral load is applied, the fuse plates yield in tension and buckle in compression to accommodate the rotation at the joint. A continuous elastic element, such as the post-tensioning rod used in this study, is

incorporated in the members to provide a self-centering force and minimize residual deformations. By achieving minimal residual deformations in the columns, the bridge may remain in service immediately after an extreme loading event. Full repair of the structure, if required, may then be accomplished by replacing the structural fuse elements.

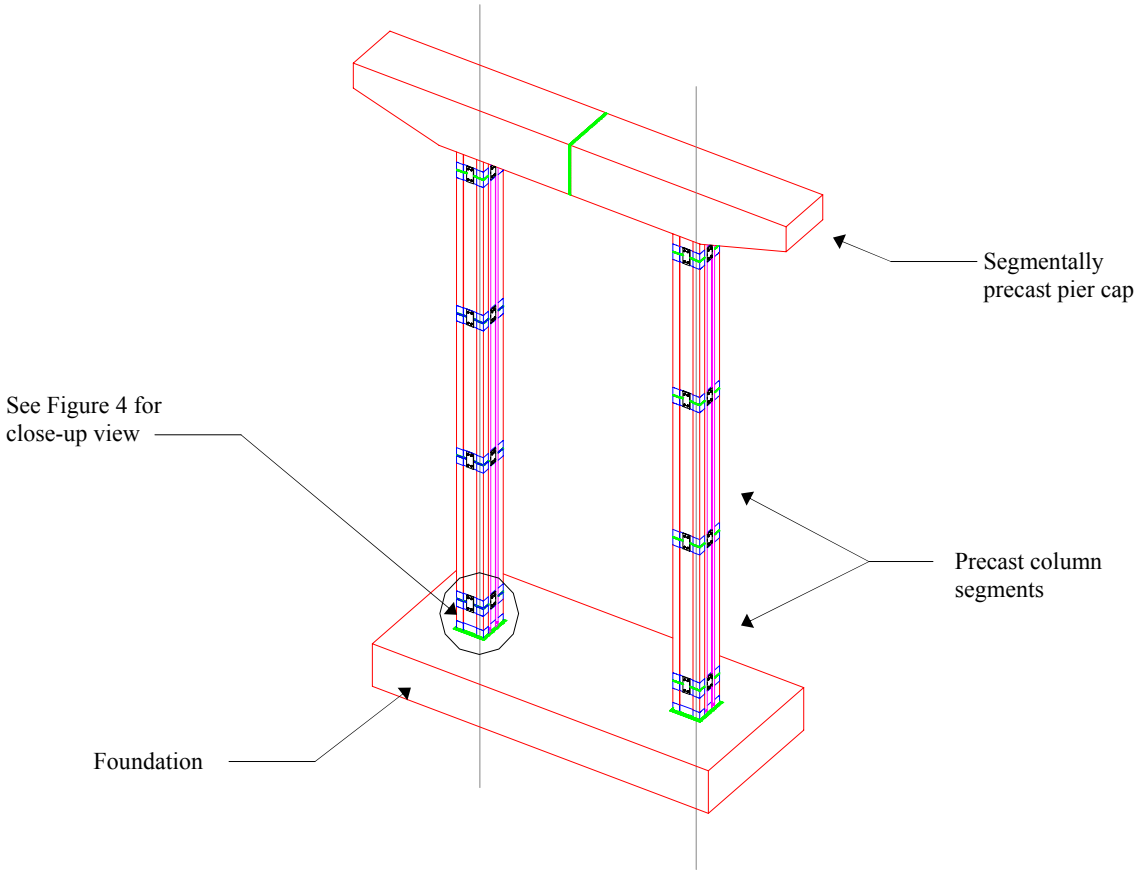

Figure 1. Basic pier assembly (isometric view).

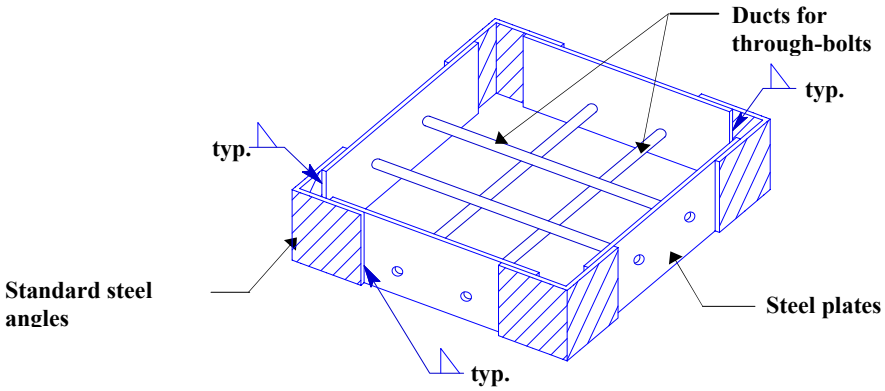

Figure 2. Steel collars at segment ends.

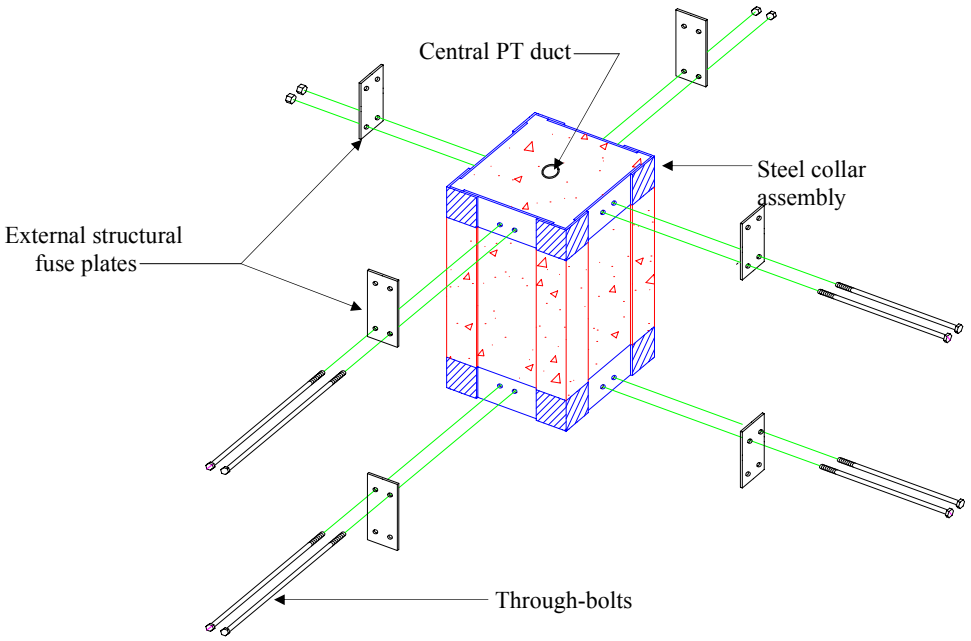

Figure 3. Single column segment with external connectors.

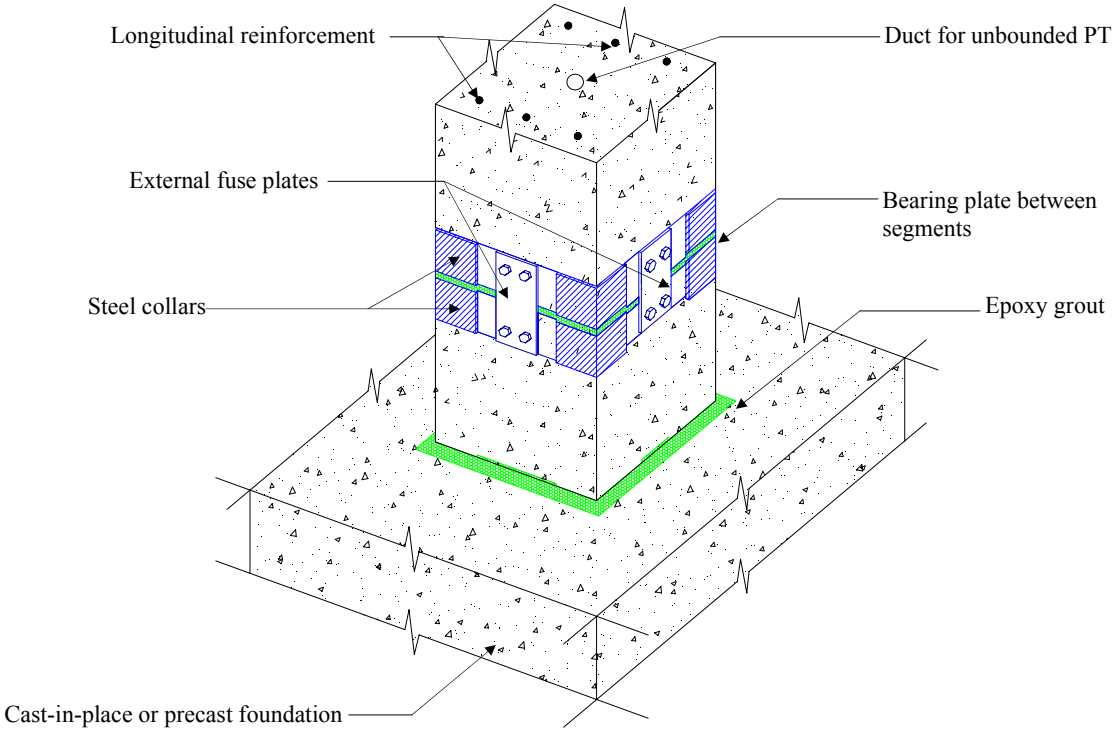

Figure 4. Close-up of typical joints.

1.3.2. Construction sequence

A possible construction sequence is as follows: Once piles are driven, a precast pile cap is placed with sockets to receive precast column segments. A vertical post-tensioning rod is threaded into an anchor cast into the bottom of the socket, and the first column segment is lowered into place. Once shimmed and leveled, flowable epoxy grout is poured into the annular socket space. A bearing plate is placed at the top of the first segment, and the next segment is subsequently lowered over the post-tensioning rod to rest on the bearing plate. External fuse plates are then bolted into position ensuring alignment and stabilizing the newly placed segment. This procedure continues until all but the uppermost column segments are in place. The uppermost column segment is epoxied into a pier cap socket and the unit is lowered onto the columns. Once all pieces are in place, cap segments are connected, external plates are secured by fully tensioning the through-bolts, and post-tensioning force is applied to the rod used for alignment. Then the pier is then ready to receive the superstructure.

This research places special emphasis on the connection designs to simplify construction. Although Figures 1–4 schematically illustrate square columns, connection details could be developed for rectangular or circular columns as well.

1.4 Research Methodology

1.4.1 Key experimental variables

Because the greatest uncertainties in this proposed system are associated with the behavior of the segment joints, cantilever column specimens for this investigation were designed to focus on the behavior of a single segment joint. Test variables investigated included the types of bearing plates, fuse plates, and amount of post-tensioning force applied. Various anchorage details and fuse plate configurations were also examined. Variables used in each test are shown in Figure 5.

One column was cast as a continuous, reinforced cantilever column to examine the behavior of the socket-type foundation connection and represent the behavior of a conventional cast-in-place column with a reinforcement ratio similar to those in the segmented columns. This

first column (Column 1) served as a basis for comparison with the subsequent five segmented columns. Columns 2-4 were cast with similar segment joint details.

Due to an unanticipated anchorage issue in these first three segmented columns, two additional segmented columns (Columns 5 and 6) were constructed with revised steel collar and end connection details. The lateral load capacity of all the segmented columns was designed to be similar to that of the control Column 1. Also shown in Figure 5 are the different materials that were selected for each investigation. Details on these materials are presented in the following paragraphs.

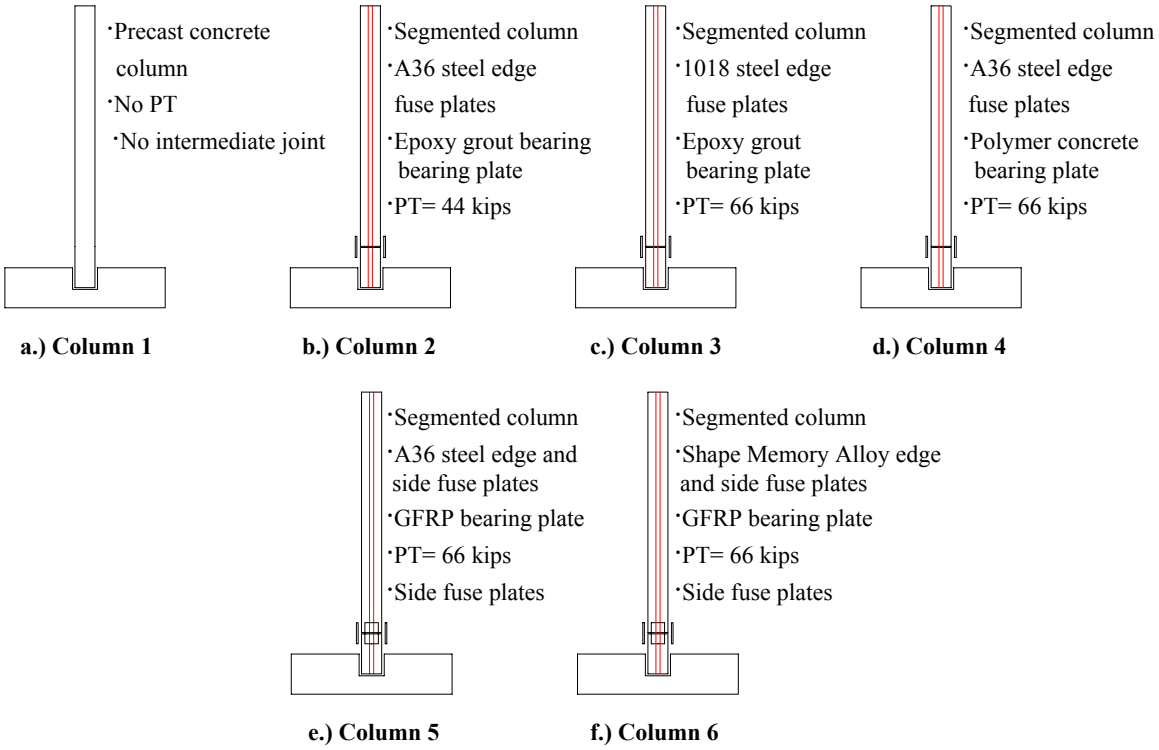

Figure 5. Test columns.

1.4.1.1 Bearing plates

The bearing plate in the precast pier system was one of the variables investigated. The bearing plate was intended to be compliant enough to transfer axial stress uniformly between segments but strong enough to withstand high shear, axial, and bending stresses. Several different types of plates were considered with desired properties that included high compressive, tensile, and shear strengths, a modulus of elasticity roughly half that of

concrete, high resistance to corrosion, low creep, and relatively low cost. Materials considered were epoxy grout, polymer concrete with steel reinforcement, glass fiber reinforced polymer (GFRP), lead, neoprene, and cotton duck.

Sikadur 32, a high modulus, flowable epoxy was mixed with Grade 37 silica sand in a 1:1 ratio for Columns 2 and 3. The modulus of elasticity was approximately 1,500 ksi, while the compressive strength of the epoxy-grout was close to 11.5 ksi. When tested in compression, this material exhibited large plastic strains without cracking.

A steel-reinforced polymer concrete plate was used in the Column 4 test. In polymer concrete, a high strength, corrosion resistant, thermosetting resin acts as the binding agent. Three-eighths inch aggregate was used in the plate, and a 2 in. by 2 in. welded wire grid was placed in the plate to reinforce against splitting. The modulus of elasticity of polymer concrete was approximately 2,400 ksi, while its compressive strength is approximately 10 ksi.

A glass fiber-reinforced polymer (GFRP) plate was used for Column 5 and 6 tests. An epoxy resin acts as the binding agent for the GFRP, with a 90-90 glass fiber orientation. The elastic modulus for the GFRP bearing plate perpendicular to the fibers was measured to be 2,000 ksi.

1.4.1.2 Fuse plates

Fuse plates in the precast pier system were another variable investigated. Desired properties include low yield stress, high plastic strain capacity, high resistance to corrosion, large ultimate elongation (~20-25%), high toughness, and low cost. Materials considered included A36 steel, 1018 carbon steel specifically manufactured to yield between 30 and 36 ksi, shape memory alloy, A242 steel, and A588 steel. The following materials were selected to be used for fuse plates.

A36 steel plates were used in Columns 2, 4, and 5 (see Figure 5). From laboratory tests, the plates were determined to have a yield stress of 42 ksi with an ultimate elongation greater than 20%. A36 plate stock is readily available in a large range of thicknesses, is easily machined and relatively low cost.

1018 carbon steel fuse plates were used in Column 3. It has a yield stress of 30–36 ksi and an ultimate elongation similar to that of the A36 steel. It was more expensive than the A36 plates and not readily available from a local steel supplier, but its low yield stress and high ultimate strain capabilities make it desirable for the segment joint connection.
Shape memory alloy (SMA) was used for the sixth column test. It had a yield stress around 50 ksi, with much less permanent elongation. Ultimate elongation was estimated to be around 11%. Although more expensive than conventional steel, the SMA plates provide the advantages of helping to self-center the column and are less likely to require replacement.

1.4.1.3 Elastic elements

Possibilities for elastic elements in the system included unbonded post-tensioning with bars or strands, external FRP strips, or external MMFX steel bars. This research investigated the effect of an elastic element using unbonded post-tensioning. The forces applied to each test column are noted in Figure 5 and ranged from 44 to 66 kips. Higher initial post-tensioning force increases the lateral stiffness of the column, increases self-centering capability, and reduces cracking in the concrete at the expense of axial capacity of the column.

2. TEST SETUP AND PROCEDURE

A combination of cyclic, quasi-static lateral loads and constant, axial dead load was applied to the cantilever column specimens tested in this investigation to simulate loading conditions on an actual pier column. The columns were fixed to the laboratory strong floor by post-tensioning precast foundation blocks to the strong floor. Concentrated lateral loads were applied near the top of the column using a hydraulic actuator. Dead load was applied by attaching a reinforced concrete load beam to the top of the column from which weights were suspended. This means of applying dead load ensured that the force remained constant and vertical in order to accurately simulate P-□ effects as the top of the column was displaced laterally with the hydraulic actuator.

2.1 Laboratory Constraints

A 2 ft. thick strong floor with tie-down locations spaced 3 ft. on centers in both directions was used for the project. A testing frame constructed of structural steel members assembled with bolted connections was used to apply lateral loads. Eight holes in the strong floor were used to attach the testing frame to the test floor. Applying 60 kips of post-tensioning force to each of the eight rods provided approximately 100 kips of frictional sliding resistance for the frame. Schematics and photographs of the frame and test setup are presented in Figures 6-8.

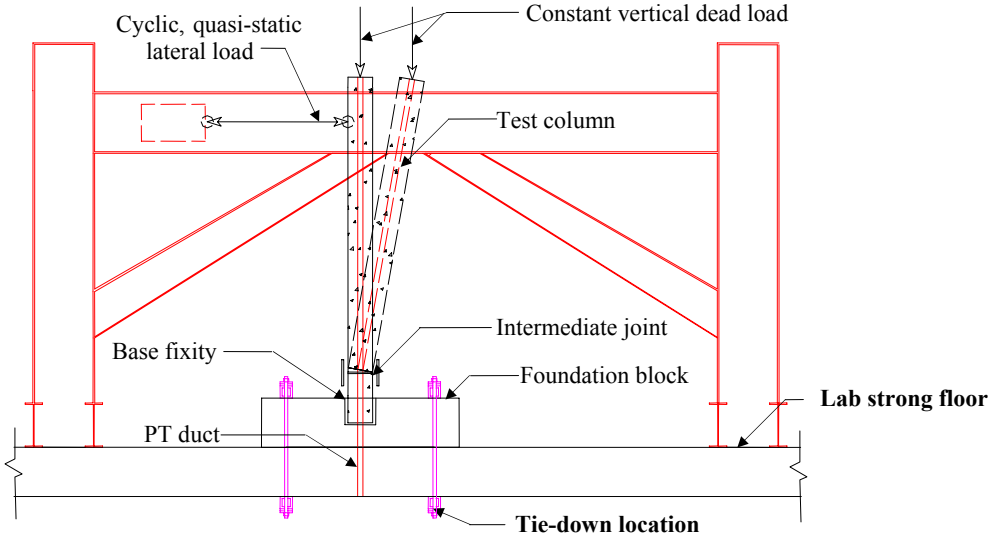

Figure 6. Test schematic.

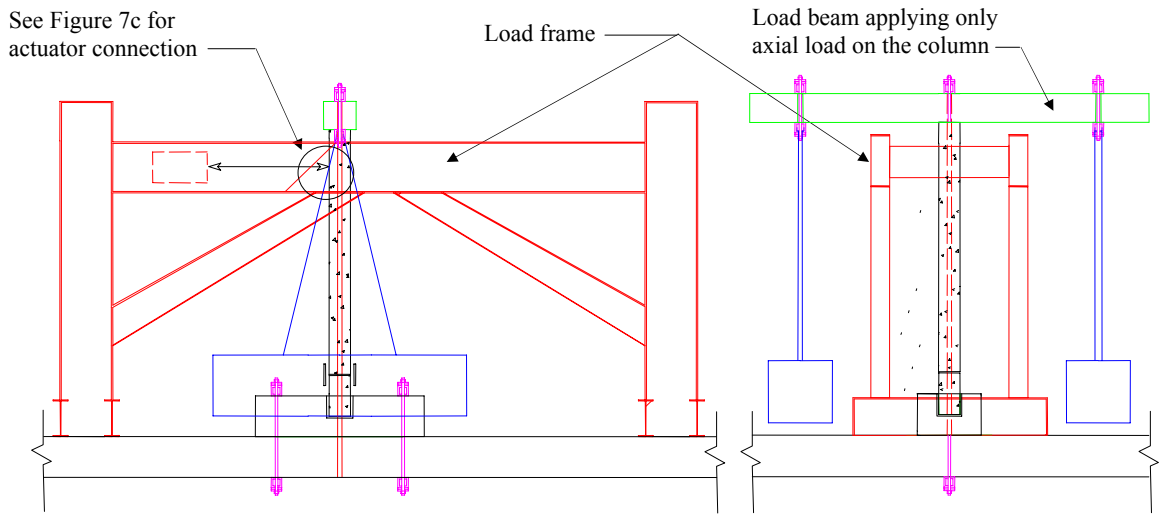

a.) Side view **b.) End view**

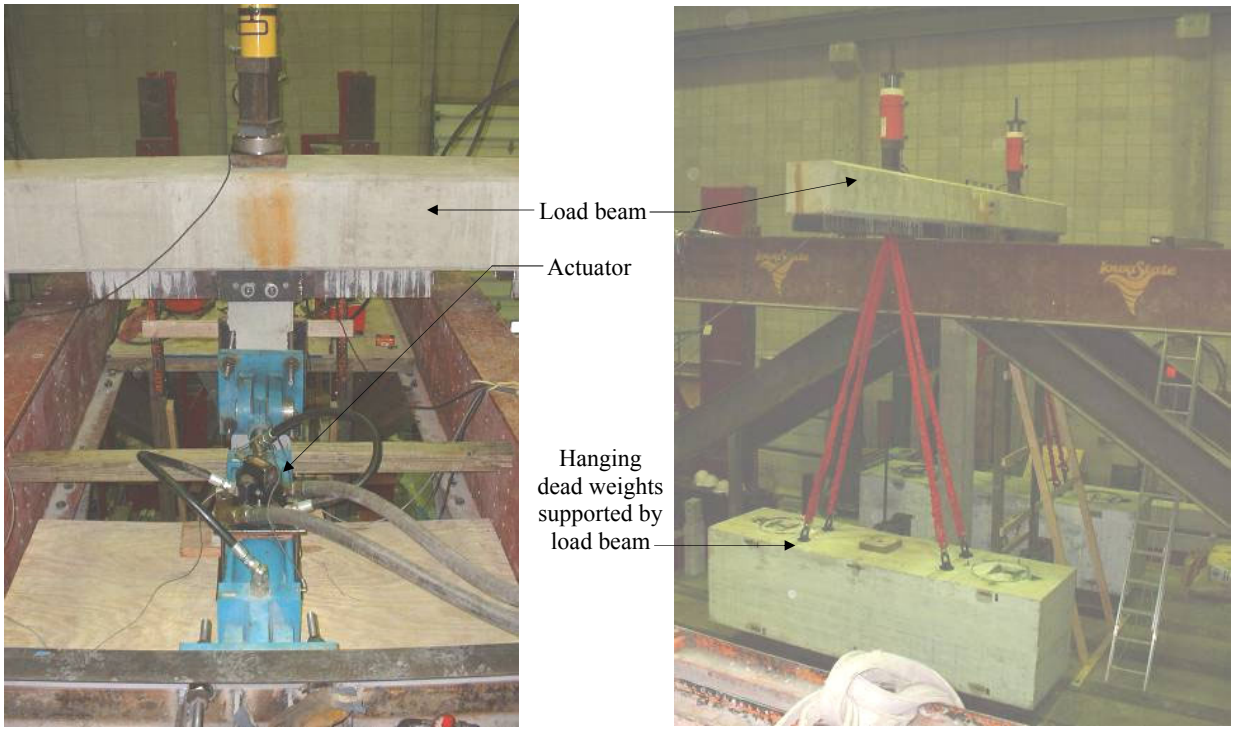

c.) Photograph of actuator connection **d.) Photograph of hanging weights**

Figure 7. Test setup.

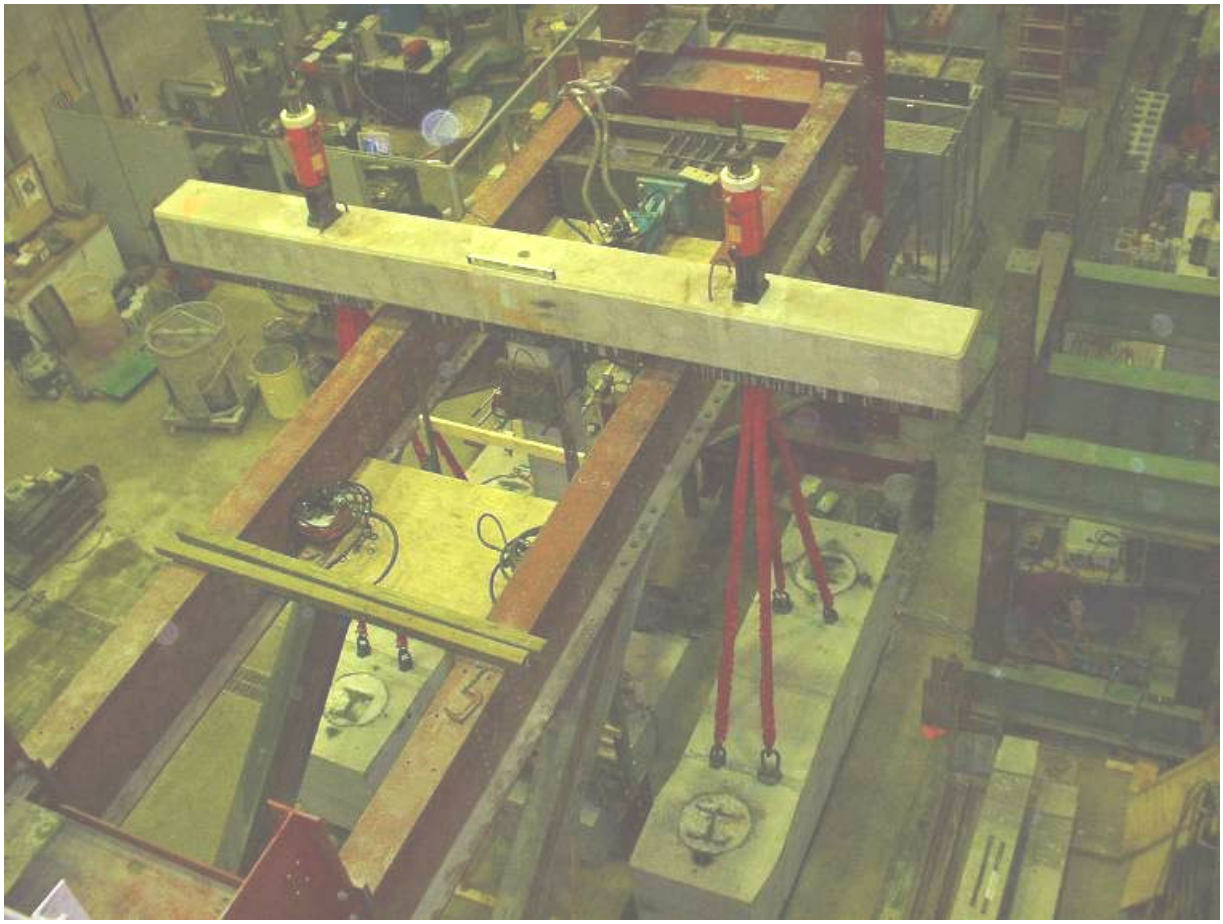

Figure 8. Photograph of load beam from above.

The frame was designed to resist much larger lateral forces than those applied in these experiments and was more than 100 times stiffer than each individual column specimen. With a maximum stroke of 24 in. (+/- 12 in.), the lateral actuator used in the tests allowed a maximum drift of 10% in both the positive (push) and negative (pull) directions. This actuator had a load capacity of +/- 100 kips, roughly 10 times the ultimate failure load of the column specimens examined. The center elevation of the actuator backplate was 11 ft.-2 in. from the strong floor, the same as the top lateral displacement transducer.

The load beam used to apply the dead load to the top of each test column was a doubly-reinforced concrete beam that was composite with a structural steel W-shape. Three holes were bored vertically through the load beam to accommodate the post-tensioning bar of the column specimen as well as the two rods that supported the concrete dead weights. The load

beam was oriented perpendicular to the direction of lateral loading and applied its own weight of 7 kips as well as the weight two large concrete blocks weighing 18.5 kips each to the top of the column. This arrangement provided 44 kips of total dead load at the top of each column.

2.2 Column Erection

The foundation blocks for each column specimen were placed inside the load frame; two ducts in the blocks, that were six feet apart, were aligned with holes in the strong floor holes for post-tensioning the blocks to the floor. Each foundation block was post-tensioned to the floor with 120 kips (60 kips/rod) providing approximately 24 kips of frictional sliding resistance. Each foundation block had been cast with a centered 15 in. x 15 in. x 13 in. deep socket to accommodate a column specimen. These details are shown in Figure 9.

a) Foundation socket **b) Foundation block**

Figure 9. Photographs of Column 1 socket and column placement.

The base of each column was placed into the socket at the center of the foundation with the overhead crane. A flowable, two-part structural epoxy (Sikadur 32) mixed in equal proportion with Grade 37 silica sand was used to grout the column segment to the foundation. The epoxy reached initial set after about four hours, at which time the bearing plate was placed on the bottom column segment. The top column segment was then lowered onto the bearing plate using the overhead crane, after which the external fuse plates were bolted to each segment. Nuts were tightened to a snug-tight fit at this stage. By connecting

the column segments with fuse plates, the column was stabilized until post-tensioning could be applied. The actuator was then connected to the column using a clevis and two bolted plates as shown in Figure 10. The actuator was fitted with clevises (i.e. hinges) at both of its ends to ensure that no concentrated moment was applied to the column through the actuator.

Figure 10. Photograph of actuator connection to column.

The load beam was then moved into position using the crane. A thin (1/4 in. thick) neoprene pad was placed on top of the top column segment to uniformly distribute the dead load to the top of the column. Two threaded rods were then used to connect the load beam to the column. Once the load beam was securely in place, the entire test column was post-tensioned to the strong floor. The dead weights were then lifted from the floor using hydraulic jacks, after which the column supported both the dead weights and the pier cap. Care was taken to ensure the dead weights were lifted simultaneously to prevent asymmetrical loading which would cause out-of-plane bending in the column during this operation.

2.3 Instrumentation

Instrumentation for each experiment included two load cells (one on the horizontal actuator to measure lateral load and one on the post-tensioning rod to measure changes in post-tensioning force as the column displaced laterally), six string potentiometers for measuring

displacement along the length of the column, eight linearly variable displacement transducers (LVDT's) for measuring vertical movement between the segments at the joints, four inclinometers for determining the rotations of the column shaft and horizontal actuator, 8–12 strain gages on the internal reinforcement, and 6–12 strain gages on the fuse plates. Internal strain gages were located on the reinforcement in both the top and bottom column segments. The gages in the bottom column segment were located at the base of the column, while the gages in the top column segment were located 1 ft above the joint (i.e. 2 ft above the base of the column). On the first three segmented specimens (Columns 2, 3, and 4), gages were placed on the corner reinforcement only. On the last two jointed specimens (Columns 5 and 6), gages were placed on all six steel reinforcement bars. The internal strain gages are shown for a 2 ft column segment in Figure 11, while the exterior instrumentation is shown in Figures 12 and 13. A wooden instrumentation frame was assembled for each test to support the lateral displacement transducers. This instrumentation frame was not in contact with the testing frame to ensure that the data acquired from the string potentiometers mounted on the frame measured absolute displacements of the test columns.

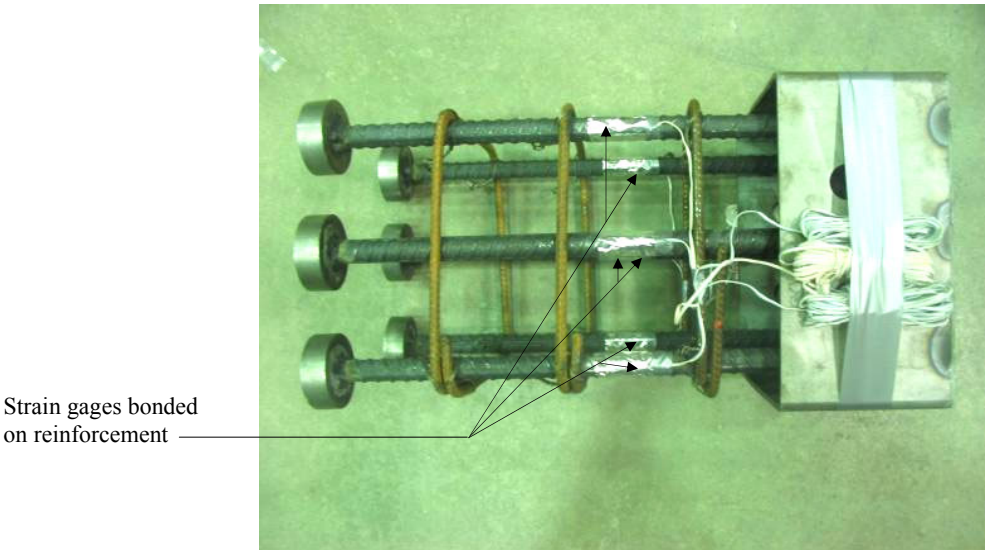

Figure 11. Photograph of strain gages on 2-ft. segment of Column 5.

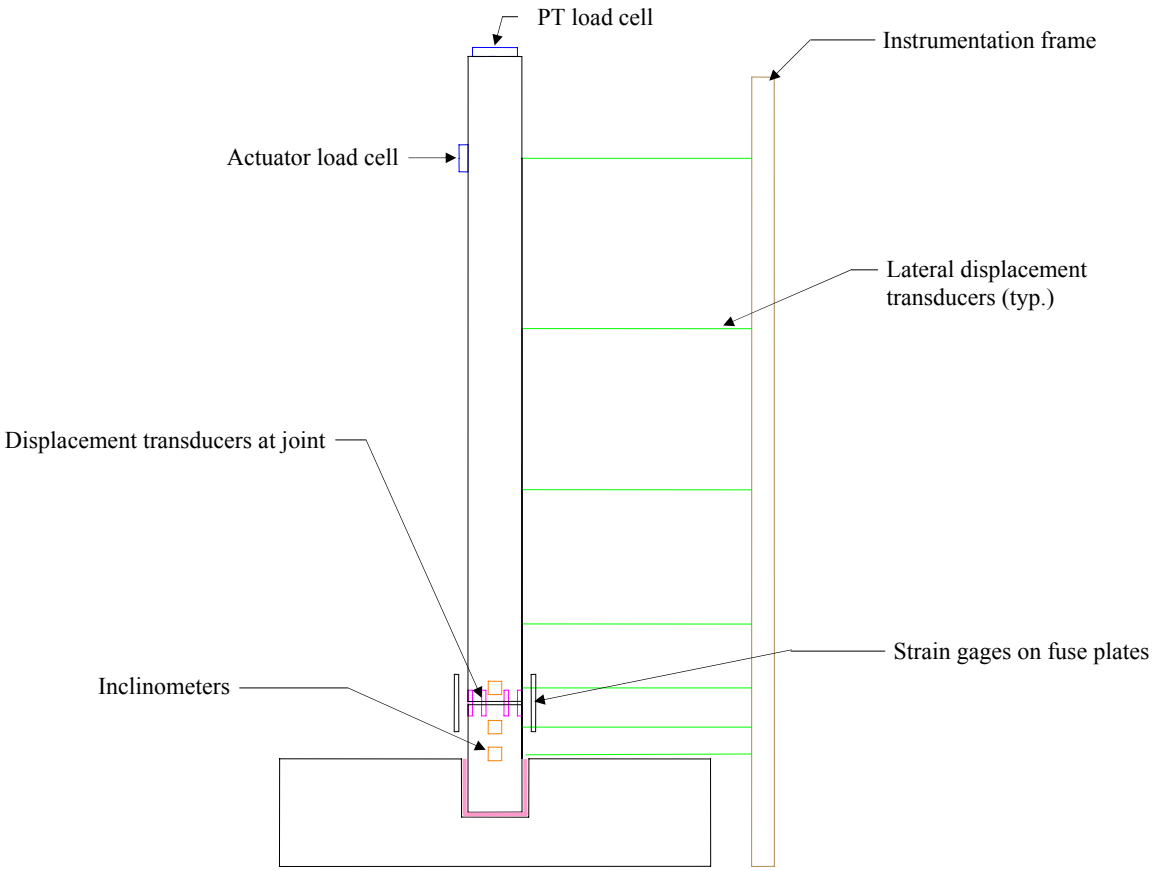

Figure 12. Instrumentation schematic.

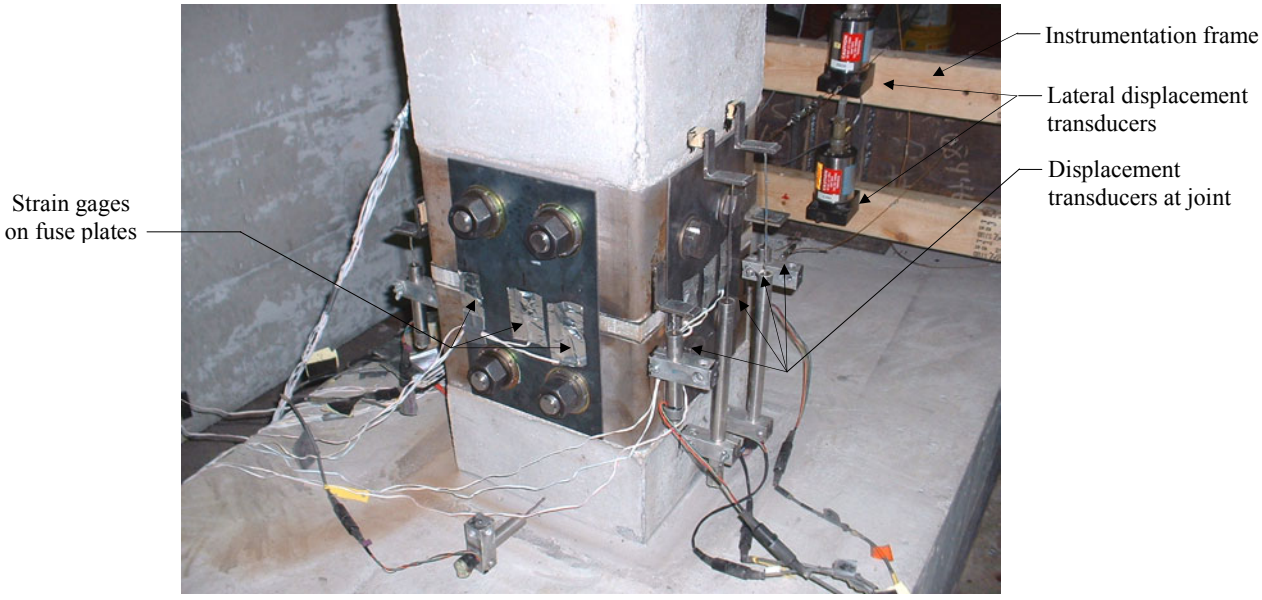

Figure 13. Photograph of instrumentation.

2.4 Testing Procedure

An MTS TestStar IIm controller was used for moving the actuator. By programming the controller with a sinusoidal wave input equal in amplitude to the maximum displacement of each cycle, the actuator was signaled to move to the peak target displacement of each loading cycle and back in a uniform period of time. A data acquisition system (DAS) was used to log data from all instrumentation employed in the experiments. The DAS recorded data once every second during the tests due to the slow, quasi-static application of lateral loads. Cyclic, quasi-static lateral loads were applied to the column specimens using displacement control. Displacement cycles increased incrementally until the column failed. Each cycle began by inducing the desired positive displacement that was desired and returning to zero displacement. The cycle was completed by inducing the same displacement in the opposite direction, and returning to zero displacement (e.g., 0 in., +1 in., -1 in., 0 in.). The specimen was examined for damage at peak displacements of each cycle, and photographs were taken every few cycles. The displacement regimen used in the tests is shown in Table 1 and Figure 14.

All segmented columns followed a similar testing procedure with one major modification. Once the column had been displaced 2.5 in. (Cycle 16), yielding and buckling of the fuse plates was apparent. To investigate effectiveness of repair, the fuse plates were replaced with new plates and the loading regimen was started over, this time continuing until the column failed.

Table 1. Displacement cycles.

Cycle	Displacement, in.	Cycle	Displacement, in.	Cycle	Displacement, in.
1	0.10	11	1.00	21	5.00
2	0.14	12	1.00	22	5.00
3	0.18	13	1.50	23	6.00
4	0.22	14	2.00	24	7.00
5	0.26	15	2.00	25	7.00
6	0.30	16	2.50	26	8.00
7	0.40	17	3.00	27	9.00
8	0.50	18	3.00	28	10.00
9	0.50	19	3.50	29	11.00
10	0.75	20	4.00	30	12.00

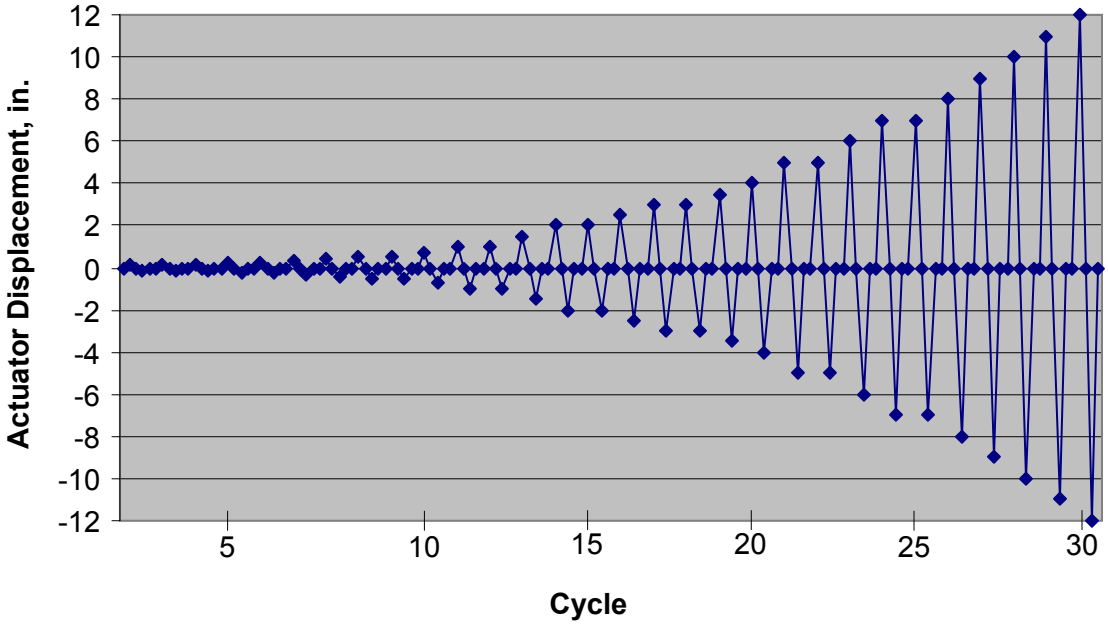

Figure 14. Displacement regimen.

3. DESIGN OF SPECIMENS

3.1 Design Approach

Specimen design began by developing a systematic approach to assessing the behavior of the proposed structure. Performance objectives associated with specific hazard levels were determined for the structure; functional-level and survival-level performance objectives were used in the design and analysis. During functional-level loading events, which are associated with a higher probability of occurrence, the performance objective is to keep the structure operational without the need for immediate repair. During survival-level loading events, which have a lower probability of occurring, the performance objective is to prevent the structure from collapsing.

As previously noted, one of the objectives of this research was to increase the event magnitude required to cause permanent, irreparable damage to the structure. By limiting most damage to the fuse plates at segment connections, the system was easily repaired and remained in its functional-level state. In this research, a desired sequence of responses to increasing lateral load which would lead to failure of the columns was developed. Due to the repairable aspect of the system, damage criteria were established for functional-level operations that would not permanently damage the structure. This preferred sequence of responses was used to size the column reinforcement, as well as determine the joint and fuse plate details.

The following response sequence was developed for the columns in terms of increasing the magnitude of applied lateral load. When a lateral load is created from an event, cracking at the base of the column is the first damage to occur in the column. The cracking will be found at or near the base, because the moment there is the largest. Due to the relatively small load required to cause cracking, this event is unavoidable from an economical design standpoint. However, with the tensile strength of concrete being neglected during design, cracking of the concrete will not diminish the overall performance of the column. Additionally, while this event is not repairable, the crack will not prevent the column from acting in an elastic manner. A decrease in initial lateral stiffness will occur due to this cracking. However, it will not affect the strength of the column when larger displacements occur. Furthermore, the

addition of unbonded post-tensioning will reduce the potential for corrosion by decreasing the widths of cracks that form.

With an increase in lateral load, the next damage to occur to the column should occur at the fuse plates connecting the column segments. To remain structurally undamaged, the longitudinal reinforcement in each precast column segment must not yield. To accomplish this, the replaceable fuse plates were designed to yield before the bonded internal reinforcement. By selecting a fuse plate material with appropriate yield strength, elastic modulus, and cross-section dimensions, the plates can be designed to yield just prior to the longitudinal reinforcement in the precast elements. By ensuring yielding of the fuse plates at a load near that required for yielding the longitudinal reinforcement, the column strength will be close to that of a non-segmented column. Furthermore, the unbonded post-tensioning in the segmented column provides additional lateral load capacity so that the lateral strength of the segmented columns may exceed that of a non-segmented column.

Once the fuse plates have yielded, they should continue to strain at nearly constant stress levels as lateral loads increase until their ultimate elongation is reached. Selecting a fuse plate material with large ultimate elongation will allow the column to experience large deflections while resisting high loads. It will also prevent the precast column segments from experiencing major damage due to yielding of internal reinforcement.

The column may continue to resist higher loads beyond yielding of the fuse plates for several reasons. If fuse plates are used on all four sides of the construction joint, the plates parallel to loading (i.e. side plates) nearer the neutral axis will not be fully yielded. Because a linear strain profile is assumed at the construction joint, the center of these plates will experience smaller strains than the fuse plates on the extreme tension and compression faces of the column. These portions of the side plates will continue to sustain increasing stresses until they too have fully yielded. Additionally, strain hardening of steel fuse plates may increase the moment capacity of the segment joints incrementally as lateral deflections increase.

With a further increase in lateral load, the construction joint may continue to sustain higher moments for the reasons previously noted. If the moment at the segment joint increases sufficiently, the longitudinal reinforcement in the column segments will begin to yield, and the column segments could no longer be considered elastic. The bonded reinforcement will

experience plastic deformation and will not return to its original state when unloading occurs. Even so, the column would still be operating at the functional-level and residual deformations will be small. The bridge could remain in service for use by emergency vehicles and effective repair could be achieved by replacing the fuse plates.

As lateral deflections are increased further, the column should continue to deflect at a nearly constant lateral load until the ultimate elongation of the fuse plates is reached. Once the tension fuse plate fractures, the force resisted by the plate will be transferred to the unbonded post-tensioning bar and the fuse plates parallel to the applied load. At this time, the post-tensioning will likely begin to yield, marking the transition from a functional-level event to a survival-level event. Until the ultimate tensile strength of the post-tensioning is exceeded, the column will remain stable; however, it will lose both its self-centering capability and its ability to be easily repaired.

3.2 Specimen Details

The 14 ft. vertical height of the column was limited by the dimensions of the load frame available for testing. A 12 in. square cross-section was selected to examine bending-dominated behavior and represent a half-scale model of a typical pier column used in Iowa with a 2.5% reinforcement ratio.

The construction joint for the segmented columns was located 12 in. above the foundation block to allow for convenient connections. This also placed the joint at a high moment region in the column. All columns had 12 in. embedment into the foundation socket to avoid pull-out and damage to the foundation block. Thus, the jointed columns were cast in 2 ft. and 12 ft. long segments.

Fuse plates and post-tensioning bars were selected and sized to ensure that yielding occurred first in the fuse plates, as well as to accommodate the bolted friction connections. Bolt sizes and types (1 in. diameter A490 bolts) were selected using AISC guidelines assuming constant clamping forces typical in steel connections. This assumption proved suspect as slippage was observed in testing. The 2.5 in. diameter central duct for the post-tensioning bar was selected to avoid small-radius bending as curvature concentrated at the joint in the specimen at high displacement levels.

All column segments were fabricated with six #7 Grade 60 steel longitudinal reinforcing bars. Three bars were placed on both the tension and compression faces of the column. Anchorage details varied in some of the columns, but the primary reinforcement remained constant in all specimens to achieve columns with similar ultimate moment capacity. Steel collars at the segment joint ends of each column segment were used to provide confinement and prevent spalling at construction joints. As previously discussed in Section 1.3 these collars also served to protect the relatively fragile concrete corners during shipping and erection as well as to provide a convenient means for connecting fuse plates with through-bolts.

3.2.1 Column 1: Control Column with no segment joint

For the longitudinal reinforcement in the control column (Column 1), the corner bars on the bottom end of the column embedded into the foundation socket consisted of two U-shaped bars. One-hundred-eighty degree hooks were used on this end for the interior two bars to achieve anchorage.

Transverse ties were spaced every foot along the height of the two column segments. On the bottom end of the column, the first stirrup was placed 5 in. from the end of the column to help confine the hooks and hoops; column reinforcement is shown in Figure 15**.**

Figure 15. Base end of control column reinforcement cage.

3.2.2 Columns 2–4: Segmented Columns

The first three segmented columns (Columns 2-4) had reinforcement details similar to those used in the unjointed control column (Column 1). U-bars were used on the construction-joint ends of the column segments for the corner bars as they were for the control column (Column 1). Similarly, the interior bars in each segment had one-hundred-eighty hooks on the construction-joint end. These U-bars and hooks were wrapped around the ducts in the steel collars in an attempt to prevent the through-bolts from pulling out of the ends of the column segments when the columns were loaded. For the 2 ft. column segment, hooks were used at the base of the reinforcement to provide anchorage. Similar transverse ties were used in these columns as in the first column. Additional column details for Columns 1-4 are shown in Figures 16-18.

a.) Columns 2-4, 2 ft. segment reinforcement **b.) Columns 2-4, 12 ft. segment reinforcement**

Figure 16. Photographs of column 2-4 reinforcement.

Figure 17. Collar for Columns 2–4.

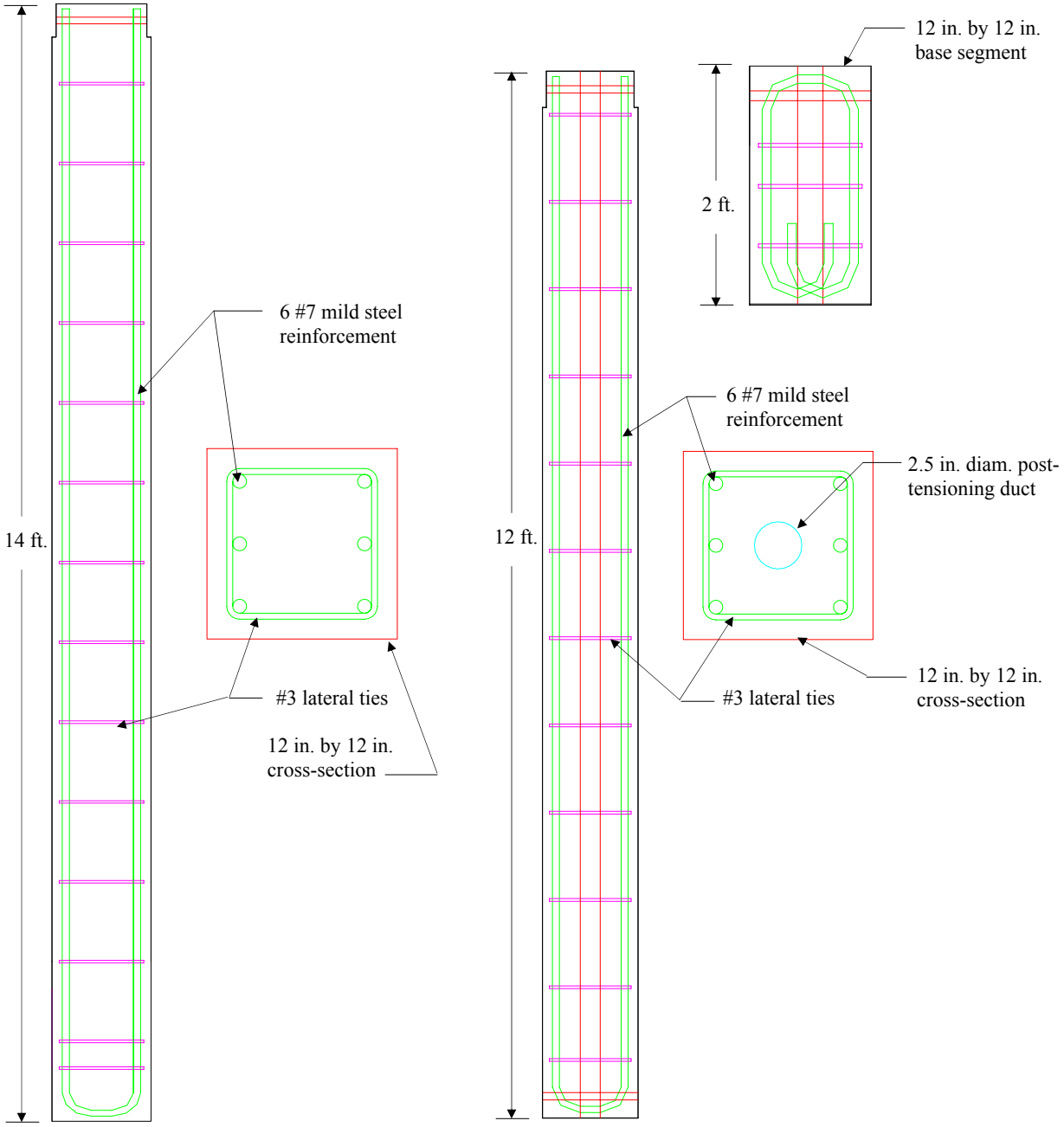

a.) **Column 1**

b.) **Columns 2–4**

Figure 18. Reinforcement in Columns 1-4.

For the first three segmented columns (Columns 2-4), the collars were fabricated from 3/16 in. thick plate and angles welded together. Holes were drilled in the plates to accommodate 1.1 in. outside diameter steel ducts for through-bolts spaced 4 in. apart on the tension and compression faces of the collar. For these three columns, fuse plates were only used on the tension and compression faces of the column.

The vertical spacing of the holes was determined by the ultimate elongation of the fuse plates. Due to the stroke limit of the actuator, the maximum deflection at the top of the columns was +/-12 in.; therefore, an opening at the construction joint was calculated to be less than 1.5 in. Since the ultimate elongation of the fuse plate steel was estimated to be 20%, a minimum spacing of 6 in. was used between the bolts connecting the fuse plates to the column segments.

3.2.3 Column 5: Segmented Column with Revised Anchorages

Column 5 was constructed using #7 longitudinal reinforcement with threaded end anchors. These anchors were welded to the steel plate at the end of the segment collar to improve anchorage of the bars and prevent bolt pull-out. The end anchors were 1 in. thick x 1.5 in. wide x 6 in. long. For Column 5, end anchors were used on all six longitudinal reinforcing bars in the 2 ft. and 12 ft. column segments. The two foot segment reinforcement and collar is shown in Figure 20. Transverse ties similar to those used in the previous columns were provided as well.

For convenience, a structural steel tube (HSS 12 in. x 12 in. x 1/4 in.) was used for the collars for Column 5 in place of the welded collars in previous specimens. The collars were sandblasted to increase the coefficient of static friction in an attempt to reduce slippage between the collars and the fuse plates observed in previous tests. Since lateral fuse plates were used on Column 5, additional through-ducts were required for the collars. The horizontal spacing of the through-ducts on the collars remained the same as the first three segmented columns; however, the vertical spacing was altered. For Column 5, the through-ducts on the lateral sides of the column were spaced ½ in. closer to the construction joint. The ducts on the extreme tension and compression faces of the column were spaced ½ in.

farther away from the construction joint. This configuration was designed so that the ducts would be in contact with each other. This can be seen more clearly in Figures 19 and 20.

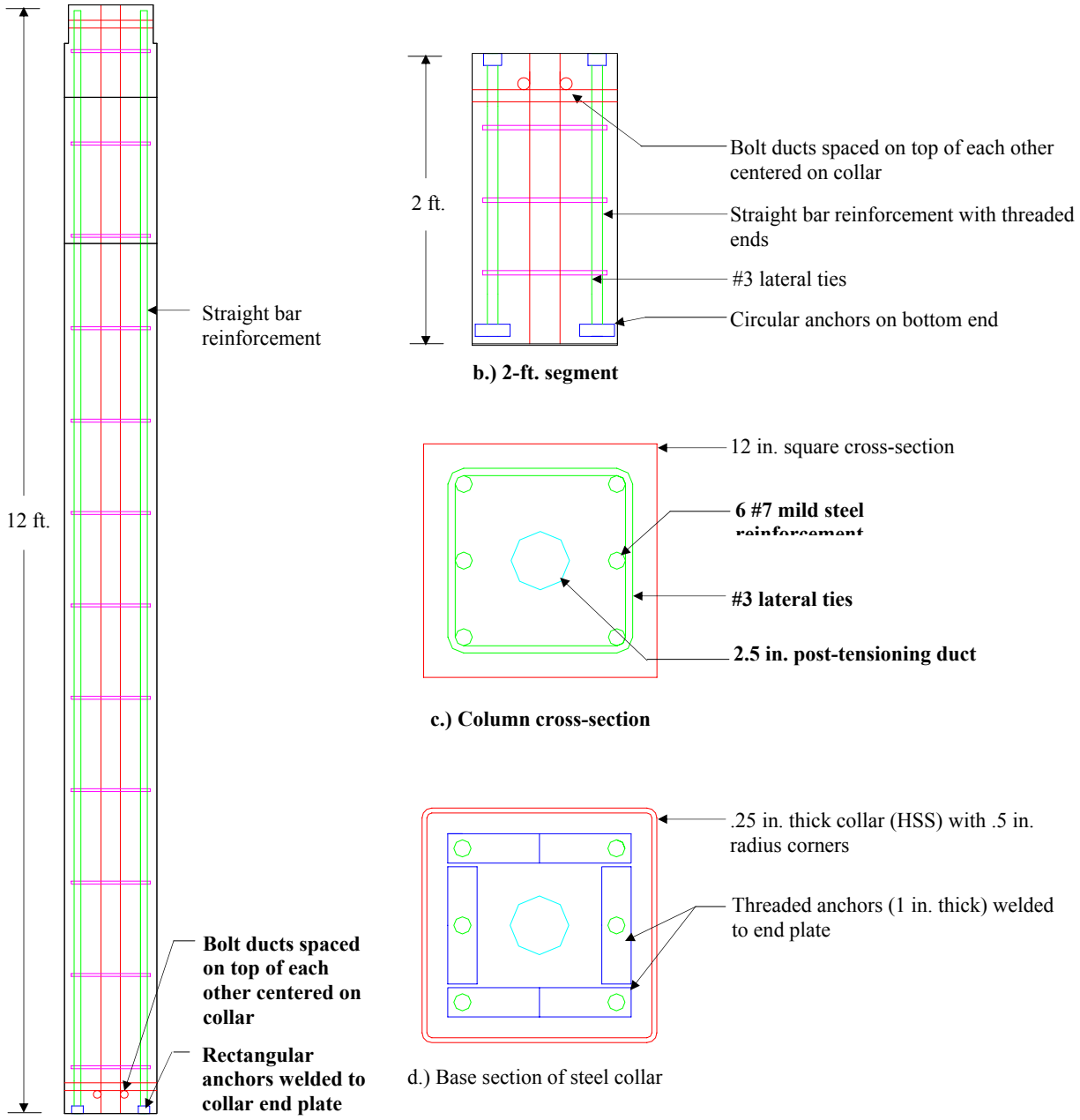

Figure 19. Column 5 details.

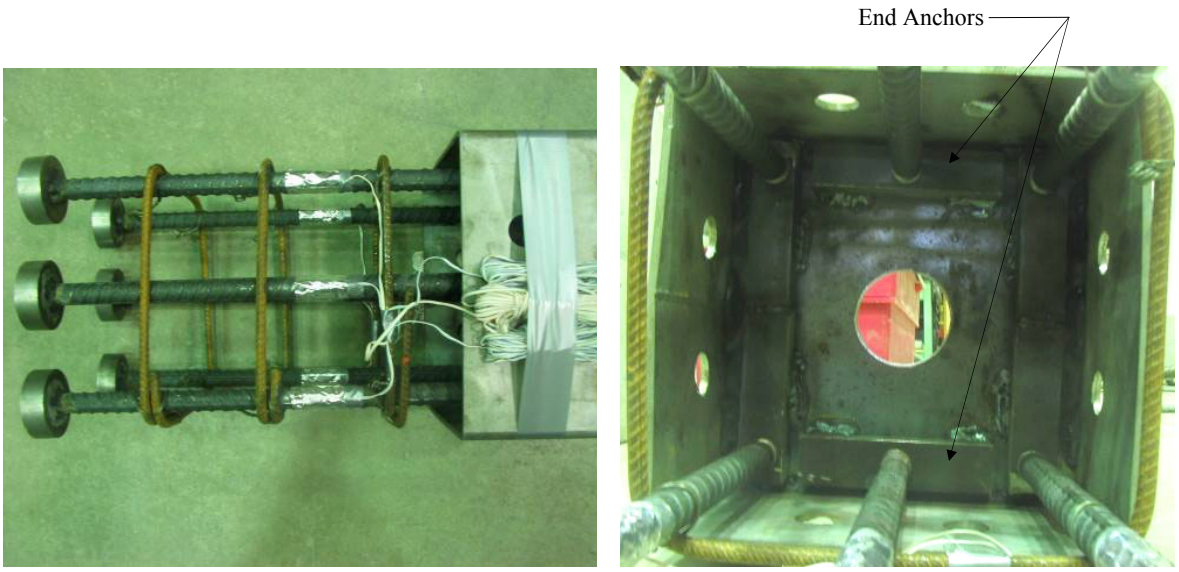

a.) Side View **b.) End View**

Figure 20. Column 5 mild steel reinforcement in the 2 ft. segment.

3.2.4 Column 6: Segmented Column with Revised Anchorages

Column 6 was also constructed using #7 longitudinal reinforcement with end anchors. Unlike Column 5, end anchors on Column 6 were used only on the center two reinforcing bars. U-bars for the corner bars were used on these columns as in Columns 2-4. Transverse ties used were similar to those in the previous specimens. The two foot segment reinforcement and collar is shown in Figure 22.

As in Column 5, a structural steel tube (HSS 12 in. x 12 in. x 1/4 in.) was used for the collars of Column 6. The only alteration from Column 5 for these collars was the vertical spacing of the through-ducts. In these collars, a 1 in. gap was provided between the pairs of ducts perpendicular to each other. The ducts for the lateral faces of the column were spaced 1 in. closer to the construction joint. The ducts on the tension and compression faces of the collars were spaced 1 in. farther away from the construction joint. This was done to provide room for additional concrete between the ducts, as well as to avoid consolidation issues in this relatively congested region. The collar used for Column 6 is shown in Figure 23, and additional details for Column 6 are presented in Figure 21.

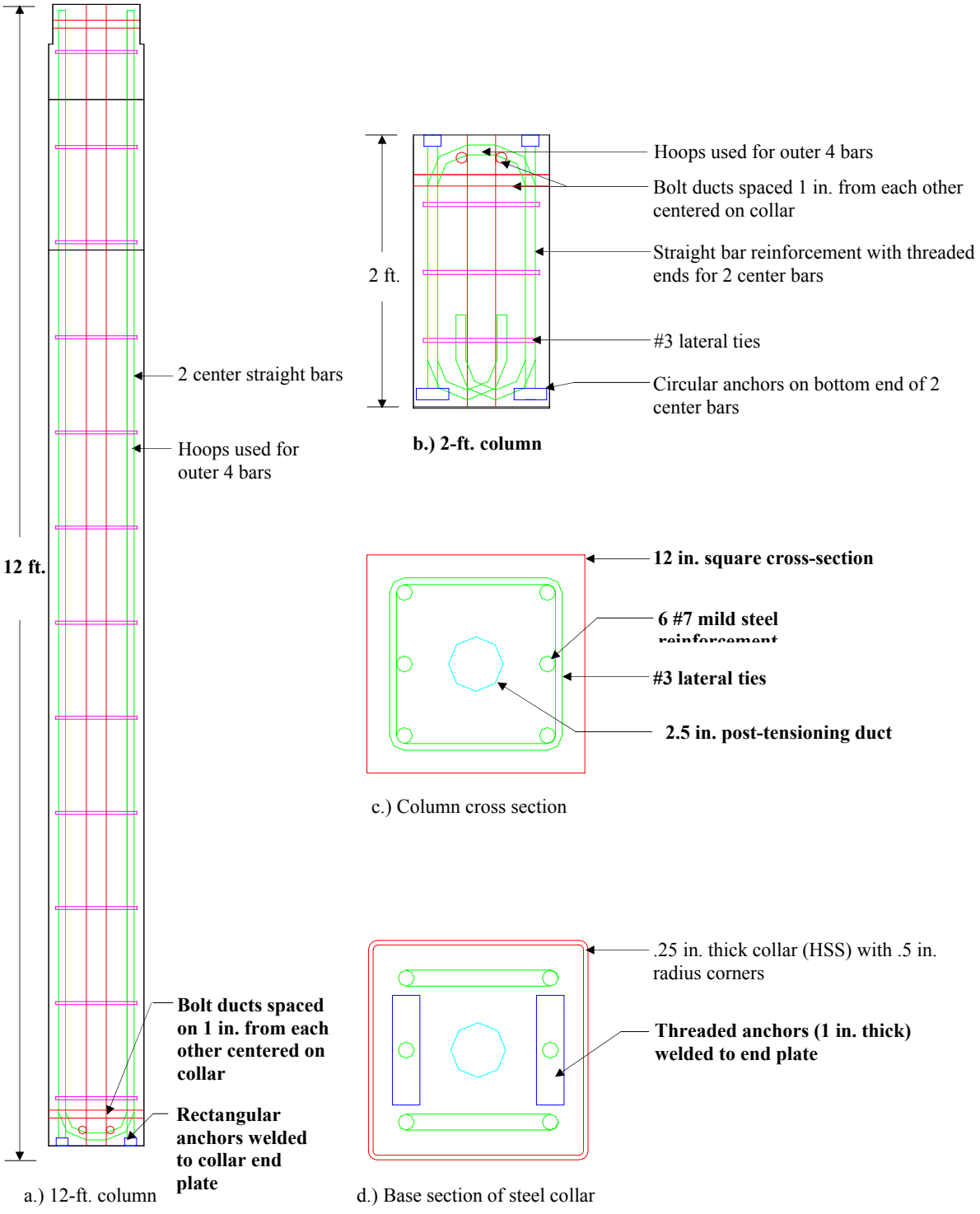

Figure 21. Column 6 details.

a.) Side View **b.) End View**

Figure 22. Column 6 mild steel reinforcement in the 2 ft. segment.

Figure 23. Column 6 collar.

4. SPECIMEN CONSTRUCTION

4.1 Foundation Blocks

Each of the foundation blocks for this series of experiments was designed to be rigidly connected to the laboratory strong floor using post-tensioning and provided a fixed base for the six columns tested. The same design and construction process was used for all of the foundation blocks, which were sized and reinforced to resist cracking under the maximum loads applied to the columns. Reinforcement details for a typical foundation block are presented in Figures 24-26.

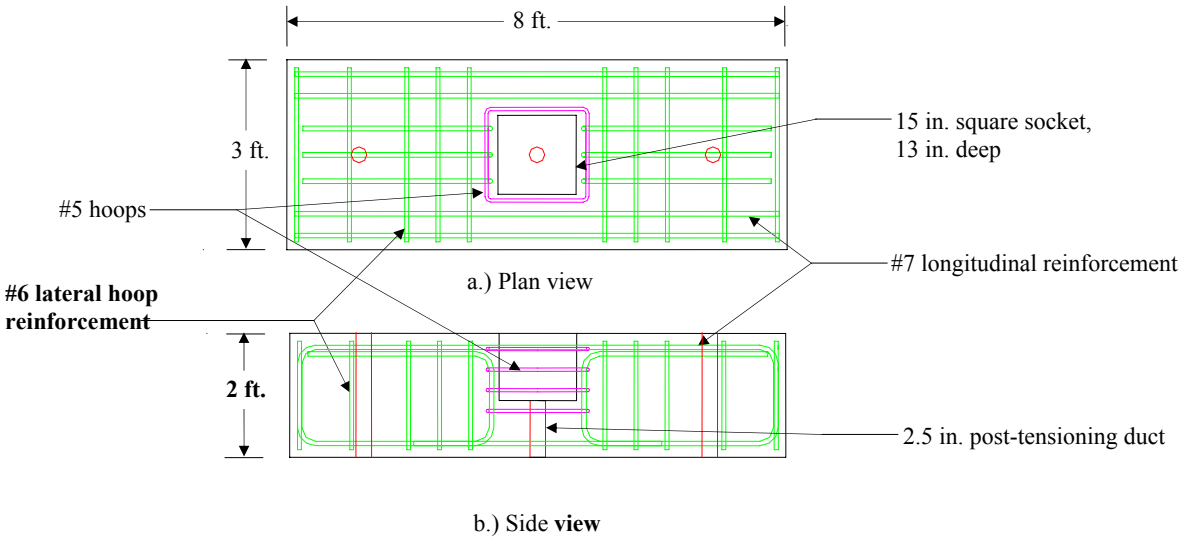

Figure 24. Foundation details.

Figure 25. Photograph of center socket reinforcement.

Figure 26. Photograph of foundation reinforcement cage.

After construction of the reinforcement cage, the boxout for the center socket (shown in Figure 27) was tied in place. As previously mentioned, this socket allowed the bottom column segment to be epoxy grouted in the foundation block. A 2.5 in. diameter hole was drilled in the center of the socket boxout to allow for the center post-tensioning duct. Two additional 2.5 in. ducts (shown in Figure 24) were spaced 3 ft. on either side of center to align with the holes in the strong floor, permitting two post-tensioned tie-down bars to secure the foundations to the lab floor. A photograph of these ducts can be seen in Figures 28.

a.) Top view **b.) Inside view**

Figure 27. Photographs of center socket boxout.

Figure 28. Photograph of foundation reinforcement and tie-down ducts in forms.

Figure 29. Photograph of boxout in forms.

4.2 Column Specimens

4.2.1 Column 1(Unjointed Control Column)

For Column 1, the reinforcement cage was first tied and positioned in standard steel forms. Strain gages were placed on the longitudinal reinforcement; four gages were located one foot from the bottom of the column on the exterior four longitudinal bars. The column's reinforcement cage positioned in the steel forms can be seen in Figures 30-32.

Figure 30. Photograph of Column 1 reinforcement.

Figure 31. Photograph of chairs and reinforcement in Column 1.

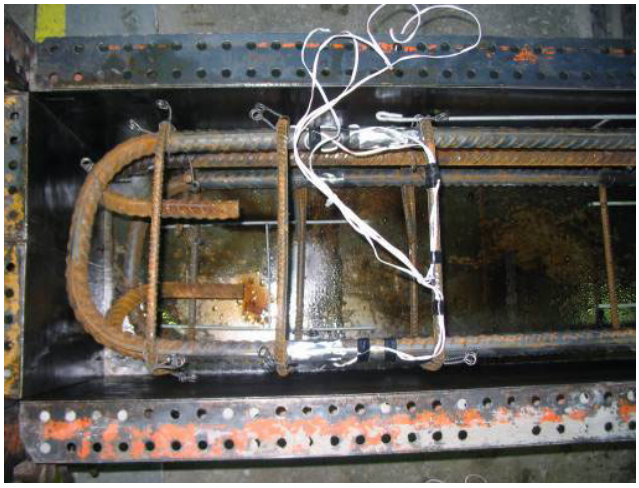

Figure 32. Photograph of base end of Column 1.

The inserts for the load beam connection were then placed in the steel forms; two 1 in. diameter ducts were held in place with plywood boxouts at the top of the column. Since these ducts would also be used as lifting points for the column, #4 reinforcing steel was used to anchor the ducts in place; these lifting inserts and reinforcing steel can be seen in Figure 33.

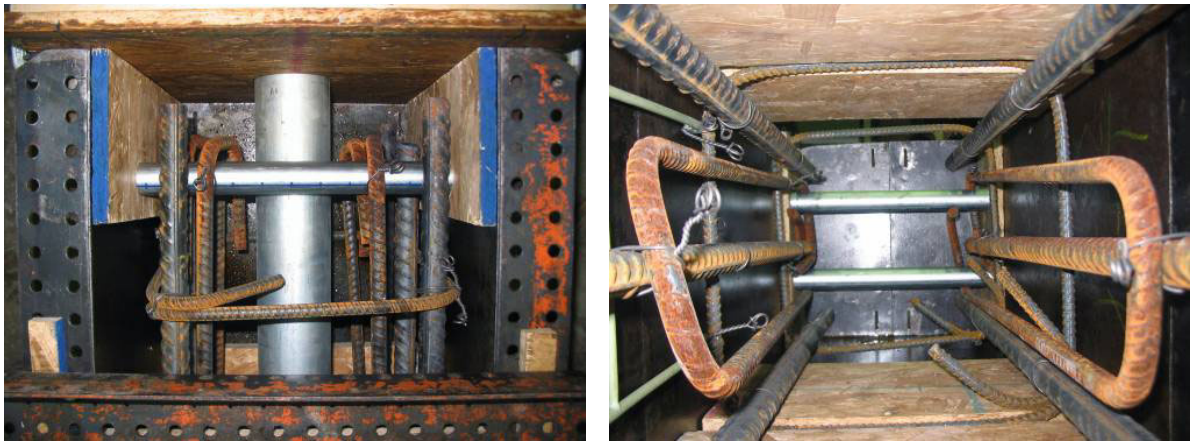

a.) Top view **b.) Inside view**

Figure 33. Photographs of lifting inserts.

4.2.2 Column 2

The 12 ft. column segment for Column 2 was constructed in a similar manner as the control column. However, several alterations were made to allow for segmented construction. As with the control column (Column 1), four internal strain gages were used in this column. They were placed 12 in. from the bottom of the column on the four corner longitudinal bars. A central duct for the unbonded post-tensioning bar was included in this segment. The steel collar was placed in the forms on the base end of the 12 ft. column. Plywood bulkheads, as seen in Figure 34, were used to cap the end of the forms and securely position the post-tensioning duct. Details of the 12 ft. Column 2 segment in the forms are shown in Figures 34-37.

The 2 ft. column segment shown in Figures 38 and 39 was constructed in a similar manner as the 12 ft. column segment. Strain gages were placed in the longitudinal direction at midheight of all four corner bars. Additionally, a steel collar identical to the one used on the 12 ft. column segment was placed on the top end of the segment.

Figure 34. Photograph of Column 2 bulkhead.

Figure 35. Photograph of Column 2 collar end.

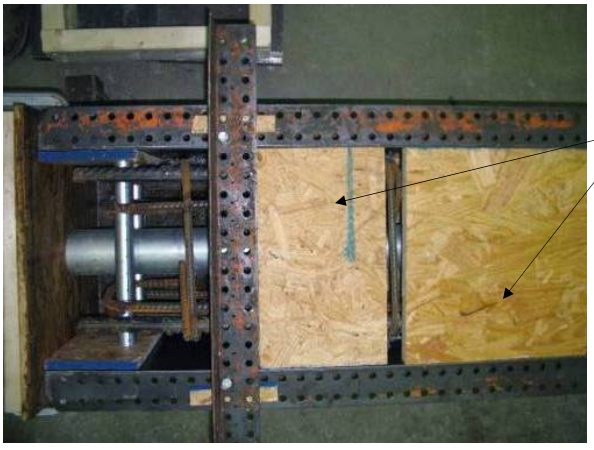

Figure 36. Photograph of top of Column 2.

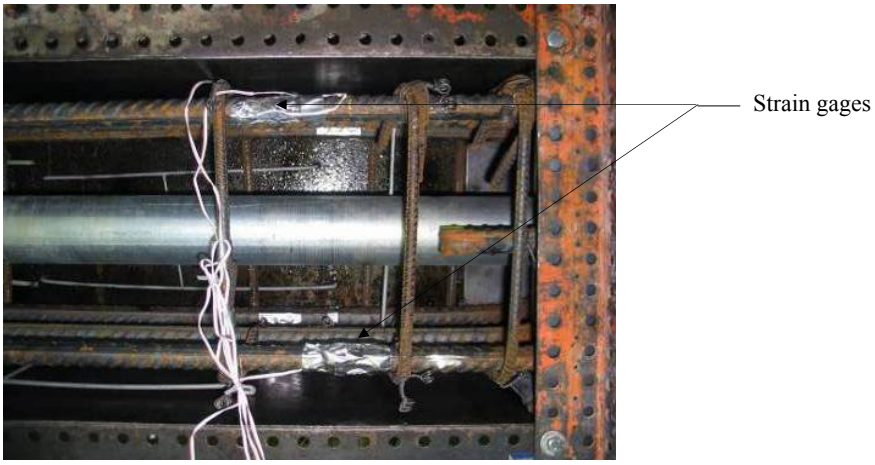

Figure 37. Photograph of Column 2 Strain gages.

Figure 38. Photograph of reinforcement of Column 2 (2 ft. column segment).

Figure 39. Photograph of Column 2 reinforcement in forms.

A typical collar used for Columns 2–4, shown in Figure 40, was constructed by welding 3/16 in. angles with 3/16 in. plates. Holes for the ducts were drilled in two of the side plates to secure bolt ducts that connected the fuse plates to each column segment. Additional information about the collars and reinforcement details was presented in Chapter 3.

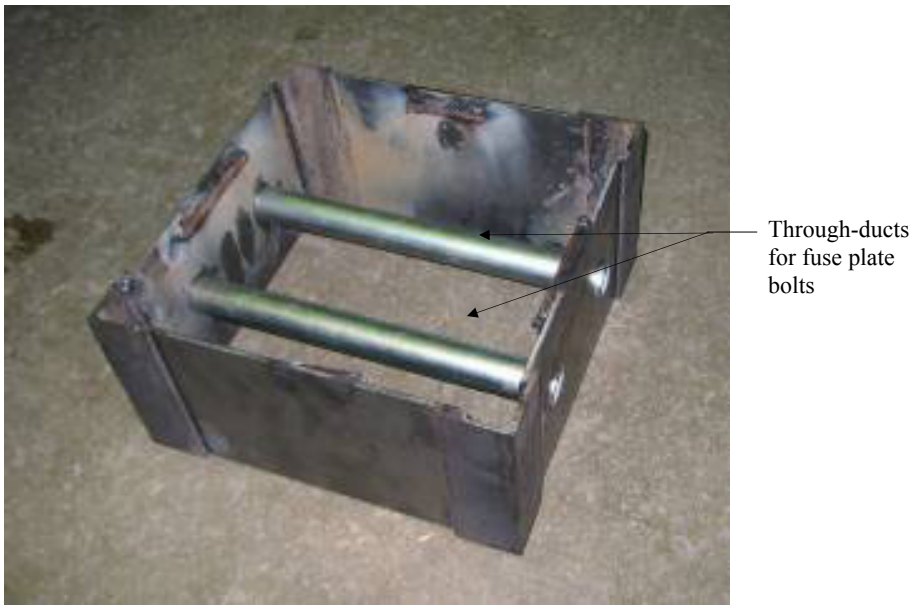

Figure 40. Photograph of Column 2 steel collar with bolt through-ducts.

4.2.3 Columns 3 and 4

The third and fourth segmented columns (Columns 3 and 4) had a similar construction process as the first segmented column with one major difference. A steel plate was welded to the end of the collars for Column 3 to assist in confining the concrete near the construction joint. A 2.5 in. hole was cut in the center of this plate to accommodate the post-tensioning duct. Due to the experimental nature of this plate, it was not included for the Column 4 collars at the time of casting. The collar used for Column 3 is shown in Figure 41; construction details of the column segments used for Columns 3 and 4 are shown in Figures 42-50.

Figure 41. Photograph of Column 3 collar and end plate.

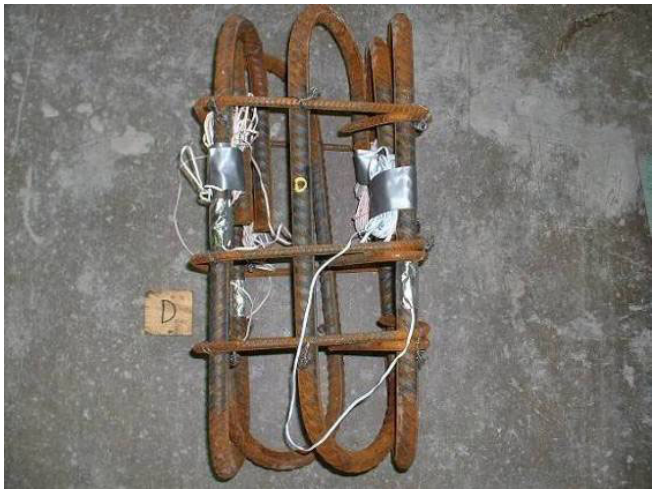

Figure 42. Photograph of Column 3, 2 ft. segment reinforcement.

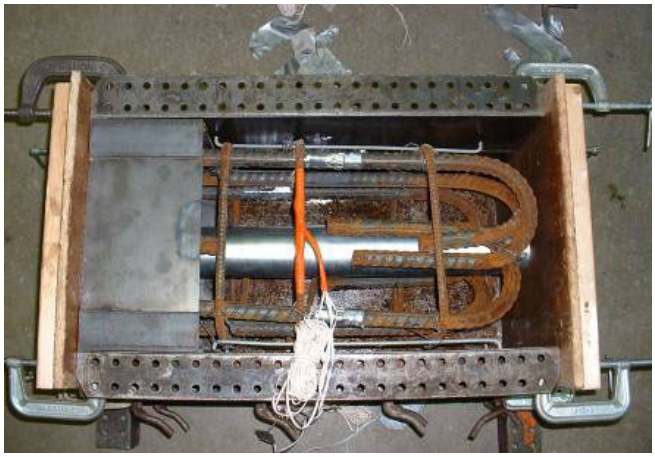

Figure 43. Photograph of Column 3, 2 ft. segment reinforcement in forms.

Figure 44. Photograph of Column 3 strain gages.

Figure 45. Photograph of Column 3 reinforcement and inserts.

Figure 46. Photograph of Column 4, 2 ft. segment.

Figure 47. Photograph of Column 4 collar region congestion.

Figure 48. Photograph of Column 4, 12 ft. segment reinforcement.

Figure 49. Photograph of Column 3 foundation reinforcement in forms.

Figure 50. Photograph of Column 4 foundation reinforcement in forms.

4.2.3.1 Additional Column 4 Alterations

Due to the behavior of the two previous segmented column tests (Columns 2 and 3), some alterations were made to the Column 4 segments after casting and prior to testing. After testing Columns 2 and 3, it was apparent that the steel plate on the end of the columns was an improvement to the system. It provided a smooth and symmetric bearing surface between the bearing plate and the column segments and reinforced against cracking of welds in the collar observed in Column 2. Since Column 4 was cast without a plate on the end of the collar, a plate was added after the column was removed from the forms. This plate was similar to that used in Column 3, and was welded to the edges of the steel collars.

The other alteration to the Column 4 segments was made in an attempt to control the collar pull-off phenomenon that occurred during the testing of Columns 2 and 3 (see Chapter 6 for a more detailed explanation on the collar pull-off phenomenon). Steel angles were affixed to each corner of the Column 4 collars to provide an additional connection between the collars and the column segments. One end of each angle was epoxied to the face of the concrete column segments, and the other was coped to reduce bending stresses and welded to the face of the steel collars. While this modification would not be made a part of a permanent design, the results of this test would be more indicative of system behavior if the collar pull-off phenomenon was prevented. The angles that were added are shown in Figure 51.

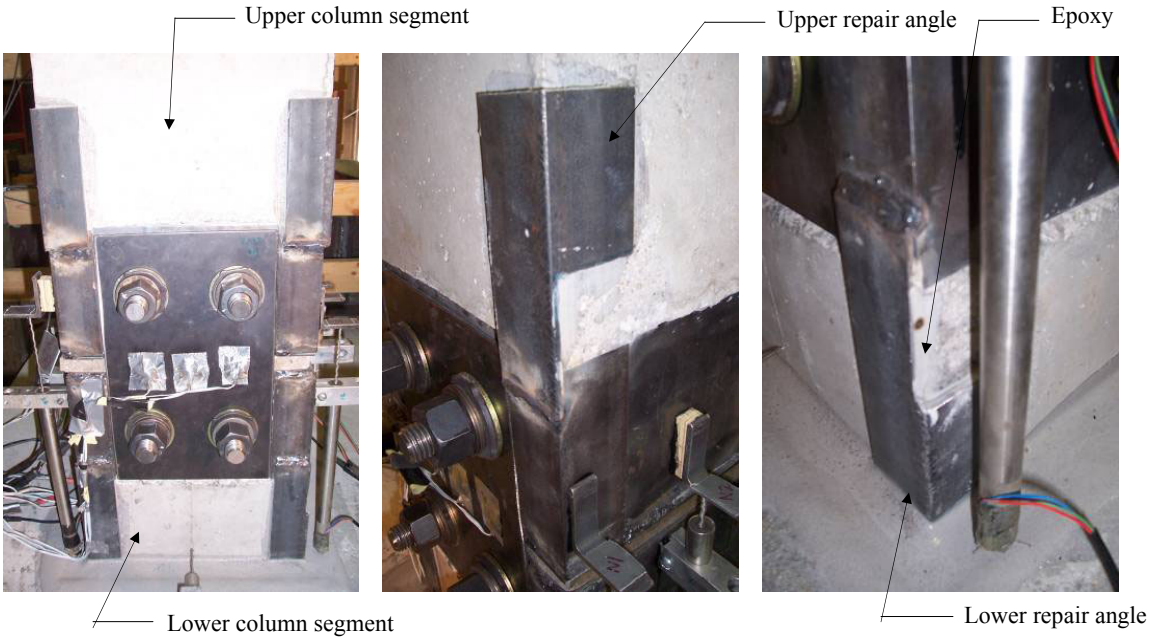

a.) Column 4 east side modifications **b.) Column 4 upper repair angle** **c.) Column 4 lower repair angle**

Figure 51. Photographs of Column 4 alterations.

4.2.4 Column 5

The fifth column had the same dimensions as the previous columns. However, due to the collar pull-off problem that occurred during testing of Columns 2–4, several reinforcement details were revised. Straight bars with threaded end anchors were used for the longitudinal reinforcement instead of bars with hoops or hooks on the ends. These anchors were welded to the end plates of the collars on the construction joint end of each column segment. Also, six strain gages (one on each bar instead of one on each corner bar) were used on both Column 5 segments. These gages were placed one ft. from the base of the 12 ft. segment and in the center of the two ft. segment as in previous columns.

Another alteration made to Column 5 concerned the steel collars. Instead of constructing them from steel plates and angles, the steel collars for Column 5 were fabricated from ¼ in. thick structural steel tubing (HSS 12 in. by 12 in. by 1/4 in.). Once the HSS sections were cut to length, they were sandblasted to increase their coefficient of static friction.

As discussed in Chapter 3, the through-bolt holes on the extreme tension and compression faces of the column were offset ½ in. farther from the ends of the columns, while the holes on the lateral faces of the collars were spaced ½ in. closer to the ends of the columns. The

collared ends of Column 5 are shown in Figures 52-55. In Figures 52 and 53, the 2 ft. column segment with straight bar reinforcement and end anchors is shown. The end plate welded to the Column 5 collars is shown in Figure 54, and the collared end in the forms prior to casting is shown in Figure 55.

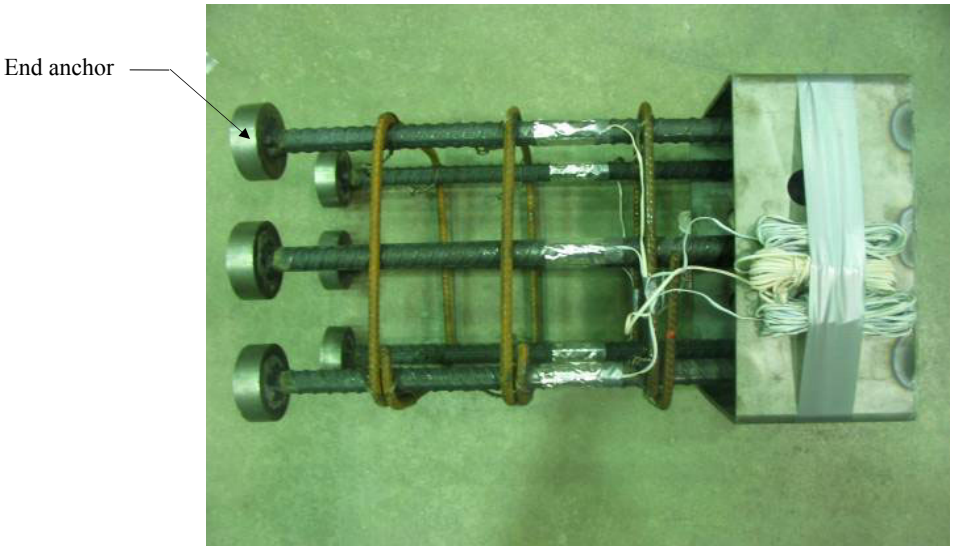

Figure 52. Photograph of Column 5, 2 ft. segment reinforcement.

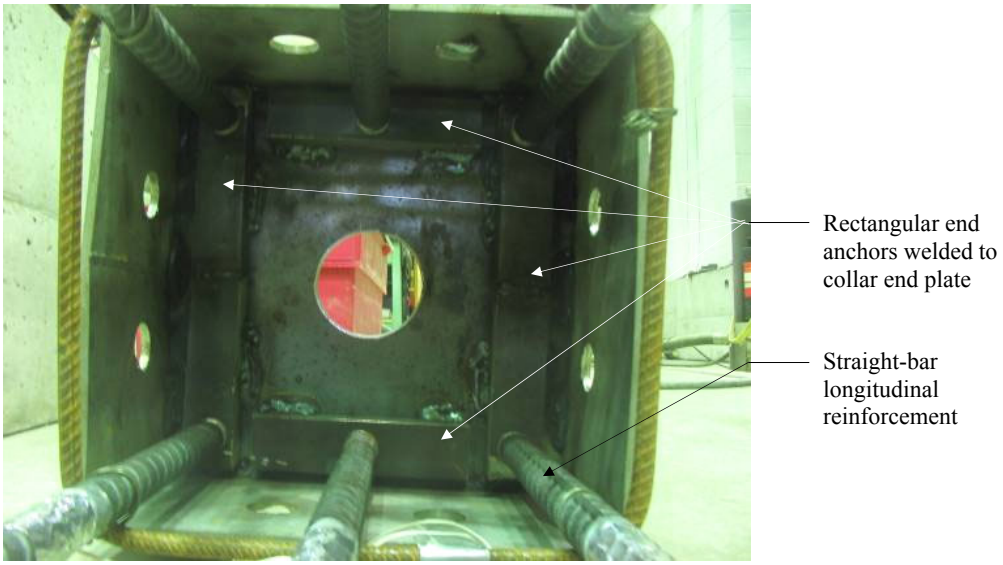

Figure 53. Photograph Column 5 collar reinforcement anchorages.

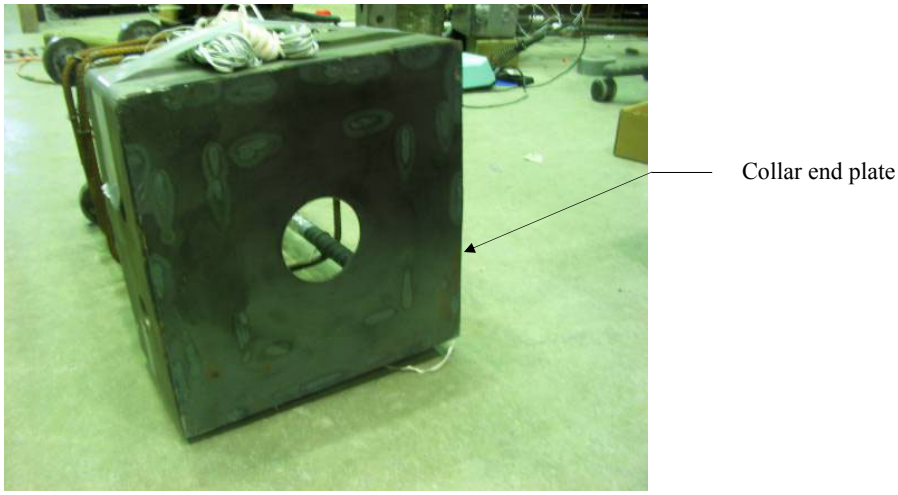

Figure 54. Photograph of Column 5 collar end plate.

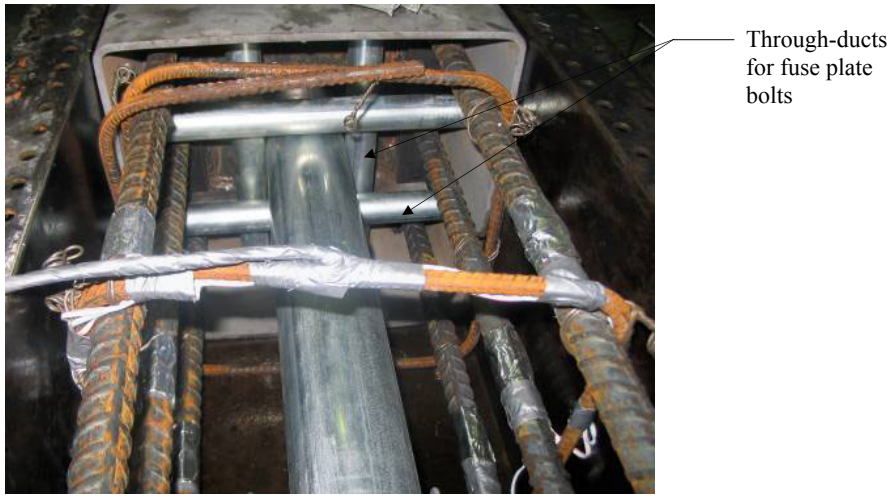

Figure 55. Photograph of Column 5, 12 ft. segment collared end.

4.2.5 Column 6

Column 6 construction was similar to that of Column 5 with some minor modifications. The #7 longitudinal reinforcing bars were used as for all previous columns, and threaded reinforcement was still used for the center two bars on the extreme tension and compression faces of the column. However, hoops were used for the outer four bars identical to those used in Columns 1–4. With the center two bars directly connected to the collars with anchors and the bolt ducts passing through the longitudinal hoops used for the outer four bars, the collar pull-off mechanism was again eliminated. This configuration is illustrated in Figure 56.

As discussed in Chapter 3, the through-bolt duct spacing was also altered for Column 6. Holes on the tension and compression faces of the column were offset 1 in. farther from the ends of the columns, while the holes on the sides of the collars were spaced 1 in. closer to the ends of the columns. The reinforcement end details, along with the collar details are shown in Figures 56-58, while the upper portion of the Column 6 12-ft. segment is shown in Figures 59 and 60.

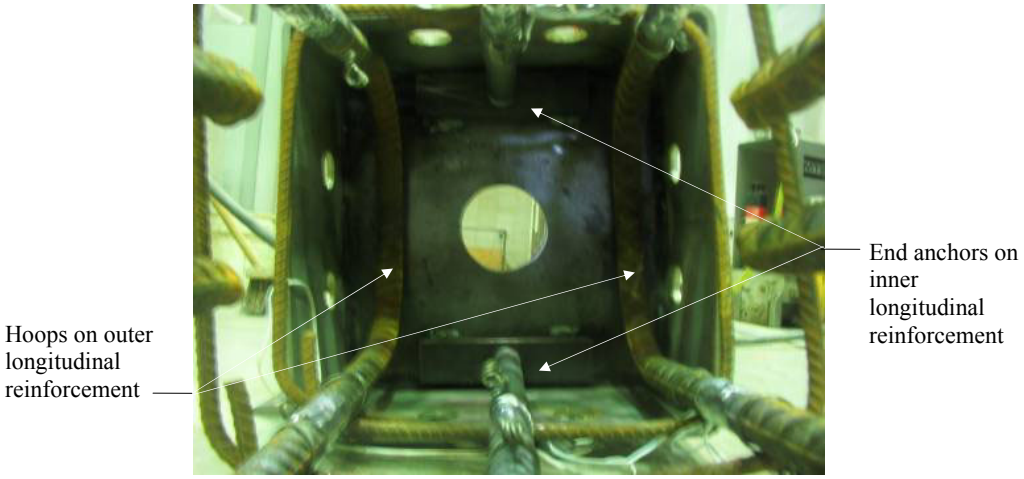

Figure 56. Photograph of Column 6 collar and end anchorage details.

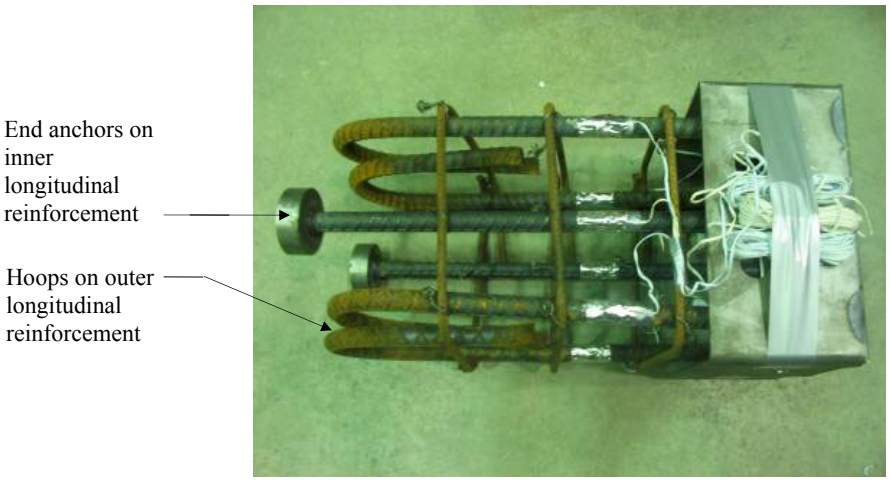

Figure 57 Photograph of Column 6, 2 ft. segment reinforcement and collar.

Figure 58 Photograph of Column 6 collar and end plate.

Figure 59. Photograph of Column 6 in forms.

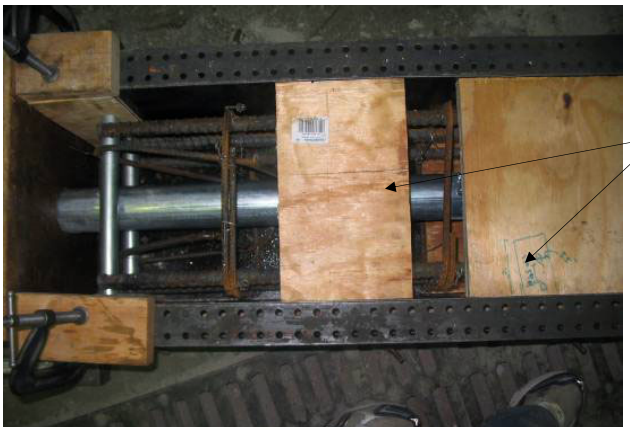

Figure 60. Photograph of Column 6 boxouts and lifting inserts.

4.3 System Impacts on Labor, Construction, and Materials

Many of the improvements with this system are associated with reduction of in-field labor and assembly of precast elements. With typical precast construction, external support (i.e., crane or temporary shoring) must be provided to support each column or segment in position while grout is placed and cured. With this system, the fuse plates can be used to precisely align and stabilize the precast column segments before post-tensioning is applied. Once the first segment is connected to the foundation, a bearing plate is placed on top of the column, followed by the second column segment. Once the second column is in place, the fuse plates can be connected between the segments to stabilize the system. Additional segments can be added in the same manner until the pier cap is placed and the post-tensioning is applied.

Labor requirements for prefabricating this system will depend on the geometry of the column cross-section and the number of bolts required for the construction joint. Angles and plate steel must be dimensioned, cut, and welded to create the collars. The process could be conveniently streamlined when a large number of elements are required. The use of standard steel shapes, like those used for Columns 5 and 6, saved labor but are not readily available in larger sizes (> 1.5 ft. square) for full-scale columns. Standardization of collar shapes would significantly reduce labor requirements during prefabrication. While prefabrication costs may be increased with this system, significant time and costs savings will be gained at the jobsite. The bearing plate used between column segments will greatly accelerate construction once the precast elements are in the field. With more conventional segmental precast concrete column construction, grouting of precast joints requires that an epoxy be used to join column segments. These segments may or may not be match-cast. Since the bearing plates can be fabricated off-site, they can be placed between column segments without any need for grout. This will significantly reduce erection time for the precast columns by eliminating labor and curing time for the grout.

The total quantity of steel used for the segmented columns may result in an increase in material costs. Steel requirements for the monolithic and segmented columns are given in Table 2. It should be noted that while the segmented columns in these experiments used nearly twice the amount of steel as the monolithic column, scaling of the models had a large

impact this ratio; typical columns would exhibit a reduction in this ratio. Again, this increase in cost can be balanced by the reduction of field labor.

Table 2. Column steel requirements

Requirements	Monolithic Column, lbs.	Segmented Column, lbs.
Bolts, collars, fuse plates		89
PT bar and duct		61
Bonded rebar and anchors	195	238
Total	195	388

The addition of the steel collars on the ends of the column segments, as well as the post-tensioning bar and anchorages, required some added materials and labor to construct. Also, due to the limited space available in the half-scale columns, segment ends were relatively congested with steel. Consolidation of the concrete became a concern, because additional vibrating was required to ensure the removal of air voids. To a large extent this congestion was a function of the reduced scale of the models. With full-scale columns, congestion of the collared ends would be significantly reduced due to the increase in volume.

While positioning post-tensioning ducts and appurtenances requires some additional labor, the advantages associated with forming and casting the segments horizontally at ground level can offset the added labor. Additionally, since all of the precast elements can be constructed off-site, their fabrication time may be effectively removed from the critical path of the construction schedule. Furthermore, the precast elements may be cast and stored indoors to optimize the curing environment for the concrete.

5. COLUMN MATERIAL PROPERTIES

Properties of the various materials used in each major component of the test columns (i.e. precast concrete segments, fuse plates, and bearing plates) were measured and are discussed in this chapter.

5.1 Bearing Plates

The bearing plate had two major structural requirements: compliancy, to transfer axial stress uniformly between segments, and strength, to withstand high shear, axial, and bending stresses. Desired properties of the plates included high compressive, tensile, and shear strengths, a modulus of elasticity approximately half that of concrete, high resistance to corrosion, low creep, and relative low cost. Materials considered were epoxy grout, polymer concrete with steel reinforcement, glass fiber reinforced polymer (GFRP), lead, neoprene, and cotton duck. The plates were 0.75 in. thick and 11.875 in. square. The plate materials selected for use in the tests are presented in Sections 5.1.1-5.1.3 of this chapter.

Cylinder compression tests complying with ASTM C 39 Standard Test Method for Compressive Strength of Cylindrical Concrete Specimens were used to determine the compressive strengths of the materials used for the bearing plates. All three pad materials used during column testing (e.g., epoxy grout, polymer concrete, and GFRP) exhibited strengths high enough that the force acting on the plate edges during large column displacements did not cause noteworthy damage to the plates. Thus, it was not possible to determine quantitatively the effect of different compressive strengths of the plate materials. Results from these tests are given in Sections 5.1.1-5.1.3 of this chapter.

In addition to the cylinder breaks, an edge compression test was performed on each type of plate to obtain a realistic stress-strain relationship. To simulate the loading applied during column tests, a 2 in. wide strip on the edge of the plates was tested in compression. From these tests, an estimate of the elastic modulus of each plate was calculated by measuring the slope of the stress-strain relationship. The GFRP plate exhibited the highest modulus during the edge compression test, while the epoxy grout plate saw the lowest modulus. While the modulus of the GFRP plate was 20% higher than the epoxy grout plate modulus, the effect of the different modulus of the three plates during column testing could not be determined,

because each plate performed satisfactorily during the tests. The edge compression test is shown in Figure 61 and the results from the tests are shown in Figure 62.

Figure 61. Photograph of edge compression test.

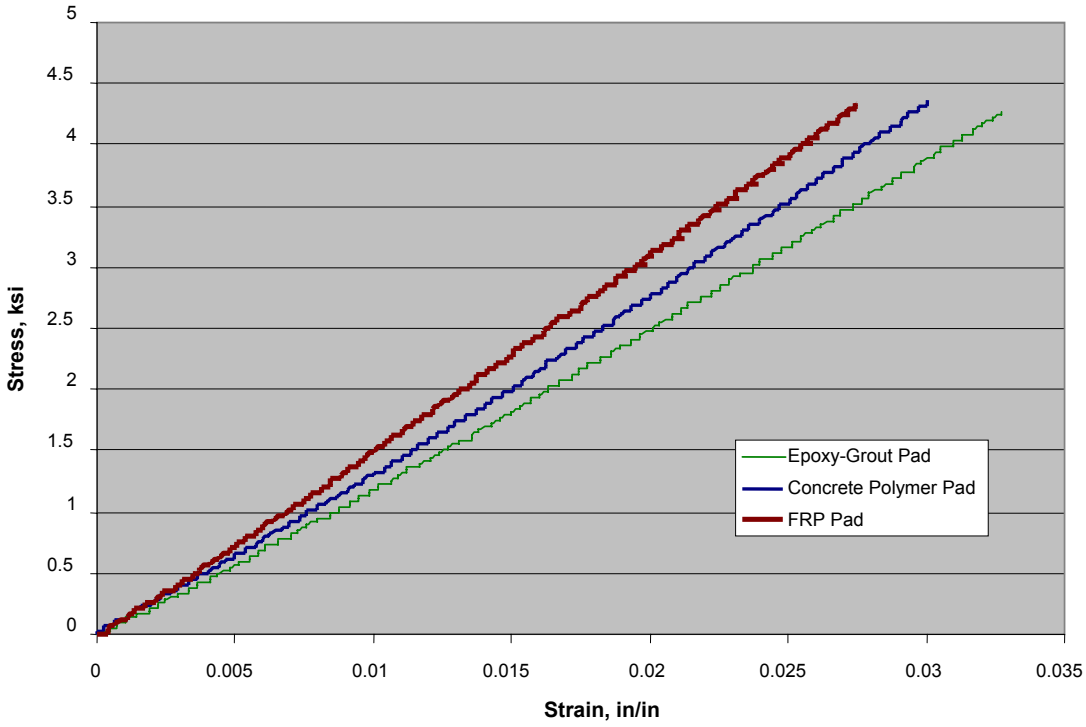

Figure 62. Bearing plate compression test results.

5.1.1 Epoxy Grout

To form the epoxy grout bearing plate, Sikadur 32, a high modulus, flowable epoxy, was mixed with Grade 37 silica sand in a 1:1 ratio. This mixture was also used to grout each column base into its foundation socket. The average compressive strength of the epoxy grout used was 12 ksi in fifteen 3 in. diameter by 6 in. long cylinder breaks, while the elastic modulus of the epoxy grout plate was 1,300 ksi. It should be noted that the elastic modulus for this material can easily be adjusted by altering the sand-to-epoxy ratio. When tested in compression, this material exhibited large plastic strains without cracking. A prefabricated epoxy grout bearing plate, shown in Figure 63, was used for Columns 2 and 3.

Figure 63. Photograph of epoxy grout plate.

5.1.2 Polymer Concrete

A steel-reinforced polymer concrete bearing plate was used in Column 4. In polymer concrete, a high strength, corrosion resistant, thermosetting resin acts as the binding agent. Three-eighths in. aggregate was used in the bearing plate, and a 2 in. square welded wire grid was cast into the plate to reinforce against splitting. The modulus of elasticity of the polymer concrete was approximately 1,500 ksi, while its compressive strength averaged 9.85 ksi in four cylinder breaks. The Column 4 plate is shown in Figure 64.

Figure 64. Polymer concrete bearing plate.

5.1.3 Fiber-Reinforced Polymer

A GFRP bearing plate was used in Columns 5 and 6; an epoxy resin served as the matrix for GFRP, while glass fiber layers provided tensile reinforcement against lateral splitting. Seventeen layers of woven fiber fabric were laid up in alternating 90^{o} orientations to construct the 0.75 in. thick plate. The elastic modulus for the GFRP bearing plate perpendicular to the fibers was approximately 1,600 ksi, and the average compressive strength of the epoxy matrix determined from 3 cylinder breaks was 13 ksi. The GFRP bearing plate is shown in Figure 65.

Figure 65. GFRP plate.

5.2 Fuse Plates

The fuse plates used in the precast pier system were another variable investigated. Desired properties for the plates included low yield stress relative to the reinforcement, large plastic strain capacity, high resistance to corrosion, large ultimate elongation, large toughness, and low cost. Materials considered included commercial grade A36 steel, 1018 carbon steel that was specifically manufactured to yield between 30 and 36 ksi, nickel-titanium shape memory alloy (SMA), A242 steel, and A588 steel. The materials used in each column are presented in Sections 5.2.1-5.2.3.

Three one-eighth in. thick strips of A36 steel, 1018 carbon steel and SMA were cut from the plate stock and tested in direct tension to determine material properties for each fuse plate type. All strips tested were 1 in. wide and 14 in. long. They were placed in the testing frame with a 9.25 in. gage length between friction grips. This gage length was chosen, because it was close to the distance between the fuse plate through-bolts connecting the column segments in Columns 5 and 6. Since testing machine table displacement was measured during the direct tension tests, the total extension of the testing strips could be used to approximate the strain capacity of the fuse plates used during testing. The results of the direct tension tests are presented in Sections 5.2.1-5.2.3.

5.2.1 Commercial Grade A36 Steel

A36 steel plates were used for the fuse plates of Columns 2, 4, and 5. From three direct tension tests, the plates were determined to have an average yield stress of 38 ksi, an ultimate stress of 52 ksi, an ultimate elongation greater than 30%, and an elastic modulus of approximately 31,000 ksi. A representative stress versus strain relationship for the A36 plates is presented in Figure 66.

5.2.2 1018 Carbon Steel

Fuse plates in Column 3 were fabricated from 1018 carbon steel. In three tests, the 1018 carbon steel strips had an average yield stress of 30.5 ksi, an ultimate stress of 48 ksi, an ultimate elongation greater than 30%, and an approximate elastic modulus of 29,000 ksi. A

representative stress versus strain relationship for the 1018 carbon steel plates is presented in Figure 67.

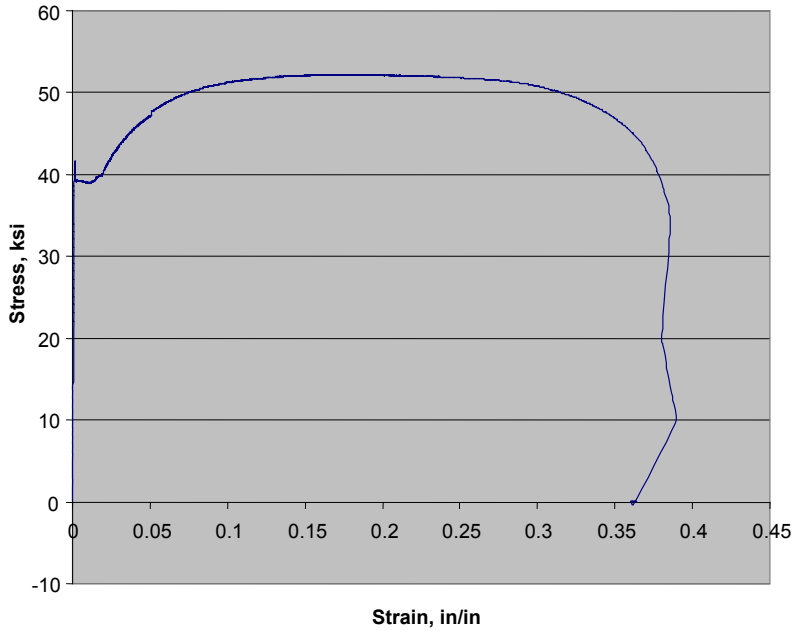

Figure 66. Typical stress vs. strain relationship for A36 steel used in fuse plates.

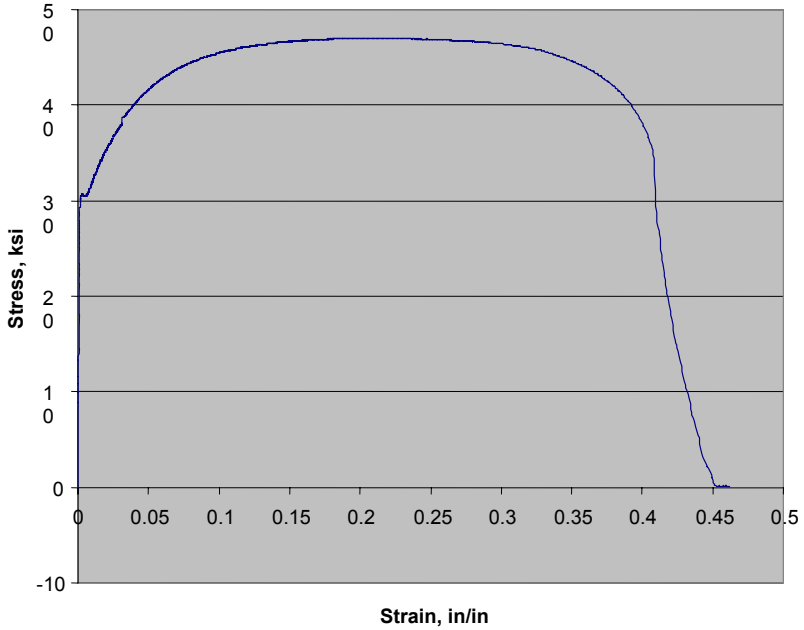

Figure 67. Typical stress vs. strain for 1018 carbon steel used in fuse plates.

5.2.3 Nickel-Titanium Shape Memory Alloy (SMA)

SMAs have the unusual property of shape recovery even when loaded beyond their linear stress-strain region. That is, they appear to yield under direct tension in a manner similar to steel but return to nearly their original length upon unloading. Shape memory alloy was used for the fuse plates of Column 6. The SMA strips exhibited a yield stress similar to commercial grade steel but with less strain capacity.

Although more expensive than conventional steel, the SMA plates had the advantages of helping to self-center the column and being less likely to require replacement following a severe loading event. Three SMA strips tested in direct tension exhibited a yield stress of 50 ksi, an ultimate stress greater than 100 ksi, and an elastic modulus of approximately 9,000 ksi. An average of 14.84% was measured for the ultimate elongation of the SMA plates. The stress versus strain relationship for the SMA plates is presented in Figure 68.

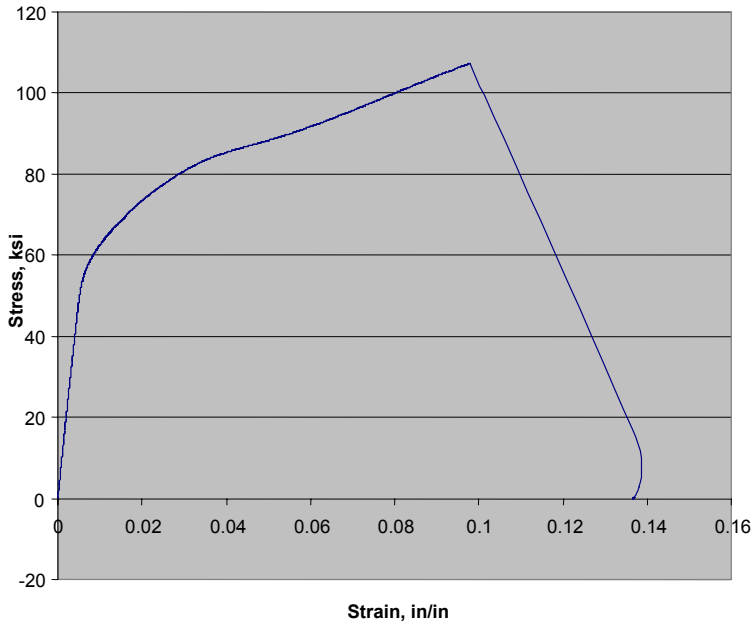

Figure 68. Typical stress vs. strain for SMA used in fuse plates.

As shown by Figures 66-68, the properties of the three tested materials varied significantly. The yield stress of the A36 steel was tested to be 6-7 ksi higher than the 1018 carbon steel, while the yield stress of the SMA was higher than both but not well defined. Ultimate elongations in the 1018 carbon steel and the A36 steel were found to be above 30%, which

will allow the pier system to sustain large displacements by permitting more rotation at each segment joint before plate fracture. The ultimate elongation of the SMA was found to be only 10%, but its high ultimate strength (~105-110 ksi) will resist larger loads before fuse plate fracture occurs. This gain in strength of the construction joint will cause the column segments to take additional rotation and subsequent damage caused by larger displacements.

5.3 Concrete

Column segments and foundations were cast in four concrete placements over the duration of the research. Each foundation used for Columns 1 and 2, as well as the 2-foot column segment for Column 2, was completed during the first casting. The second casting included the control column (Column 1) and the 12-foot segment for Column 2. Completed in the third casting were all elements for Columns 3 and 4, while each element for Columns 5 and 6 was completed during the fourth casting.

Concrete cylinders that complied with ASTM C 192 Standard Practice for Making and Curing Concrete Test Specimens in the Laboratory were made during all concrete castings. However, two cylinders were tested at 3, 7, 14, and 28 days of age for each of the castings inadvertently instead of three cylinders. The cylinder testing followed ASTM C 39 Standard Test Method for Compressive Strength of Cylindrical Concrete Specimens. Concrete used in all columns was a normal weight mix with maximum 3/8 in. aggregate to address congestion in the small-scale specimens. The specified strength was 5 ksi, and 28-day breaks from 6 in. diameter by 12 in. long cylinders ranged from 5 to 6 ksi as shown in Figure 69. Two cylinders, whose strengths are shown in Table 3, were also tested on the day of each column test.

Table 3. Test-day concrete cylinder strengths.

Test Column #	Cylinder 1, psi	Cylinder 2, psi	Average, psi
Column 1	5340	7220	6280
Column 2	6320	6610	6490
Column 3	5830	5690	5760
Column 4	5900	5900	5900
Column 5	6040	6080	6060
Column 6	5670	6200	6200

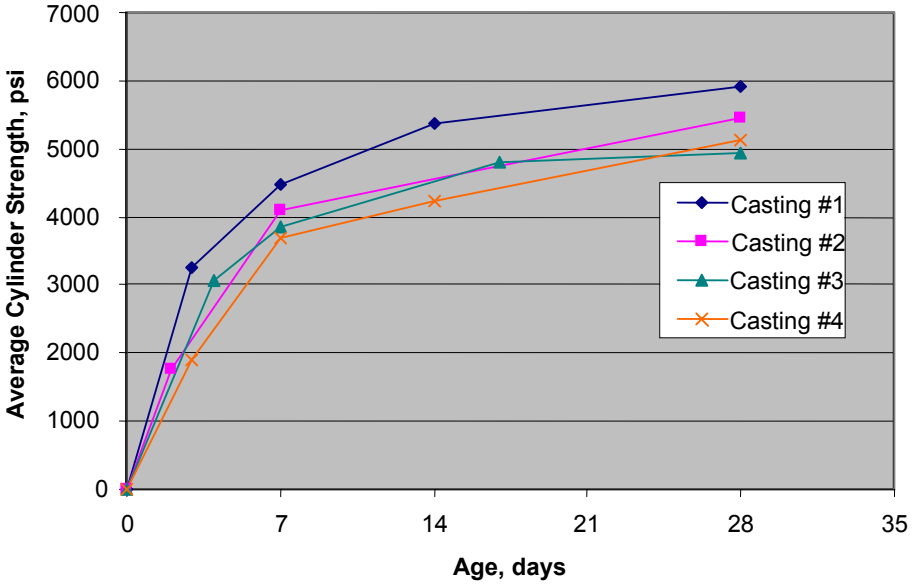

Figure 69. Concrete strength gain.

6. QUALITATIVE TEST RESULTS AND DESCRIPTION OF DAMAGE

Qualitative descriptions of failure sequences for each column are presented in this chapter, accompanied by numerous photographs showing these qualitative results. Quantitative measurements from the various tests are presented in Chapter 7. Results of the various material tests (e.g., compressive strength of concrete, tensile strength of fuse plate materials, etc.) were presented in Chapter 5.

6.1 Loading Conditions and Terminology

The load applied by the actuator, which was oriented in the east/west direction, is shown in Figure 70. During each positive (push) half-cycle, the actuator displaced the column to the west, while during each negative (pull) half-cycle, the actuator displaced the column to the east. As discussed in Chapter 1, 44 kips of dead load was applied to each column. This load consisted of the dead weights, load beam, and column, which was included in the dead load because most of the instrumentation was located at the base of the column. Furthermore, while no post-tensioning was applied to Column 1, 44 kips of post-tensioning was applied to Column 2, and 66 kips of post-tensioning was applied to Columns 3-6.

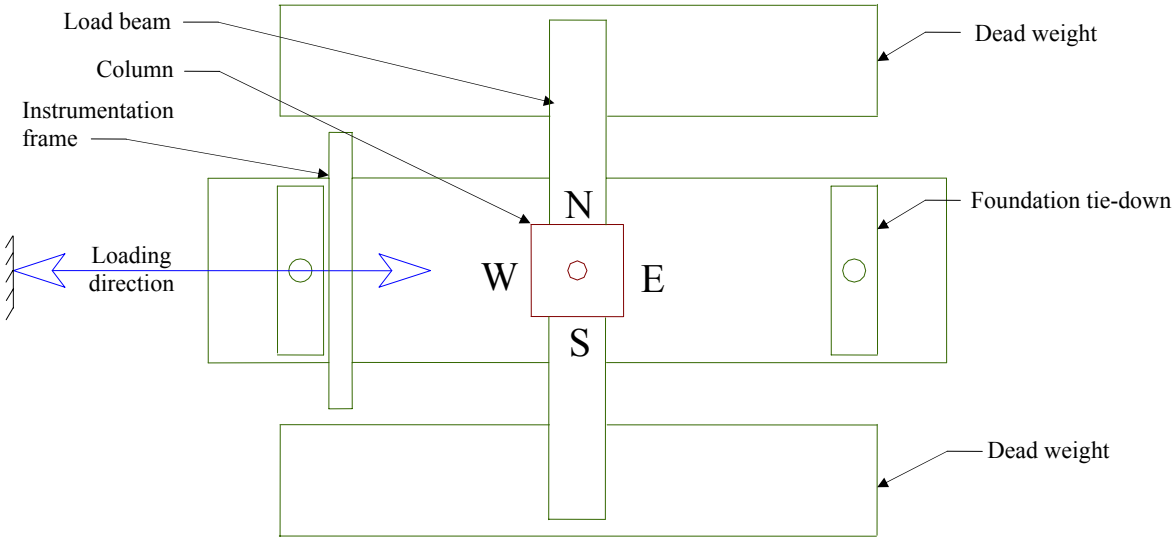

Figure 70. Top view of test setup showing column orientation in test frame.

Also note the terminology used in the following test descriptions relative to the condition of the segmented columns: “a” indicates a displacement cycle prior to replacement of fuse

plates while “b” indicates a displacement cycle after replacement of the original fuse plates. Thus, the test regimen for a segmented column would have both a Cycle 10a and 10b, since the test procedure was repeated after the original fuse plates were replaced.

6.2 Column 1 Results

Testing of Column 1 commenced and continued to a +/- 9.0 in. lateral displacement. No post-tensioning was applied to this column to replicate the behavior of a conventional, cast-in-place column. Incremental damage accrued over the imposed displacement regimen is presented in Figures 71-84. Cracking across the east and west column faces was first observed on Cycle 7 (displacement = +/- 0.40 in.). On the positive (push) half-cycle, cracking was observed 3 in. above the base on the east face; on the negative (pull) half-cycle, three full cracks across the column face were noted 3 in., 16 in., and 24 in. above the base on the west face. These initial cracks are shown during Cycles 8 and 11 in Figures 71 and 72, respectively.

Cracks continued to expand and develop further up the column as cycles continued and lateral loads increased (see Figures 73 and 74). From Cycles 20 to 22, several areas on the compression face of the column began to exhibit localized compression damage and are denoted by hatched areas drawn on the column faces (see Figures 75 and 76). Major compression damage that localized in the southwest corner of the column was observed on Cycle 20 (displacement = +/- 5.0 in.) (see Figures 77a and 78). As the previously observed damage increased on subsequent cycles, the column began to tilt to the south, perpendicular to the axis of loading. On Cycle 21 (displacement = +/- 5.0 in.), Column 1 attained its maximum lateral load of + 9.7 kips.

Additional cycles produced more spalling of concrete, most notably on the southwest corner of the column near the base (see Figures 79-81), a reduction in lateral load, and further tilting of the column to the south (see Figure 82). It was observed during Cycle 25 that the load beam was in contact with the testing frame (see Figure 82a). On Cycle 27 (displacement = +/- 9.0 in.), the damage was severe enough that the longitudinal reinforcement in the column was visible and exhibited clear signs of buckling (see Figures 82-84). Furthermore, the lateral load applied to the column had fallen off sharply, and the column was in danger of becoming

unstable. Therefore, testing was stopped after Cycle 27. Quantitative lateral load versus displacement data are presented in Chapter 7.

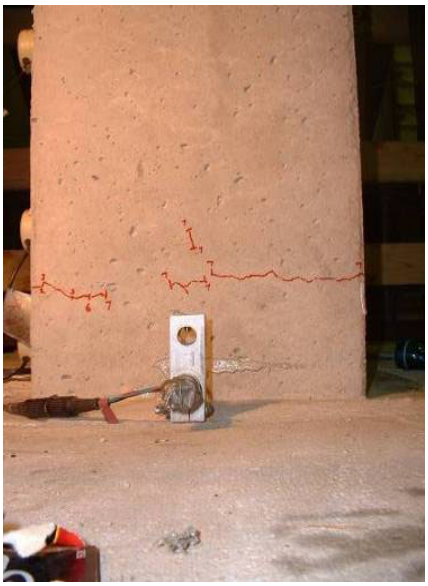

a.) East face initial cracking

b.) West face initial cracking

Figure 71. Photographs of Column 1 - Cycle 8.

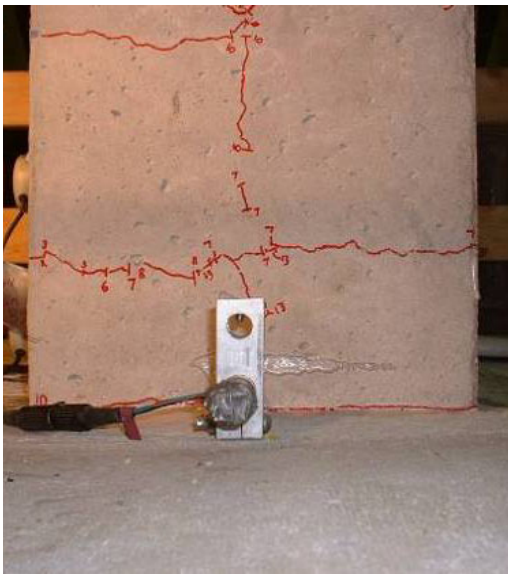

a.) East face

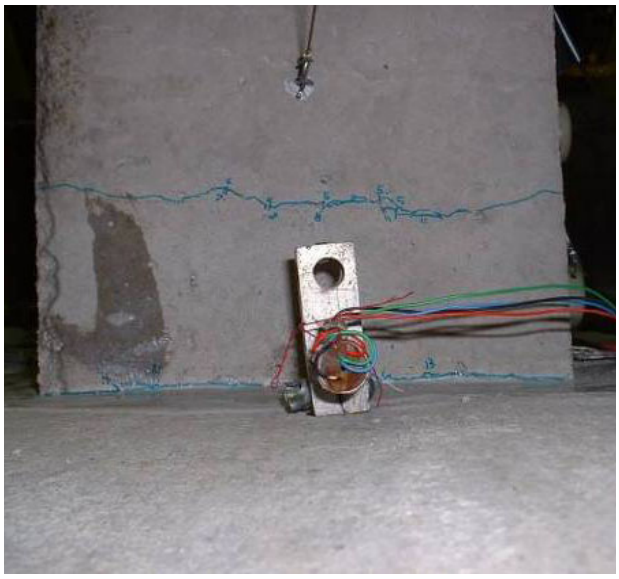

b.) West face

Figure 72. Photographs of Column 1 - Cycle 11 base cracking.

a.) Southwest corner view of progressive cracking b.) Progressive cracking on the east face

Figure 73. Photographs of Column 1 - Cycle 11 progressive cracking.

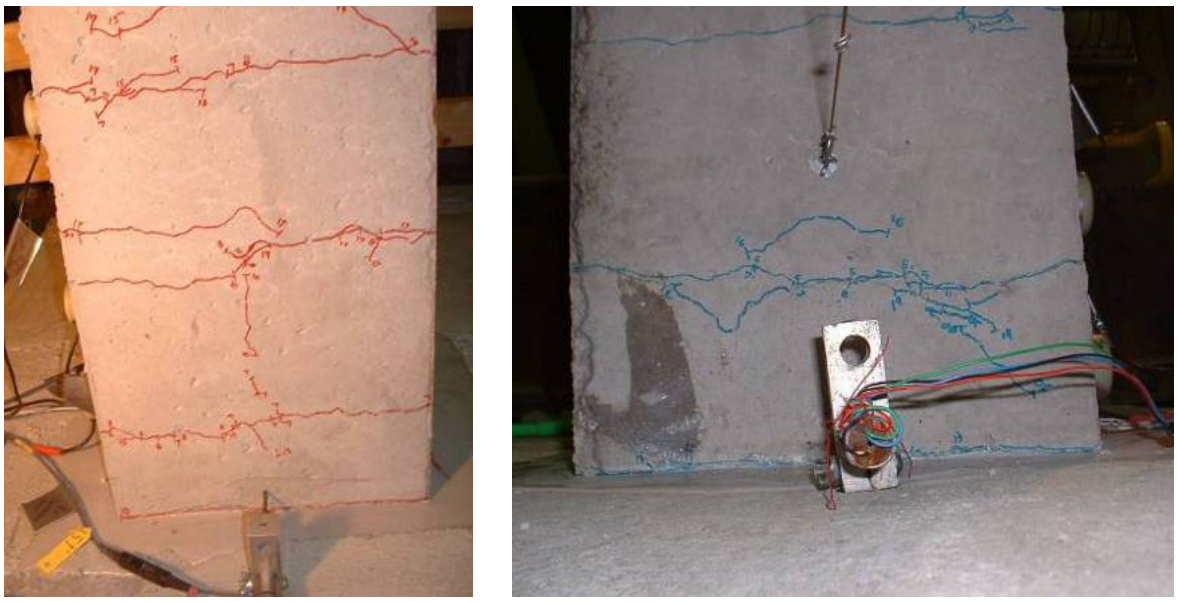

a.) East face cracking b.) West face cracking

Figure 74. Photographs of Column 1 - Cycle 14.

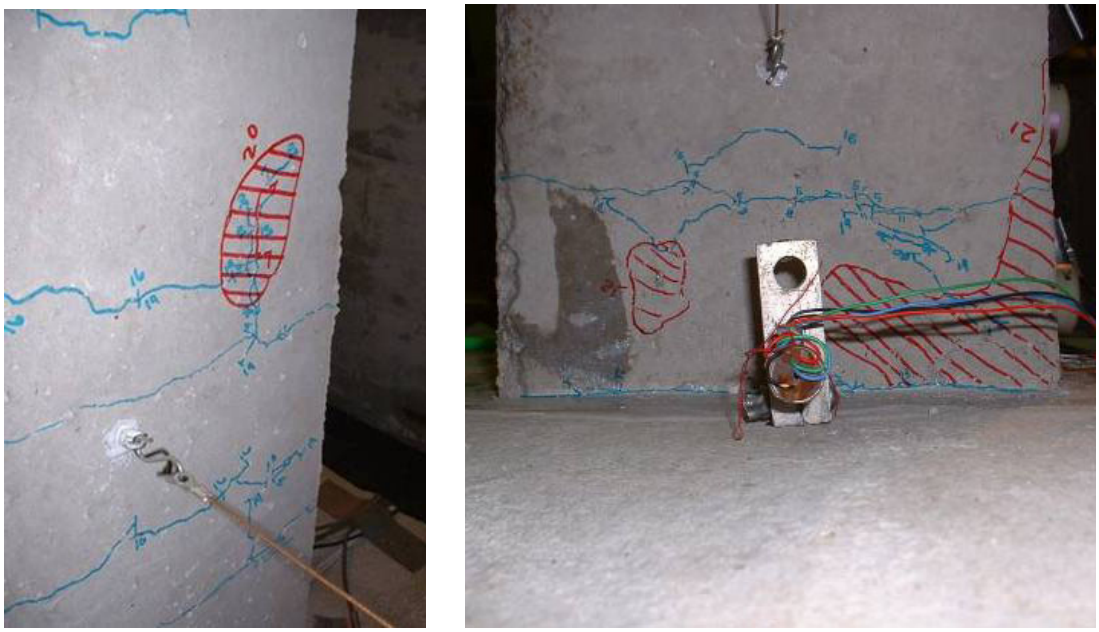

a.) West face initial compression damage b.) Localization of compression damage on southwest corner

Figure 75. Photographs of Column 1 - Cycle 20.

a.) Southwest corner compression damage b.) East face initial compression damage

Figure 76. Photographs of Column 1 - Cycle 22.

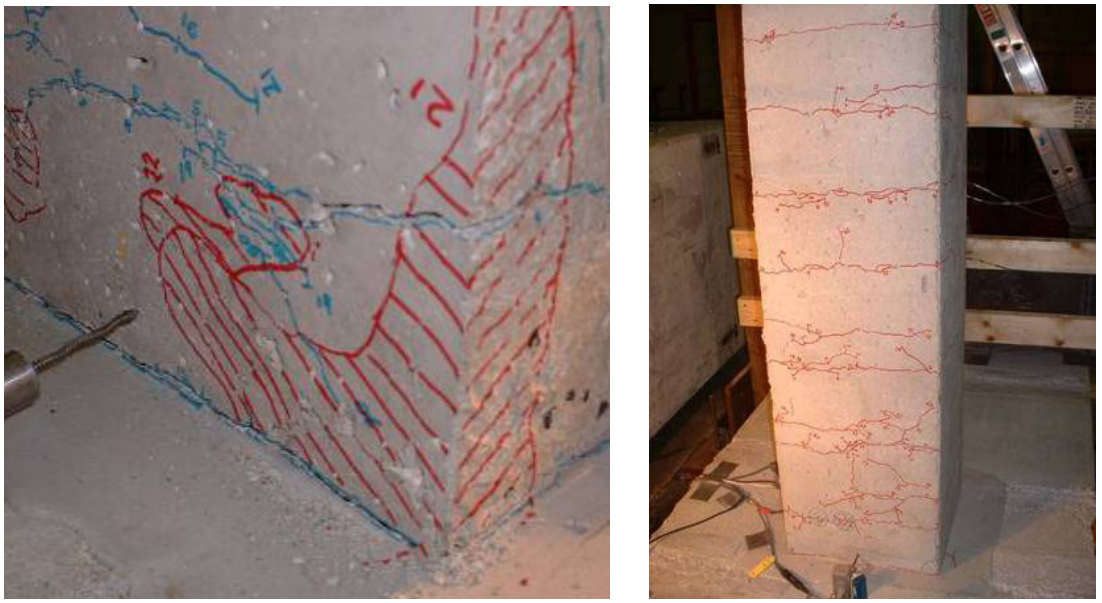

a.) Southwest corner compression damage **b.) East face crack progression**

Figure 77. Photographs of Column 1 - Cycle 23.

Figure 78. Photograph of Column 1 – Cycle 24 damage to southwest corner

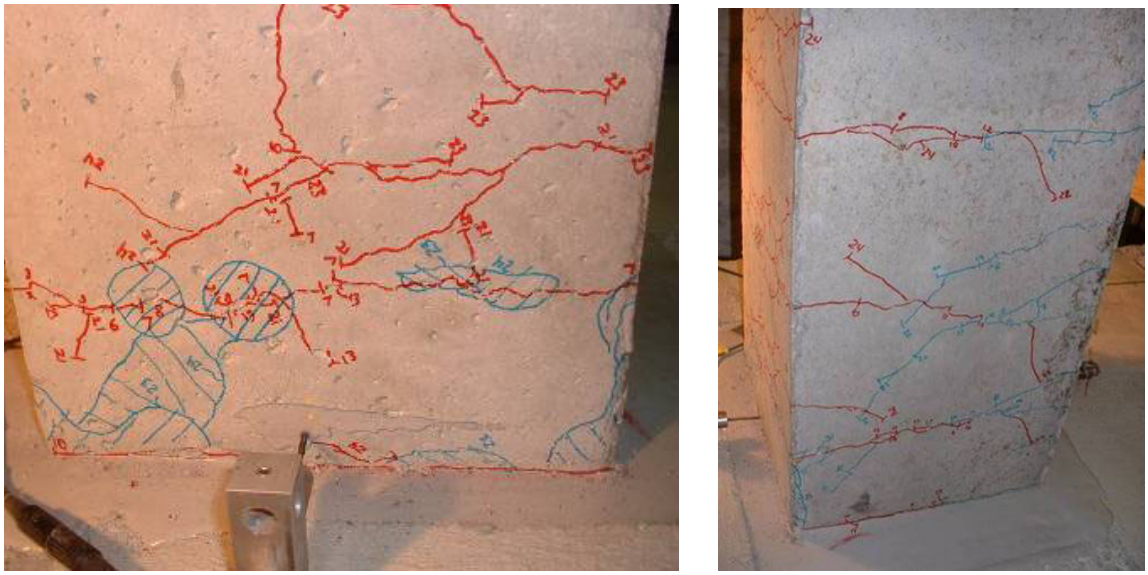

a.) East face damage b.) North face crack progression

Figure 79. Photographs of Column 1 - Cycle 24.

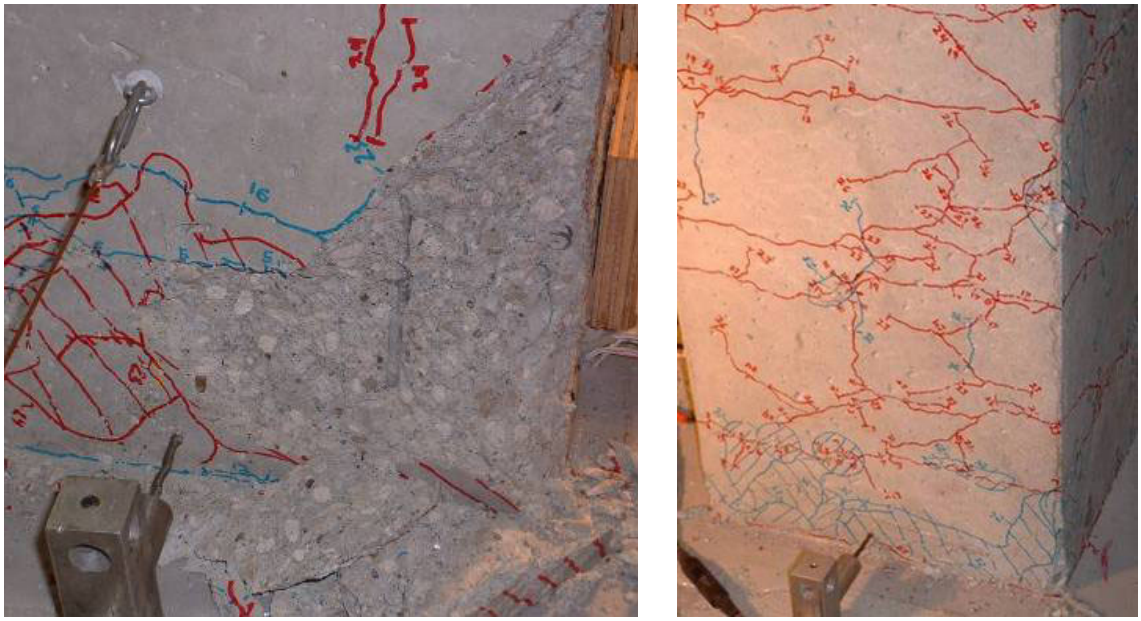

a.) Southwest corner damage b.) East face damage

Figure 80. Photographs of Column 1 - Cycle 25.

a.) Severe spalling of southwest corner

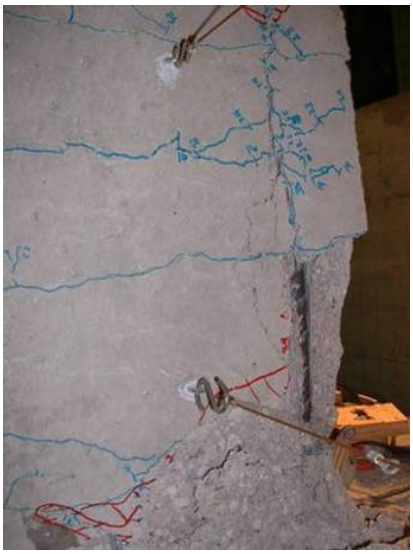

b.) Visible southwest corner reinforcement

c.) North face cracking/spalling

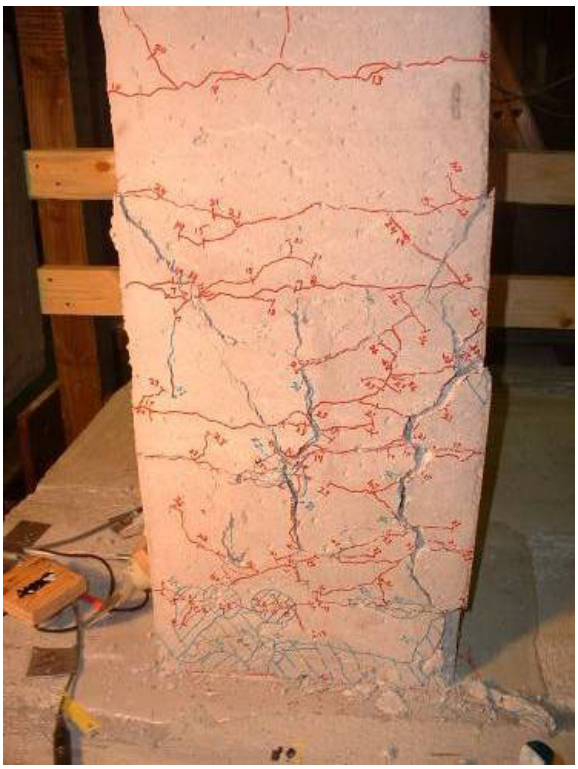

d.) East face bulging due to buckled reinforcement

Figure 81. Photographs of Column 1 - Cycle 26.

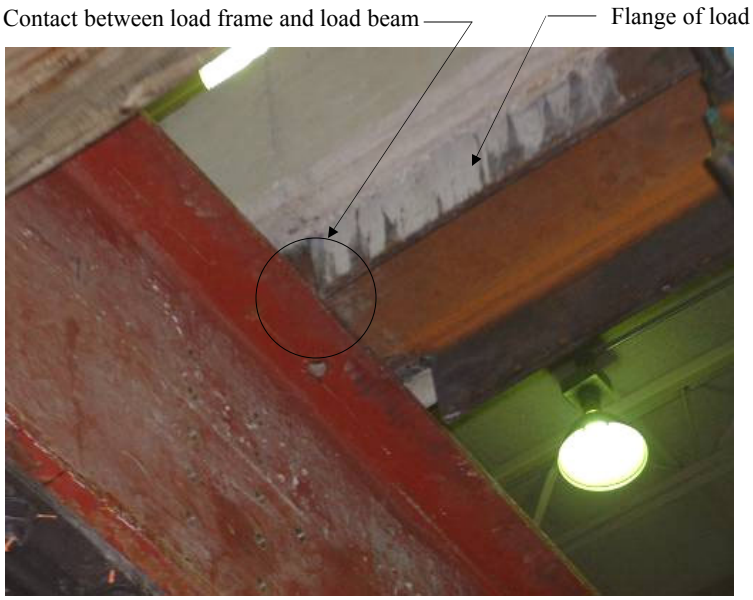

a.) Frame impingement with underside of load beam

b.) East face reinforcement exposed

c.) North face cracking/bulging

d.) West face damage

Figure 82. Photographs of Column 1 - Cycle 27 damage/frame impingement.

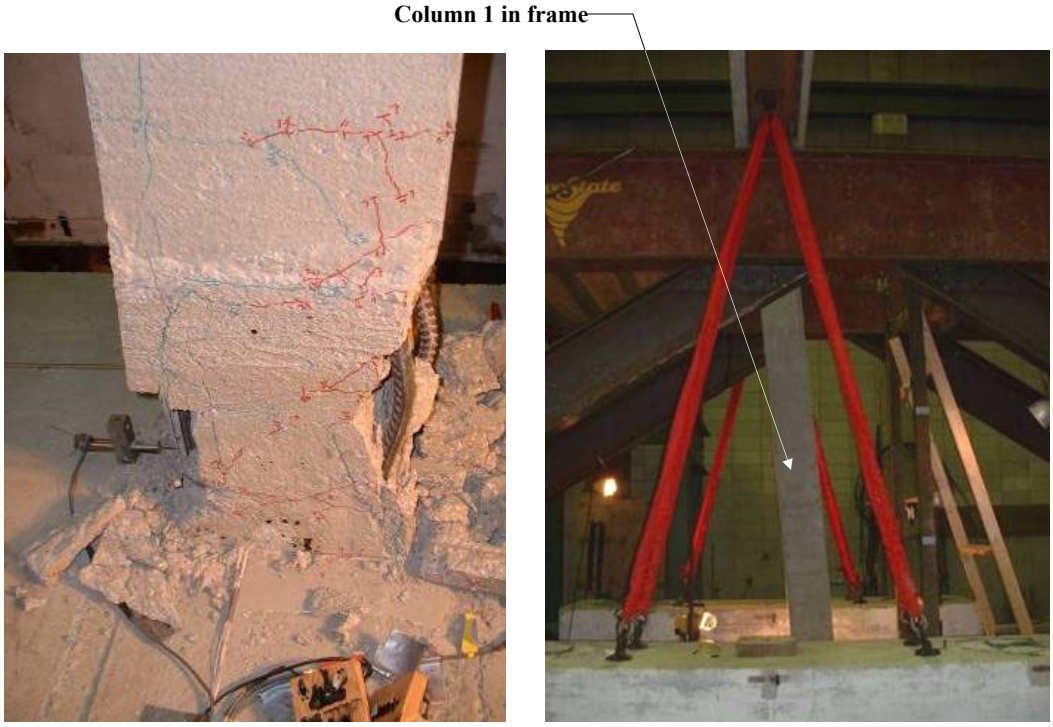

a.) South view of damage

b.) Column deformation on pull half-cycle

Figure 83. Photographs of Column 1 - Cycle 27 damage and deformation.

c.) Final damage to east face

d.) Final damage to south face

Figure 84. Photographs of Column 1 – After testing

Behavior of the control column closely matched that expected of a conventional, cast-in-place column in the field with the exception of the localized failure at the southwest corner (see Chapter 7 for quantitative comparisons). Cracking initially occurred near the base of the column and spread upward as lateral loads and deflections increased. Peak loads occurred near the time that yielding of the bonded reinforcement occurred and was followed by a period of increasing lateral displacements at or near the peak load. This continued until rotational capacity near the base of the column was reached and ultimate failure, marked by buckling of longitudinal bars and crushing of core concrete, occurred.

6.2.1 Frame Impingement

During the last three positive (push) half-cycles of + 7.0 in., + 8.0 in., and + 9.0 in. displacements, the load beam impinged on the load frame when displacements exceeded + 7.0 in. This impingement and the associated tilting to the south occurred only on the positive portions of the loading cycles. This caused spuriously high lateral load readings on these half-cycles. Testing was continued beyond the + 7.0 in. displacement, because the problem did not occur on the negative (pull) half-cycles. Thus, testing was continued until failure occurred on the negative half of Cycle 27. Due to this occurrence, only the data collected for negative half-cycles for the three largest displacement cycles were considered reliable and indicative of typical column behavior.

6.3 Column 2 Results

Testing of Column 2 commenced and continued to a +/- 6 in. displacement. The incremental damage accrued over the imposed displacement regimen is illustrated in Figures 85-92. Cracking across the entire column was first observed on Cycle 10a (displacement = +/- 0.75 in.) (see Figure 85). On the positive (push) half-cycle, cracking occurred 2 in. above the base of the column on the east face; on the negative (pull) half-cycle, cracking occurred at the base of the west face of the column. Also during Cycle 10a, "pinging" in the fuse plate on the tension side of the column was heard, indicating slippage in the slip-critical connection between the fuse plate and the steel collar. "Pinging" was heard on each consecutive cycle in the tension fuse plates throughout the remainder of Test a. During Cycles 11a to 16a, small

cracks formed every 8 in. to 12 in. across the column for several feet above the construction joint (see Figures 86 and 88). The fuse plate in compression began to buckle on Cycle 13a (displacement = +/- 1.5 in.) and is shown buckling during Cycle 14a in Figure 87b. During Cycle 15a, the crack that formed between the upper column collar and the concrete grew noticeably (see Figure 88). Since Cycle 16a was the predetermined cycle to replace fuse plates, testing was stopped and new plates were mounted on the column. At this juncture, a peak load of + 6.39 kips had been applied to the column.

Following replacement of the fuse plates, testing was restarted and continued without additional cracking until Cycle 11b (displacement = +/- 1.0 in.), when several cracks were found at the base of the column. Slippage of the fuse plates was again noted during Cycle 12b (displacement = +/- 1.0 in.). During Cycle 15b (displacement = +/- 2.5 in.), the segment joint began to open significantly. Reverse curvature in the fuse plates at the top and bottom edges (see Figure 89) was also noted on the negative (pull) half of Cycle 15b indicating bolt bearing at the slip critical connection.

During Cycle 18b, loss of control of the actuator occurred at + 0.4 in. displacement, shaking the column. This was the first occurrence of a problem with actuator control that would hinder testing throughout the remainder of the project. This loss of actuator control was caused by a malfunctioning servo valve that persisted despite reconditioning of the valve by the manufacturer. Further explanation of the actuator control problem is discussed in Section 6.3.1.

Compression damage above the top collar was noted on Cycle 19b (displacement = +/- 3.5 in.) on the northwest and northeast corners of the column. On Cycle 20b (displacement = +/- 4.0 in.), the actuator control problem occurred at + 1.5 in. displacement on the positive (push) half cycle. An increase in gap width at the upper segment's collar interface, as well as a fractured weld on the upper steel collar (see Figure 91), was also noted on Cycle 20b. On the remaining cycles, the crack at the failed weld in the collar continued to widen. On Cycle 22b (displacement = +/- 6.0 in.), the crack between the upper collar and column segment began to open significantly, clearly causing rotation that was designed to occur at the segment joint. This indicated that the upper collar and through-bolts were pulling off the upper column segment, causing irreparable damage to the segment. This phenomenon is shown during

Cycle 23b in Figure 92b. Also during Cycle 22b, a crack was observed on the northwest corner of the bearing plate. The test was stopped after Cycle 23b due to the opening of the crack between the collar and column; it was evident that the decrease in load at each displacement was due to this phenomenon. A maximum load of + 6.64 kips was observed during Column 2's test on Cycle 14a (displacement = +/- 2.0 in.), while a maximum displacement of 6.0 in. was recorded for the test. At + 6.0 in., a load of + 4.48 kips was achieved, while a - 3.27 kip load was achieved at - 6.0 in. Quantitative lateral load versus displacement is shown in Chapter 7.

6.3.1 Actuator Control Problem

As previously described, the control problem with the actuator occurred several times during testing of Columns 2–6, delaying the tests. While moving to a specified displacement, the malfunctioning valve in the actuator would periodically get stuck. In an attempt to reach the displacements called for by the controller, the stuck valve would ram back and forth, causing the actuator to cycle quickly and violently. Limited quantifications could be made as to the magnitude of load, displacement, and damage caused by these events since data were collected at one second intervals. However, forces in the range of 12–15 kips were recorded several times.

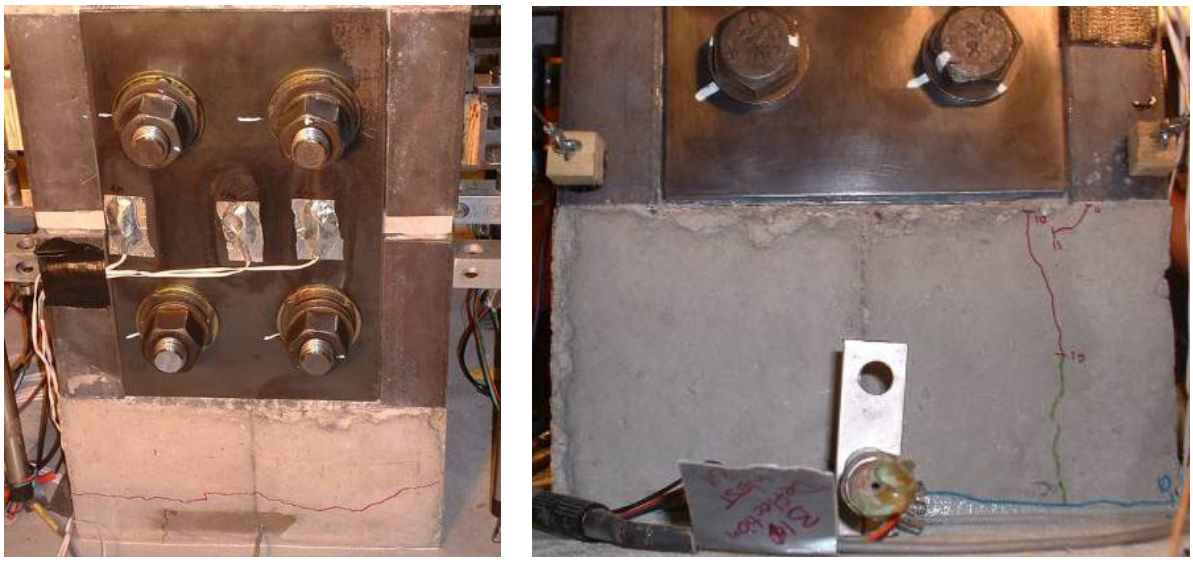

a.) East face **b.) West face**

Figure 85. Photographs of Column 2 – Cycle 11a initial cracking.

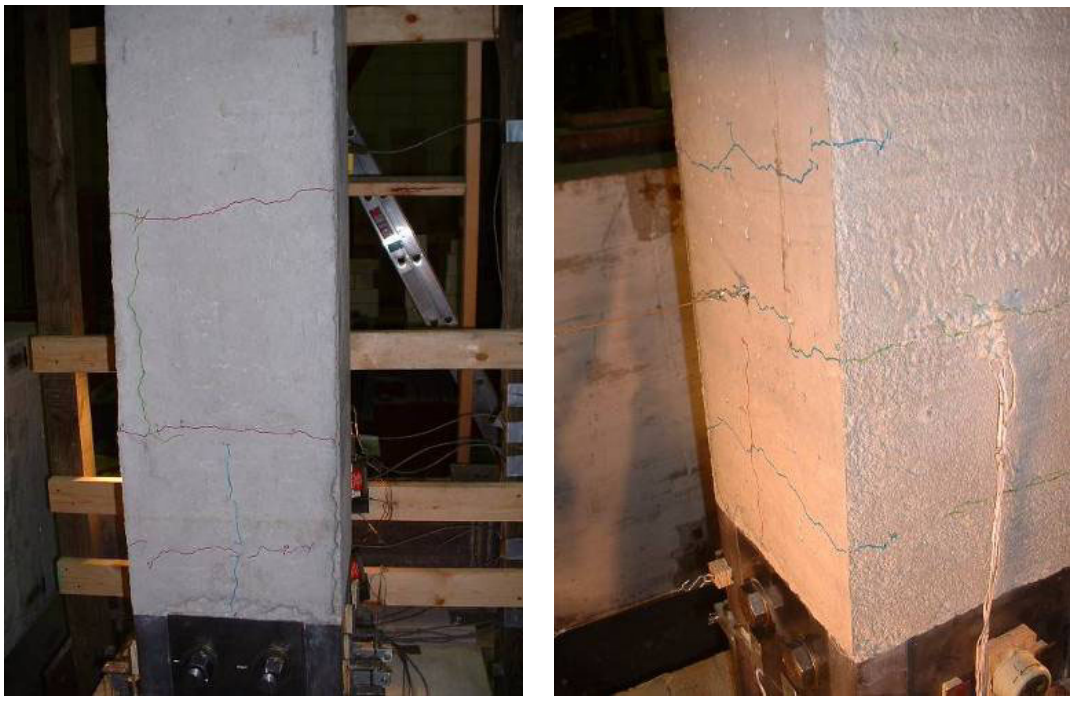

a.) East face crack progression b.) Southwest corner crack progression

Figure 86. Photographs of Column 2 – Cycle 11a upper column crack progression.

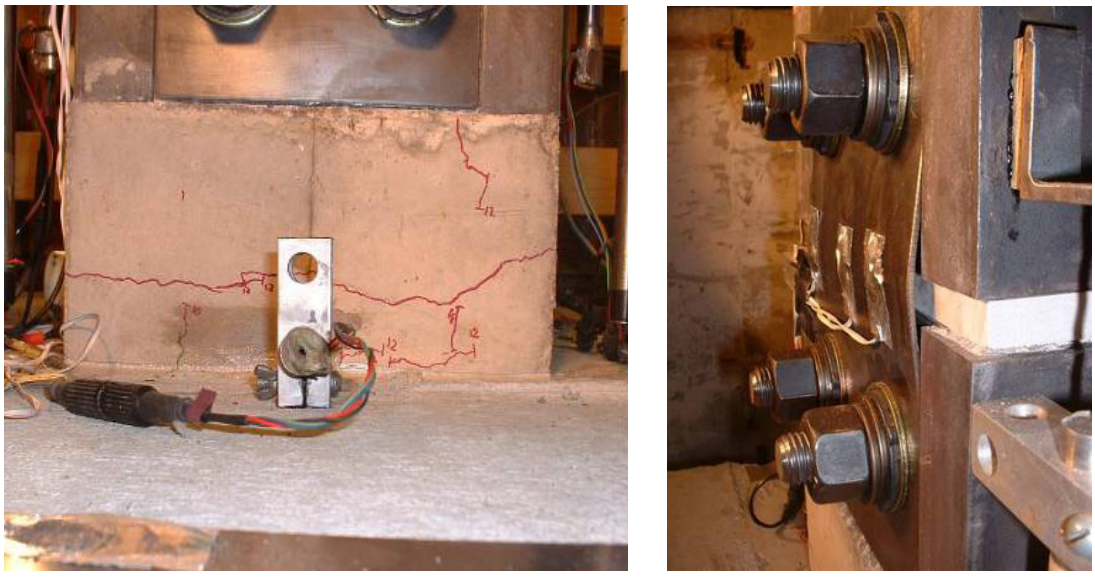

a.) East base cracking b.) Initial buckling of east plate

Figure 87. Photographs of Column 2 – Cycle 14a.

a.) East face

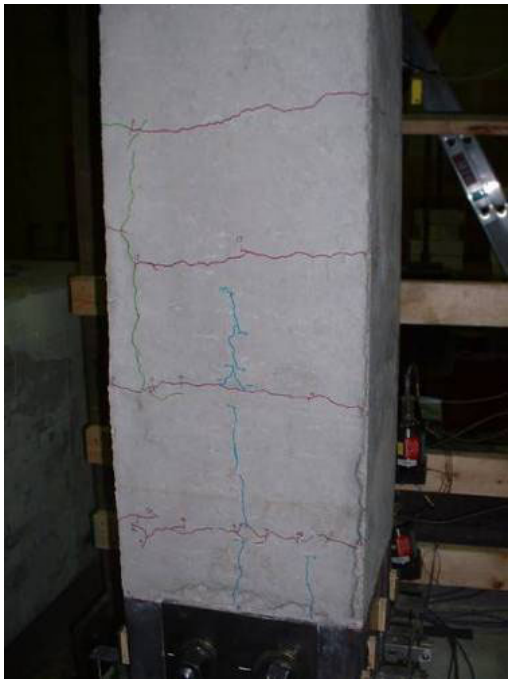

b.) East face crack progression

c.) East face cracking above top collar

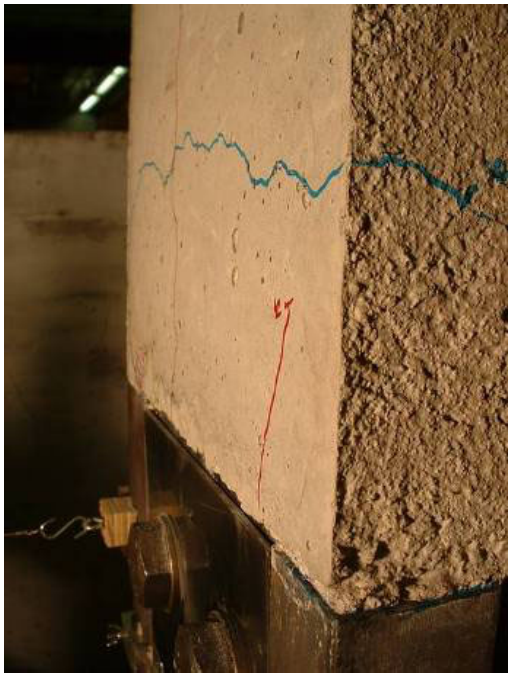

d.) Southwest corner collar/column interface

Figure 88. Photographs of Column 2 – Cycle 15a.

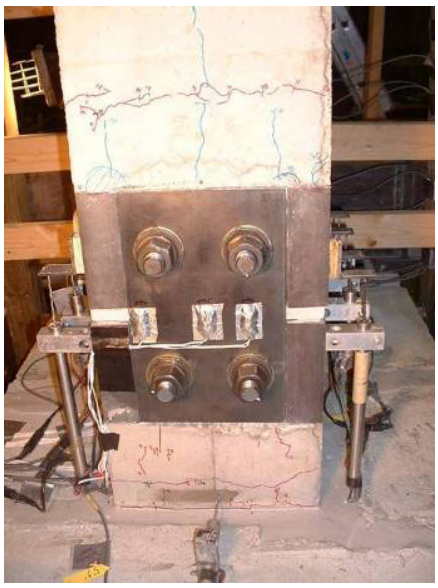

a.) East face

b.) Northeast corner collar/column interface

c.) West collar/column interface

d.) Buckling of replaced west plate

Figure 89. Photographs of Column 2 – Cycle 16b.

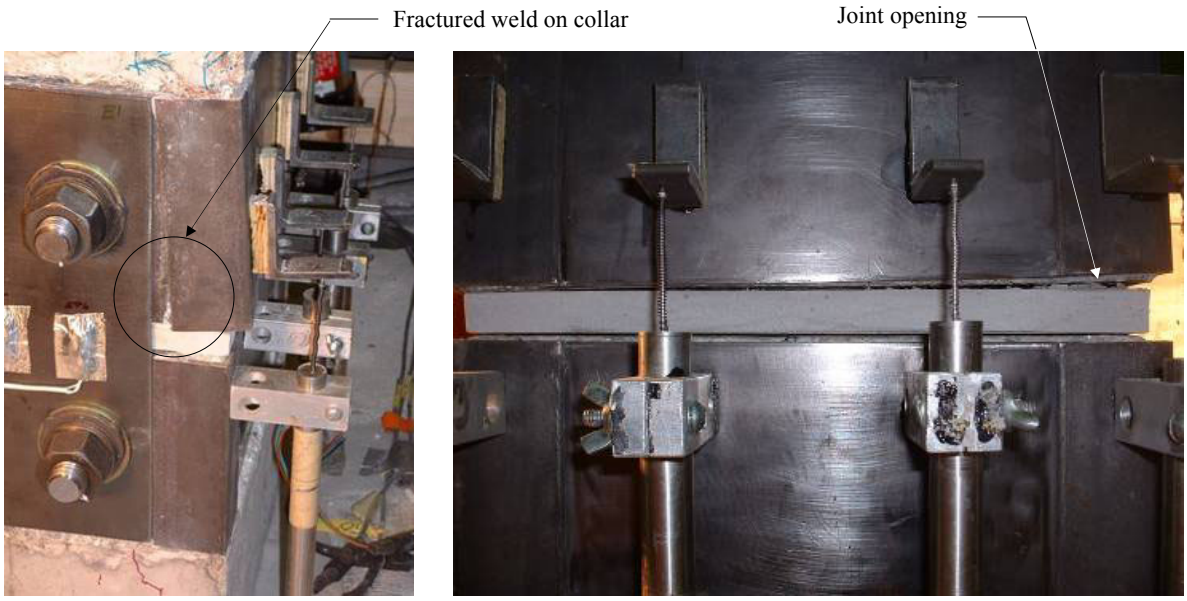

a.) Northeast collar angle fracture **b.) North face collars and construction joint opening**

Figure 90. Photographs of Column 2 – Cycle 21b.

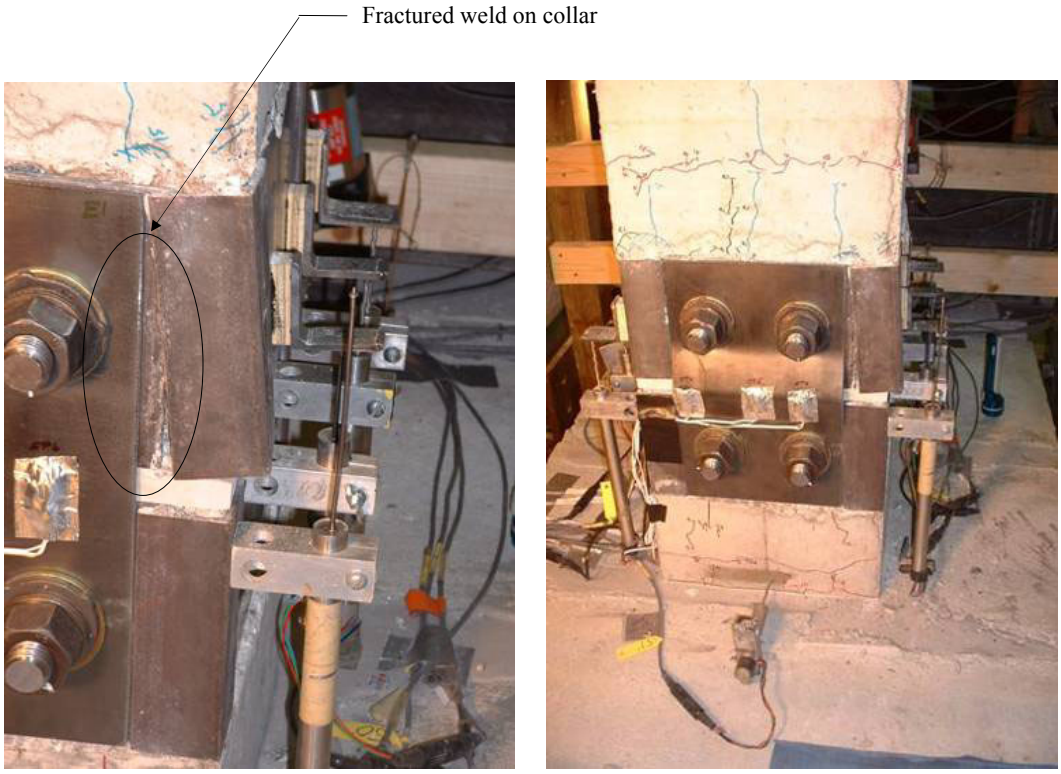

a.) Northeast collar angle fracture **b.) East face final cracking and angle fracture**

Figure 91. Photographs of Column 2 – Cycle 23b east face.

a.) East plate buckling during last cycle

b.) West collar/column interface final crack width

c.) Northwest corner of bearing plate

d.) Column tilt during negative half-cycle

Figure 92. Photographs of Column 2 – Cycle 23b.

Test 2 initially responded as predicted at low loads and displacements. However, detailing problems soon became apparent as the steel collar and through-bolts began to pull off the end of the upper column segment. Since Columns 3 and 4 had already been cast by the time Column 2 was tested, the problems were remedied in Columns 5 and 6 as described in

Chapter 3. The collar pull-off problem led to premature failure of Columns 2–4, so meaningful comparisons of behavior with the control column at large displacements could not be made. The premature failure mode did, however, give valuable insight into important detailing issues at the ends of the precast segments.

6.4 Column 3 Results

Testing of Column 3 commenced and continued until +/- 9.0 in. displacements were reached. The incremental damage accrued over the imposed displacement regimen is illustrated in Figures 93-105. Cracking across the entire column was observed on Cycle 10a (displacement = +/- .75 in.) (see Figures 94 and 95). On the positive (push) half-cycle, cracking occurred at the base of the column on the east face, as well as 1 ft. above the top collar; on the negative (pull) half-cycle, cracking occurred 1 in. above the base on the west face of the column. During the next several cycles, small cracks formed every 6 in. to 10 in. up the column face for several feet above the construction joint (see Figures 97a and 97b).

On Cycle 13a, a loss of control of the actuator occurred at a - 0.59 in. displacement. Also, on Cycle 13a, minor compression damage was observed around the collar. Buckling could be seen in the compression fuse plates, and a small amount of compression damage was noted in the bearing plate on the west side on Cycle 14a (displacement = +/- 2 in.) (see Figure 98). Loss of control of the actuator also occurred on Cycle 16a at + 0.47 in. By Cycle 16a, the fuse plates had buckled to a large degree when under compression indicating that they had yielded in tension on previous cycles. This was also the predetermined cycle to replace fuse plates, so testing was stopped and new fuse plates were mounted on the column. At this juncture, a peak horizontal load of +/- 6.30 kips had been applied to the column.

After replacing the fuse plates (see Figure 98), the displacement regimen was restarted. "Ticking" was heard in the east plate on Cycle 15b indicating slippage between the fuse plate and the collar. On Cycle 16b (displacement = +/- 2.5 in.), the crack opening was noted between the top collar and the column segment (see Figure 99). Actuator problems occurred again on Cycle 17b (displacement = +/- 3.0 in.) at - 0.30 in. At this point, the gain control was turned down in an attempt to regain control of the actuator.

During the next several cycles, additional slippage at the fuse plate was observed, and, as during Column 2 testing, the crack between the top collar and column continued to open. This concentrated the rotation at that location instead of at the construction joint. The fuse plate buckling and opening gap at the segment joint can be seen for several cycles in Figures 100-103. Additionally, curling of the top of the west fuse plate can be seen in Figure 104a, providing further evidence of the slippage and bearing of the fuse plates on the collar through-bolts.

The test was stopped on Cycle 27b (displacement = +/- 9.0 in.) due to the opening of the crack between the collar and column and the decrease in applied load. A maximum load of + 6.34 kips was observed during Cycle 16a (displacement = +/- 2.5 in.) of the Column 3 test; a maximum displacement of + 9.0 in. was also observed for the test. At + 9.0 in., a load of + 4.23 kips was achieved, while a - 3.51 kip load was achieved at - 9.0 in. Quantitative lateral load versus displacement for the Column 3 test is given in Chapter 7.

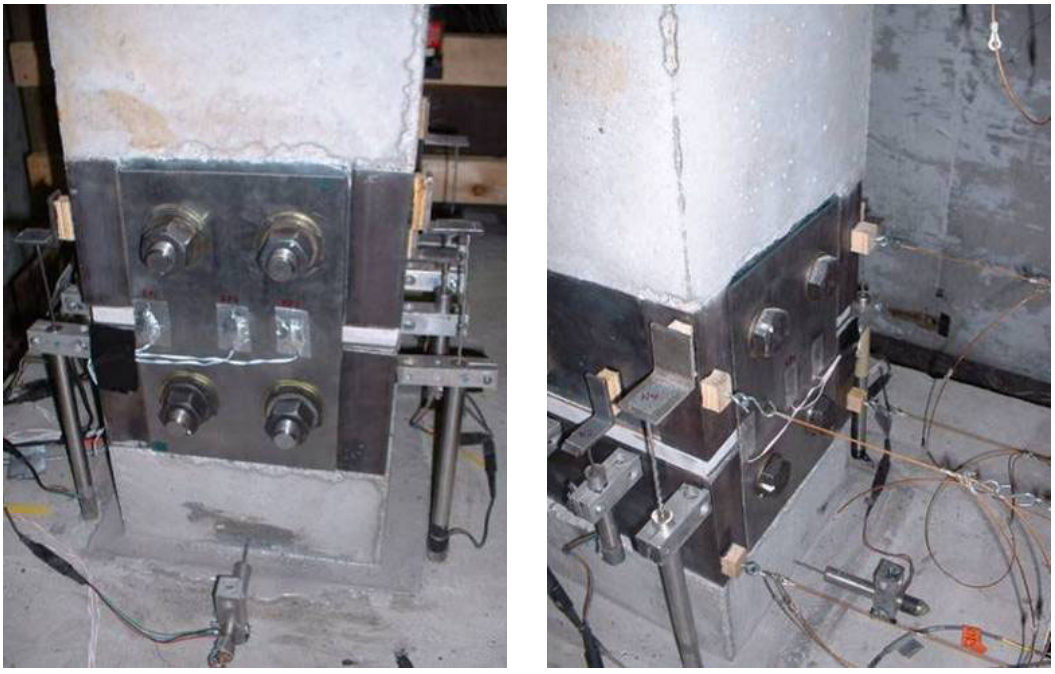

a.) East face **b.) West face**

Figure 93. Photographs of Column 3 – Prior to testing.

a.) East face crack progression

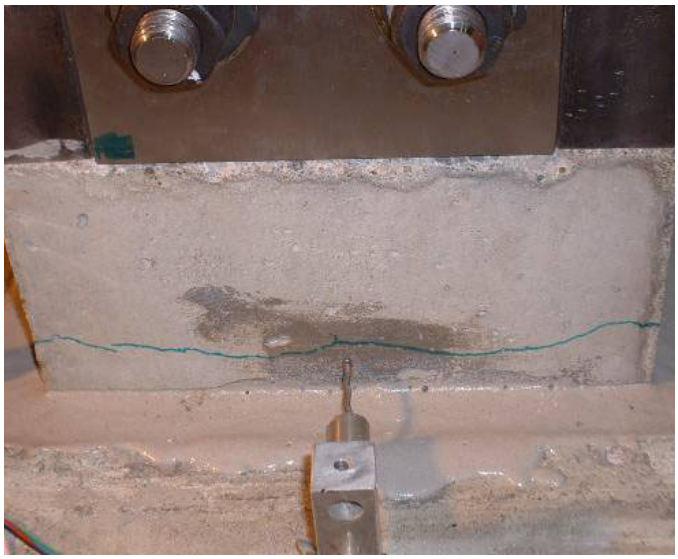

b.) East base initial cracking

Figure 94. Photographs of Column 3 – Cycle 10a east face.

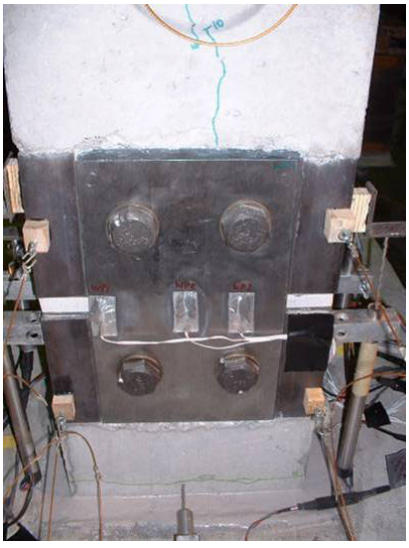

a.) West face crack progression

b.) West base initial cracking

Figure 95. Photographs of Column 3 – Cycle 10a west face.

a.) East plate and column face b.) West plate and column face

Figure 96. Photographs of Column 3 – Cycle 14a fuse plates.

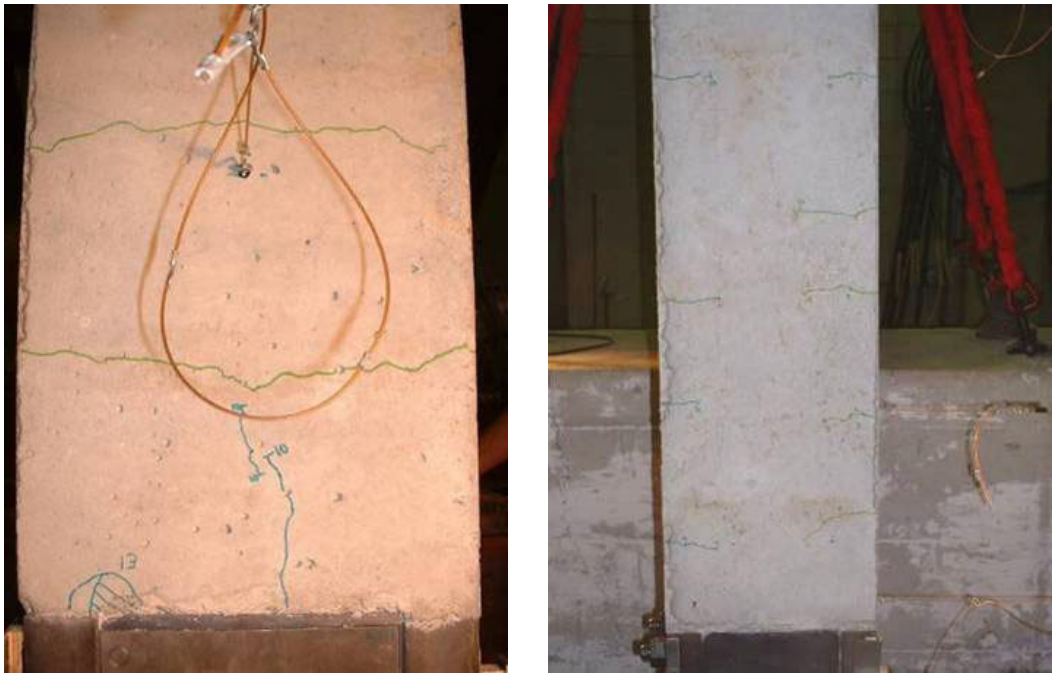

a.) West face cracking above collar b.) North face crack progression

Figure 97. Photographs of Column 3 – Cycle 14a.

a.) East replacement fuse plate **b.) West replacement fuse plate**

Figure 98. Photographs of Column 3 – Replacement fuse plates.

a.) Northeast corner interface opening **b.) Northwest corner interface opening**

Figure 99. Photographs of Column 3 – Cycle 16b.

Figure 100. Photograph of Column 3 – Cycle 18b west face damage.

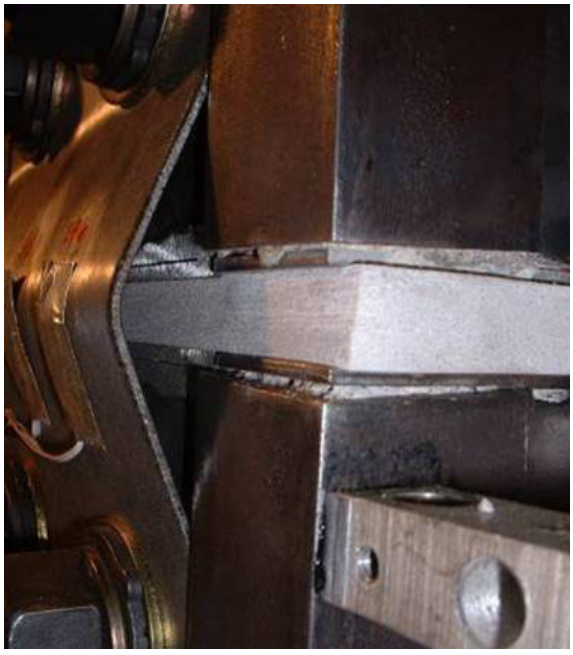

Figure 101. Photograph of Column 3 – Cycle 19b east fuse plate buckling.

Figure 102. Photograph of Column 3 – Cycle 21b joint opening during push half-cycle.

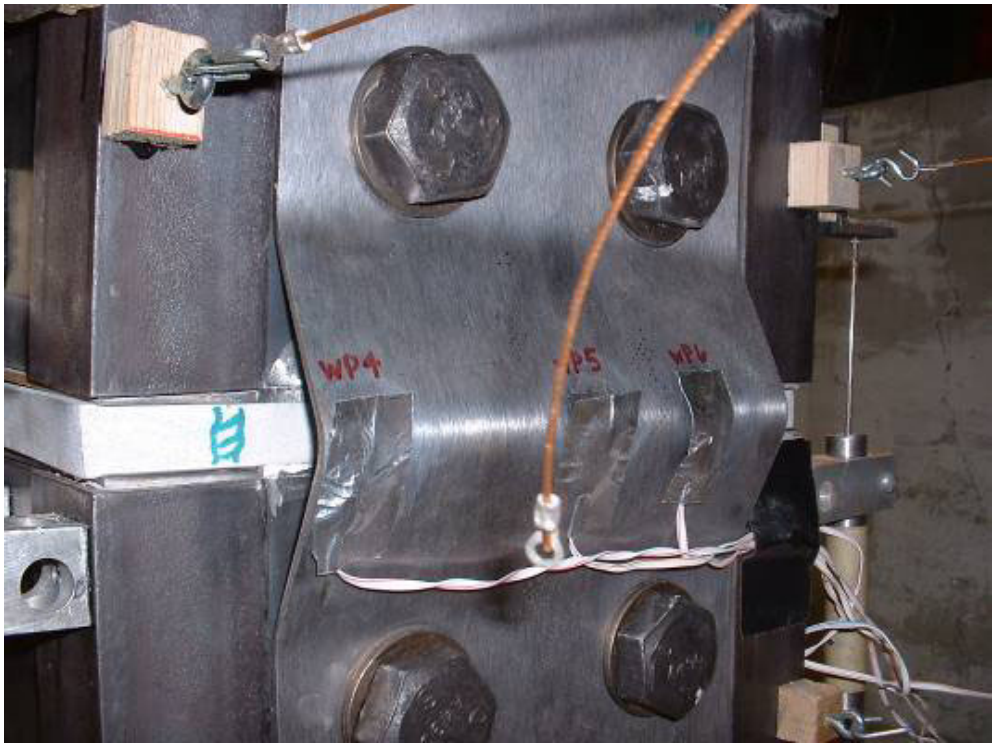

Figure 103. Photograph of Column 3 – Cycle 21b West fuse plate buckling.

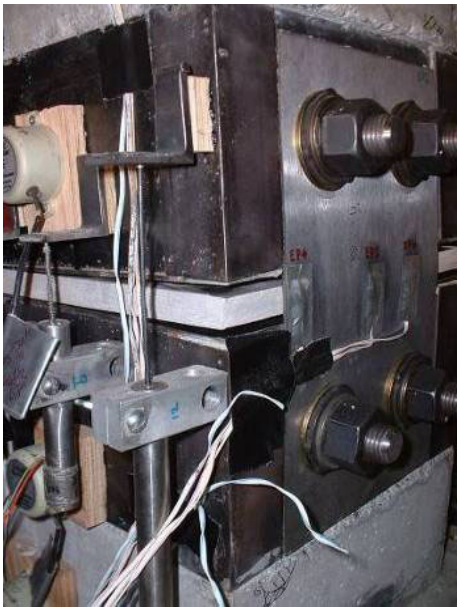

a.) Southeast corner joint opening

b.) Southeast corner interface opening

c.) West bolt bearing causing plate curling

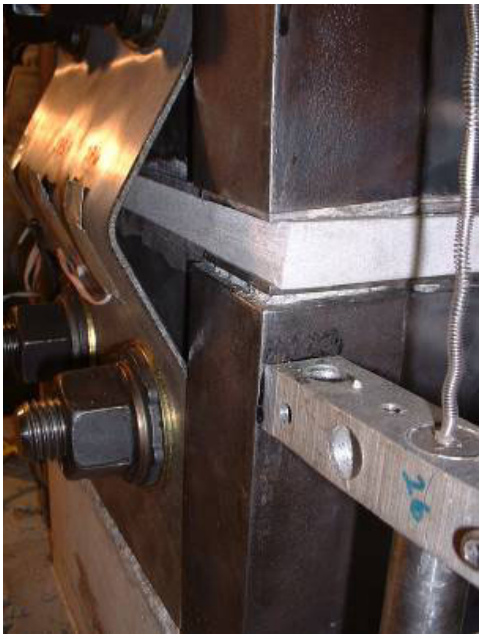

d.) East fuse plate buckling

Figure 104. Photographs of Column 3 – Cycle 21b pull half-cycle.

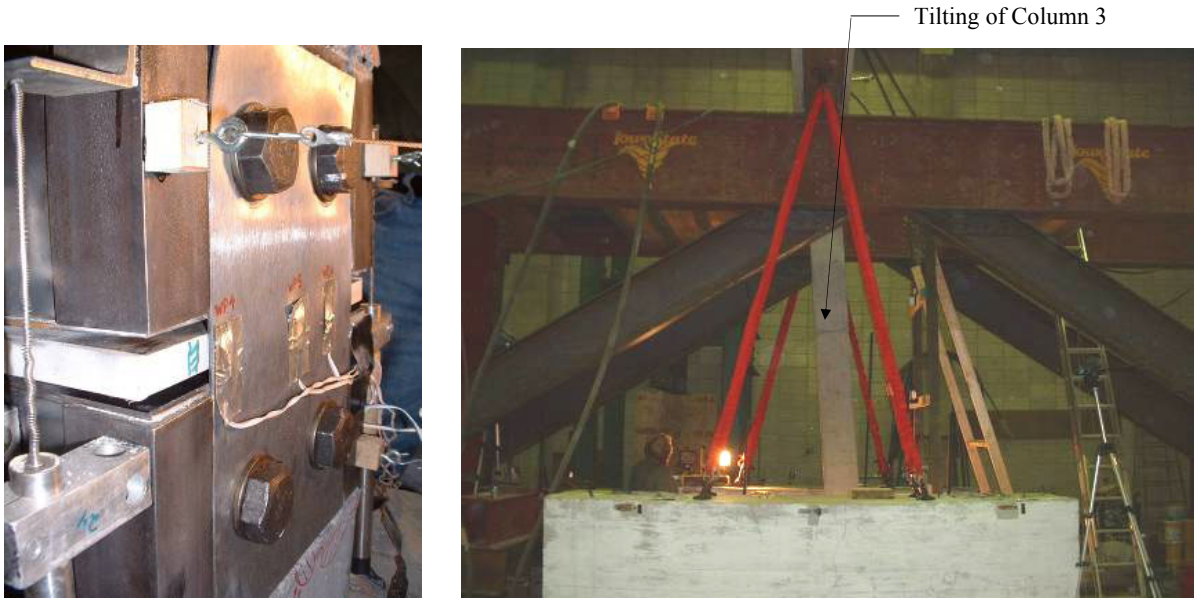

a.) Northeast corner joint opening **b.) Pull half-cycle column deformation**

Figure 105. Photographs of Column 3 – Cycle 22b.

As with Column 2, Column 3 failed prematurely from the same detailing problem discussed previously. Prior to initiation of this mechanism, the column's behavior proceeded as expected. The pull-off mechanism and associated detailing needs were clearly identified and demonstrated in this test.

6.5 Column 4 Results

Testing of Column 4 commenced and continued out to a +/- 6.0 in. displacement. Because Column 4 was cast with the same internal reinforcement details that led to premature failure in the previous two columns, external retrofit angles were attached to the collars in an attempt prevent the same failure mechanism from occurring (see Figure 106). The added reinforcement is described in detail in Chapter 4. The incremental damage accrued over the imposed displacement regimen for the Column 4 test is illustrated in Figures 107-118. The first signs of damage to Column 4 were cracks that formed around the repair angles on Cycle 5a and 6a (displacements = +/- .26 in. and +/- .30 in.). A horizontal crack 3 in. above the top collar was noted on Cycle 7a (displacement = +/- .40 in.) on the east face (see Figure 108). Cycles 10a and 11a (displacements = +/- .75 in. and +/- 1.0 in.) produced more cracking above the top collar, as well as a full crack across the base on the east and west sides (see

Figure 109). Small cracks were noted on the corner of the bearing plate on Cycle 15a (see Figures 110b and 111a). On Cycle 14a (displacement = +/- 2.0 in.), several "pinging" sounds were heard from the west fuse plate during the negative (pull) half-cycle, indicating the onset of slippage. Slippage between the tension fuse plate and the collar was observed on Cycle 15a (displacement = +/- 2.5 in.) as well. Actuator control problems then occurred on Cycle 15a at + 0.42 in. displacement and on Cycle 16a at + 0.40 in., - 0.46 in., - 1.71 in., and - 1.09 in. Also, on Cycle 16a, the upper segment exhibited severe cracking around the external retrofit angles (see Figure 112), and the fuse plates in compression had clearly buckled. Since this was also the predetermined cycle to replace fuse plates, testing was stopped and new plates were mounted on the column. At this time, a peak horizontal load of + 6.32 kips had been applied to the column.

a.) Northwest corner of column **b.) South side of column prior to testing**

Figure 106. Photographs of Column 4 – Column prior to testing.

a.) Northwest retrofit angle on bottom column segment **b.) West face prior to testing**

Figure 107. Photographs of Column 4 – Cycle 7a.

Figure 108. Photograph of Column 4 – Cycle 7a east face.

a.) East face crack progression b.) Incipient cracking at southeast retrofit angle

Figure 109. Photographs of Column 4 – Cycle 11a.

a.) Cracks forming around southeast retrofit angle b.) Northeast corner bearing plate compression damage

Figure 110. Photographs of Column 4 – Cycle 15a.

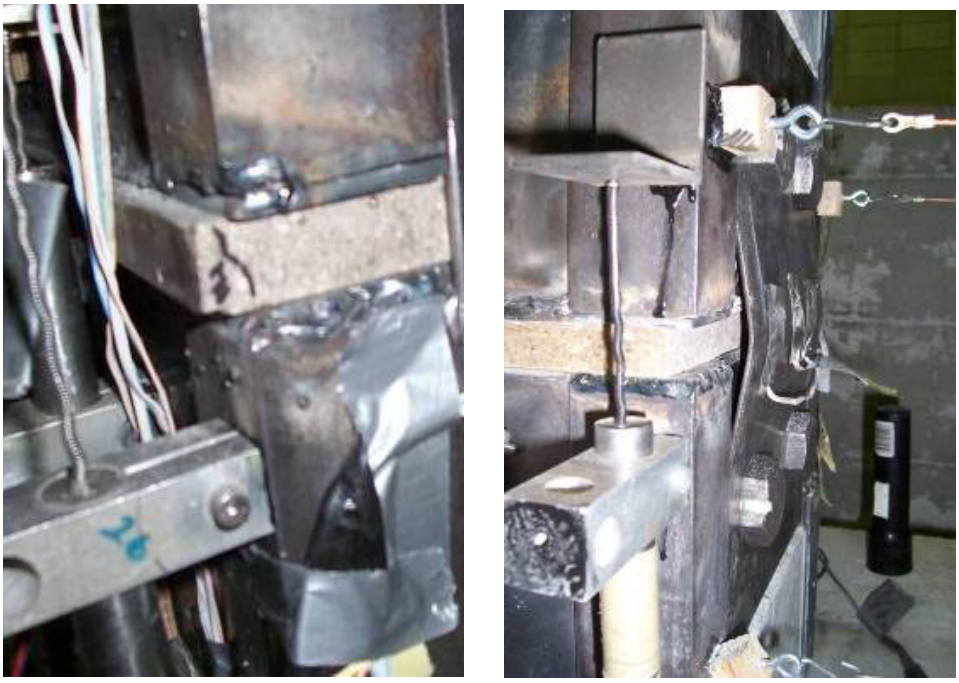

a.) Damage to bearing plate in southeast corner **b.) West fuse plate buckling**

Figure 111. Photographs of Column 4 – Cycle 15a joint.

Figure 112. Photograph of Column 4 – Cycle 16a southeast retrofit angle damage.

Figure 113. Photographs of Column 4 – Start of test 4b.

Figure 114. Photograph of Column 4 – Cycle 19b west face of upper column segment.

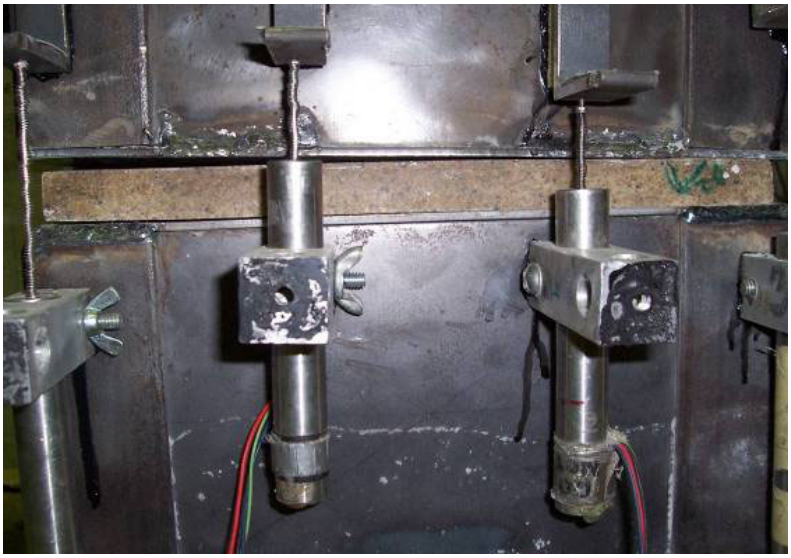

a.) North face joint opening during push half-cycle **b.) East face column damage**

Figure 115. Photographs of Column 4 – Cycle 21b north and east faces.

a.) South side view of retrofit angle failure **b.) Upper column segment damage**

Figure 116. Photographs of Column 4 – Cycle 21b south and west faces.

a.) Northwest corner damage

b.) Upper segment damage and retrofit failure

c.) North face damage and retrofit angle failure

d.) Northeast corner fuse plate buckling

Figure 117. Photographs of Column 4 – Cycle 22b.

After replacing the fuse plates, the displacement regimen was restarted. The damage accrued in the column up to this point can be seen in Figure 113. Actuator control problems continued to increase in frequency and magnitude throughout the remainder of the Column 4 test. From Cycles 19b to 22b, damage to the upper column segment increased and the upper

repair angles became detached from the column face (see Figures 114-117). By this point, rotation of the column concentrated almost exclusively at this location as the collar again pulled off the end of the segment. Testing of Column 4 was stopped after Cycle 23b, as it was again evident that the decrease in load at each displacement was due to this pull-off phenomenon. A maximum horizontal load of + 6.39 kips was observed on Cycle 19b (displacement = +/- 4.0 in.) and a maximum displacement of 6.0 in. was observed for the test. At + 6.0 in., a load of + 4.45 kips was achieved, while a - 5.16 kip load was achieved at - 6.0 in. Quantitative lateral load versus displacement data from the testing of Column 4 are presented in Chapter 7.

The attempt to reinforce the collar (described in Section 4.2.3.1) against pull-off was unsuccessful as behavior of Column 4 was similar to that observed in Columns 2 and 3. Once again, little could be determined about the ability of the column to withstand its design load due to the premature failure mode. However, Tests 2, 3, and 4 allowed selection of the most effective fuse plate and bearing plate materials for subsequent tests of Columns 5 and 6, as well as identification of key detailing issues for the segmented columns.

6.6 Column 5 Results

Testing of Column 5 commenced and continued to a + 11.14 in. displacement on the positive (push) half-cycle and a -12.00 in. displacement on the negative (pull) half-cycle, using the entire stroke of the actuator. The + 12.00 in. displacement was not able to be reached, because the difficult nature of positioning the column caused the column to be slightly to the east of the center of the actuator shaft. Column 5 is shown before testing in Figure 118, and the incremental damage accrued over the imposed displacement regimen is shown in Figures 119-139. Cracking across the entire column base was noted during Cycle 10a. On the positive (push) half-cycle, cracking occurred at the base of the column on the east face (see Figure 119). Cracks also formed approximately every 6 in. up the column for several feet. On the negative (pull) half-cycle, cracking occurred at the base of the west face of the column. Testing was halted on Cycle 11a (displacement = +/- 1.0 in.), because the load-displacement cable to the DAS had become disconnected during the first portion of testing. Thus nearly all the data measured over these cycles were lost. Once the load-displacement cable was

reconnected, testing was restarted at Cycle 1a. It should be noted that the load-displacement curve remained nearly linear during this portion of testing. However, cracking that took place during this portion of testing may have caused a reduction in the initial lateral stiffness as indicated by the recorded data for Column 5.

After restarting the test, additional cracks formed across the column on Cycle 13a (displacement = +/- 1.5 in.) (see Figures 121 and 122). On Cycle 14a (displacement = +/- 2.0 in.), a small amount of compression damage was noted under the collar on the west face of the column (see Figure 123). This minute chipping was observed on previous specimens and was caused by the collar bearing on the surface of the concrete column. The depth of chipping was limited to the thickness of the collar and could be eliminated in the future by placing a small gap or indentation in the concrete at this location. Additional small regions of compression damage were marked on the positive (push) cycles of Cycles 15a and 16a (see Figure 125). By Cycle 16a, the fuse plates were visibly buckling. Since this was also the predetermined cycle to replace fuse plates, testing was stopped and new fuse plates were mounted on the column. At this time, a peak horizontal load of + 7.45 kips had been applied to the column during the positive (push) half-cycle, while a horizontal load of - 8.53 kips had been applied during the negative (pull) half-cycle.

The displacement regimen was then restarted with the second set of fuse plates. Testing continued without incident or additional cracking until Cycle 17b (displacement = +/- 3.0 in.) when the actuator control was lost briefly. Fuse plate buckling that occurred during Cycle 18b can be seen in Figure 126. Testing was stopped again after Cycle 18b due to several large actuator incidents and was resumed the following day after several adjustments were made to the control system. Cycles 19b and 20b (displacements = +/- 3.5 in. and 4.0 in.) were completed before another actuator incident halted testing again. A lateral load during this incident was recorded at 15 kips, possibly causing internal damage to Column 5 and initiation of slip in the fuse plate connections.

After setting interlocks and increasing the dither in the control system in an attempt to improve actuator control, testing was resumed. On Cycle 21b, several "pings" were heard in the plates, indicating slipping between the plates and the steel collars. Prior to the previous actuator incidents, no evidence of slippage had been noted. On the negative (pull) half-cycle

of Cycle 21b, the top of the west plate began to curl due to this slippage and subsequently began bearing on the through-bolts. This condition continued on each cycle and can be seen during Cycle 23b in Figure 128b. With each significant "pinging" noise, a loss of load was also observed while displacement of the column continued. Slippage and the resulting bearing condition continued during each cycle until the full stroke of the actuator was reached (see Figures 128b, 130a, 130b, 133, 134c). Despite this slippage, the gap opening at the column segment continued to widen throughout the remainder of the test (see Figures 127b, 131a, 132c, 135a, 136c, 137b) and the crack width at the interface between the upper column segment and collar remained small. The final condition of the west fuse plate and the condition of Column 5 are shown after Cycle 30 in Figure 138. Post-test damage for all sides of Column 5 can be seen in Figure 139.

The maximum column displacement that was achieved on the positive (push) half-cycle of Cycle 30b was + 11.14 in. and was associated with a + 6.97 kip load. On the negative (pull) half-cycle, the column was displaced - 12.00 in., at which a - 6.86 kip load was achieved. After returning to zero displacement on Cycle 30b, the residual force on the column was less than 200 lbs. The maximum force on the column of + 8.88 kips was achieved on Cycle 21b (displacement = +/- 5.0 in.). Quantitative lateral load versus displacement data for Column 5 are presented in Chapter 7.

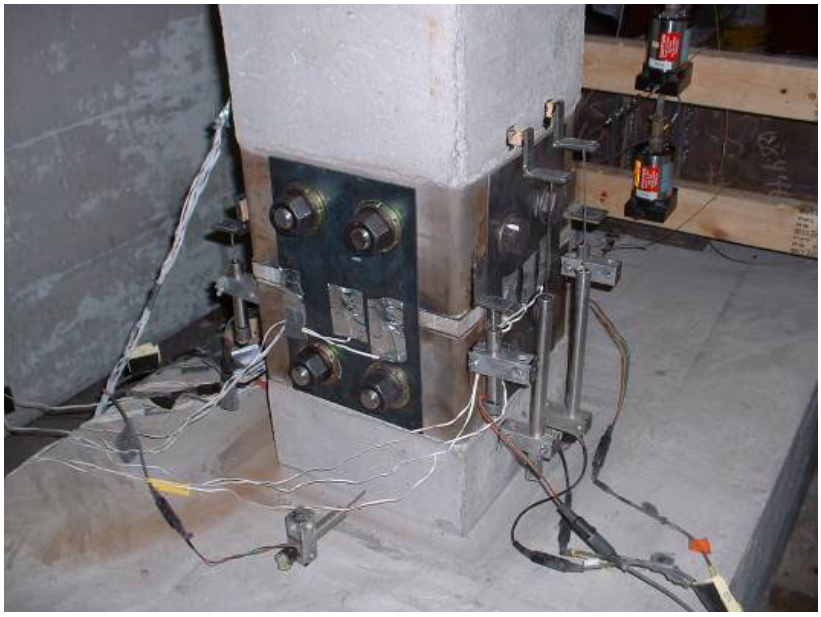

Figure 118. Photograph of Column 5 – Prior to testing.

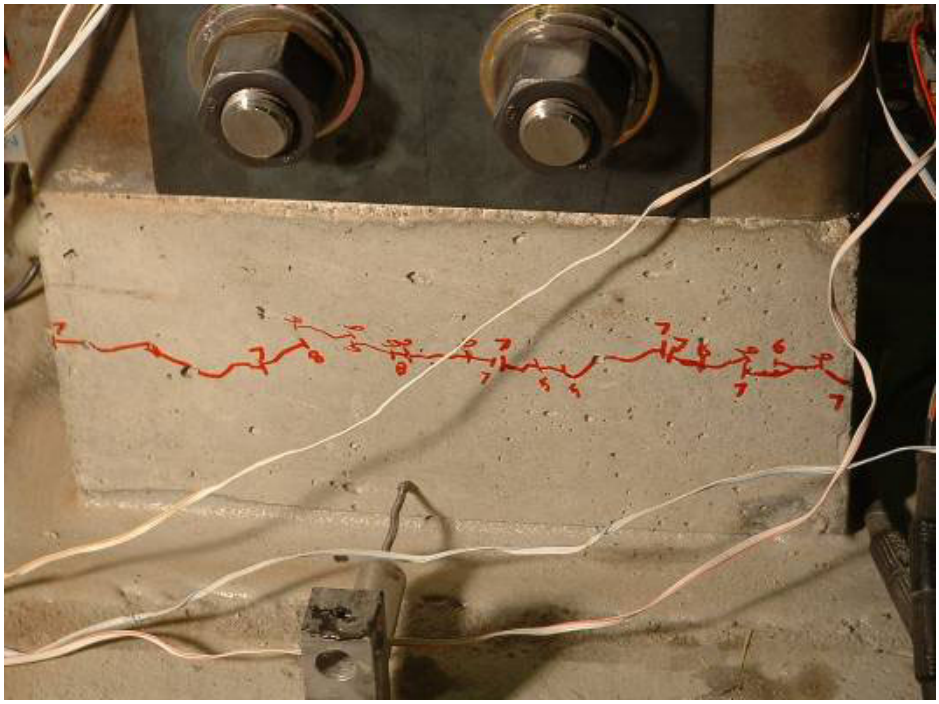

Figure 119. Photograph of Column 5 – Cycle 10a east face initial cracking.

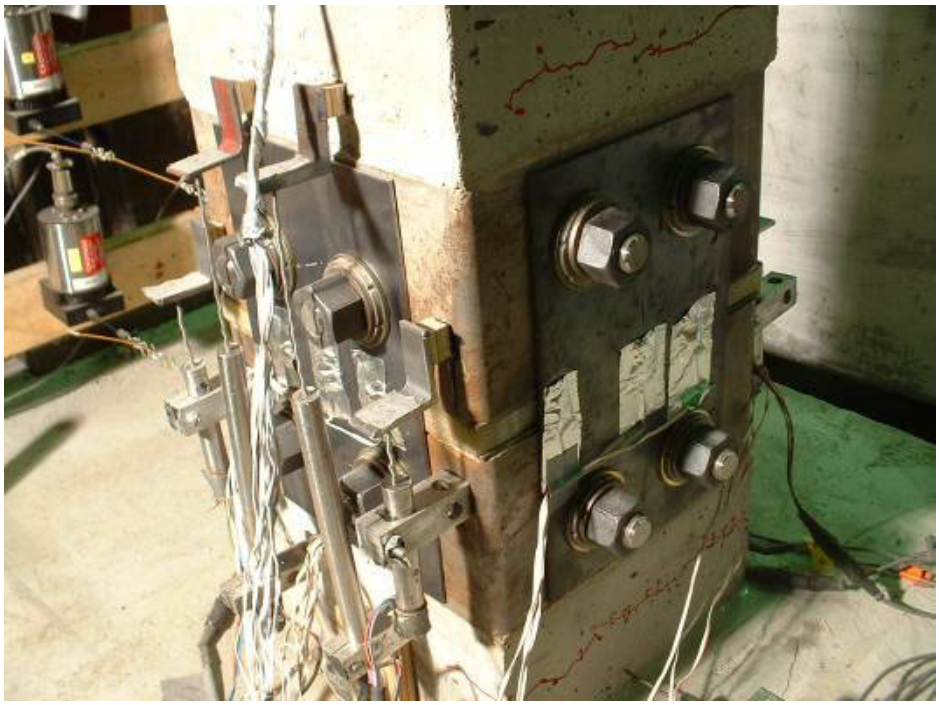

Figure 120. Photograph of Column 5 – Cycle 10a southeast corner view of cracking.

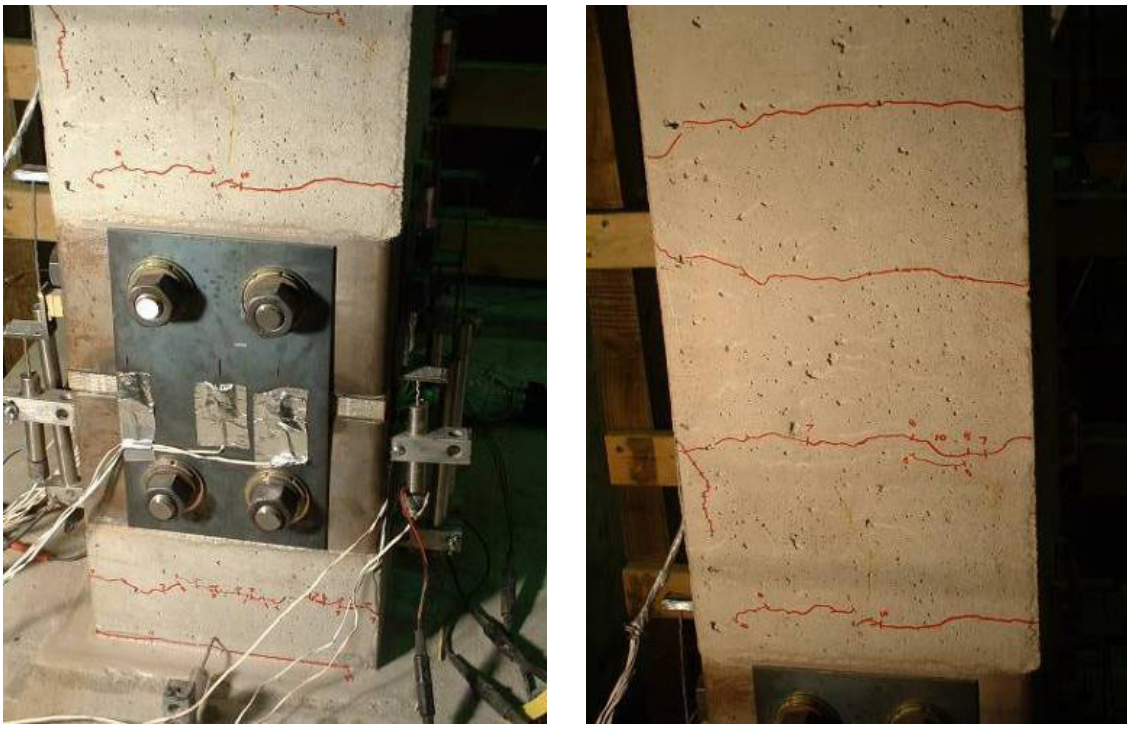

a.) Cracking around column joint b.) Upper segment crack progression

Figure 121. Photographs of Column 5 – Cycle 13a east face.

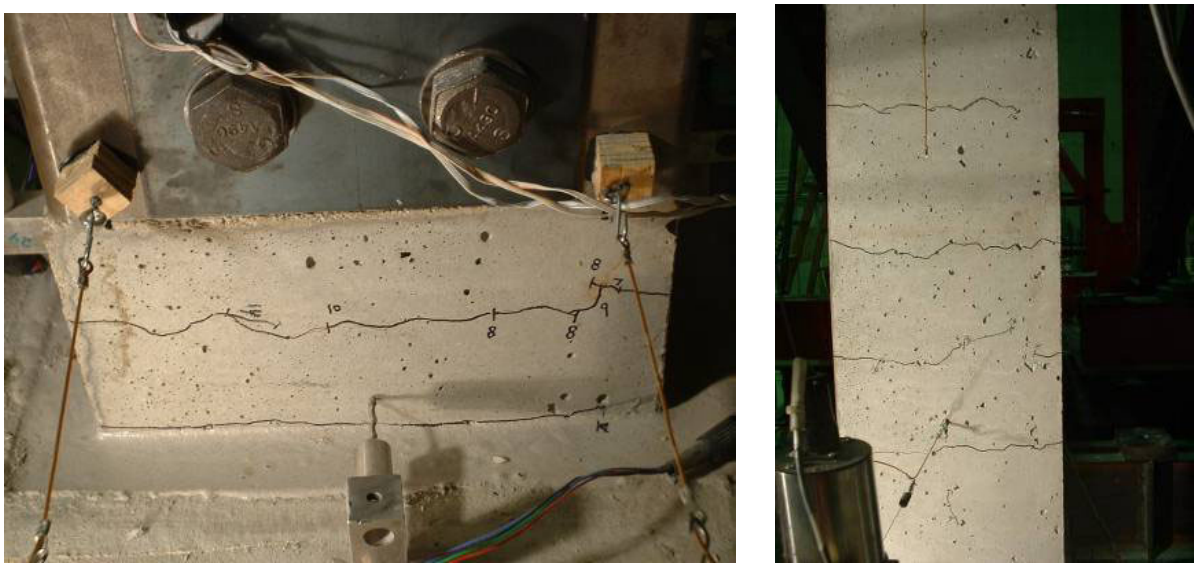

a.) Cracking at the base of the west face b.) Upper segment crack progression

Figure 122. Photographs of Column 5 – Cycle 13a west face.

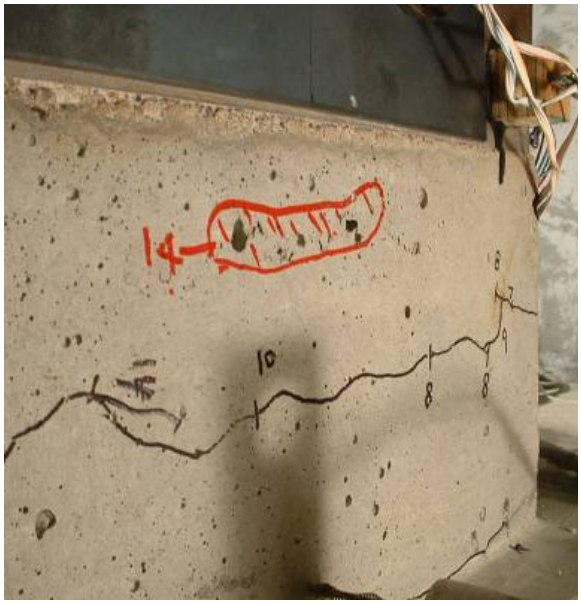

a.) West face at base b.) East plate initial buckling

Figure 123. Photographs of Column 5 – Cycle 14a west face.

a.) West face compression damage and cracking at base b.) East fuse plate buckling

Figure 124. Photographs of Column 5 – Cycle 15a.

a.) Upper segment compression damage

b.) West fuse plate initial buckling

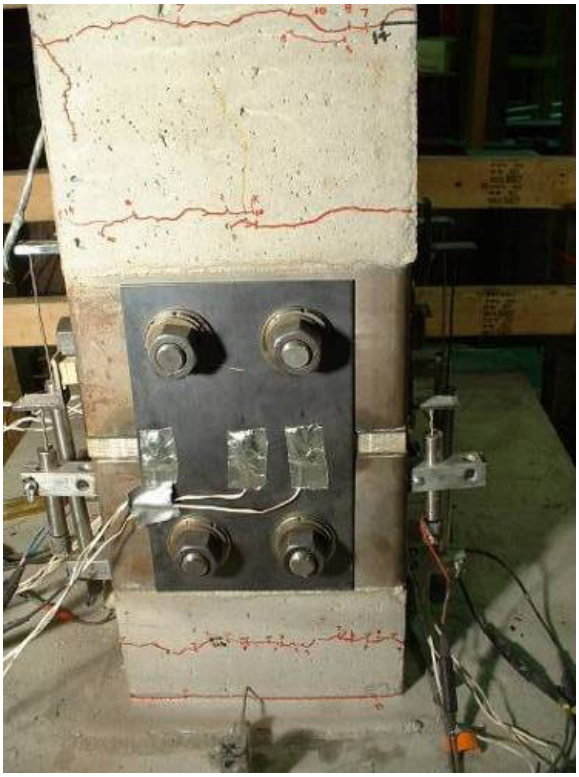

a.) West face cracking at the end of Test 5a

b.) East plate buckling in compression

Figure 125. Photographs of Column 5 – Cycle 16a.

Figure 126. Photographs of Column 5 – Cycle 18b west fuse plate buckling.

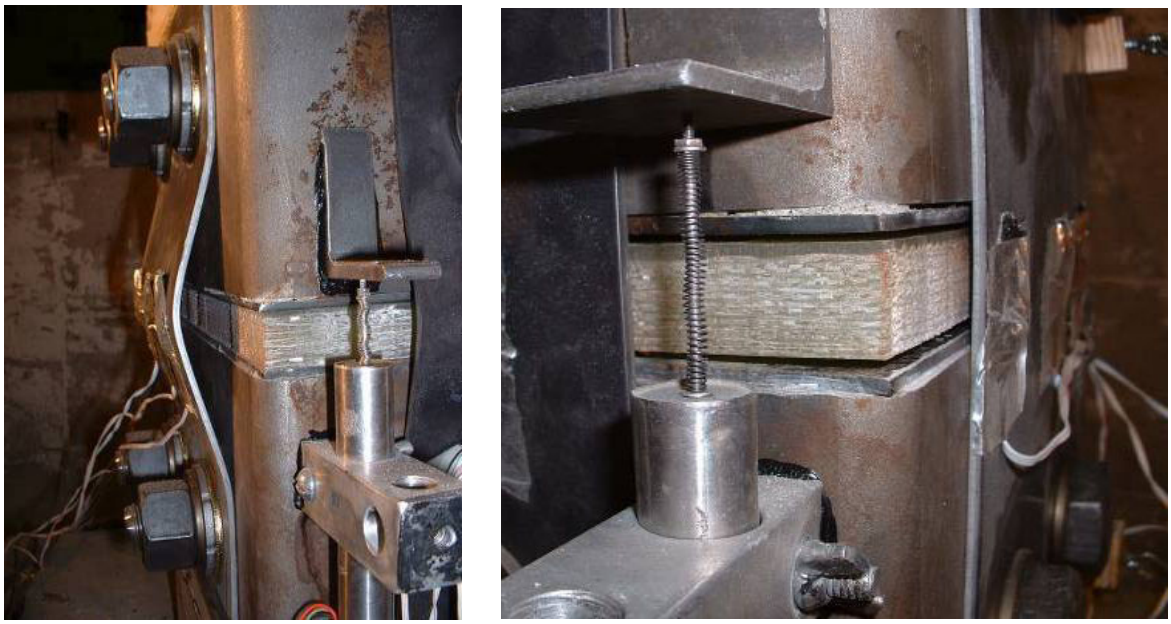

a.) East fuse plate buckling **b.) West joint opening during pull half-cycle**

Figure 127. Photographs of Column 5 – Cycle 21b.

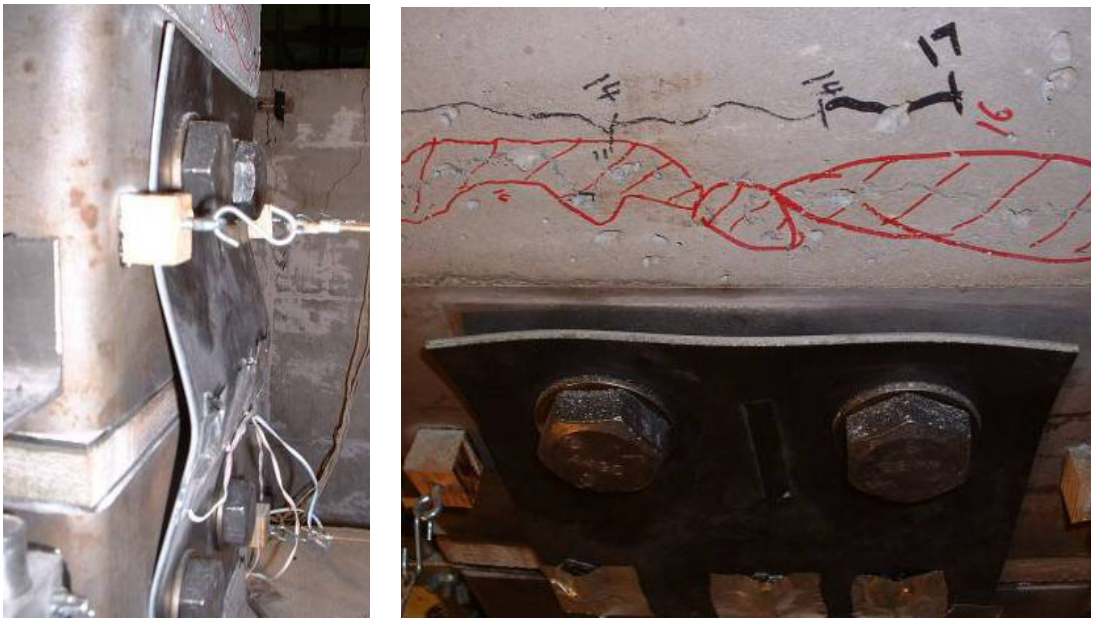

a.) West fuse plate buckling b.) Bolt bearing on west fuse plate causing plate curling

Figure 128. Photographs of Column 5 – Cycle 23b.

a.) Southeast corner joint opening b.) East joint opening during push half-cycle

Figure 129. Photographs of Column 5 – Cycle 24b joint opening.

a.) West face damage and fuse plate buckling

b.) Southwest corner fuse plate buckling

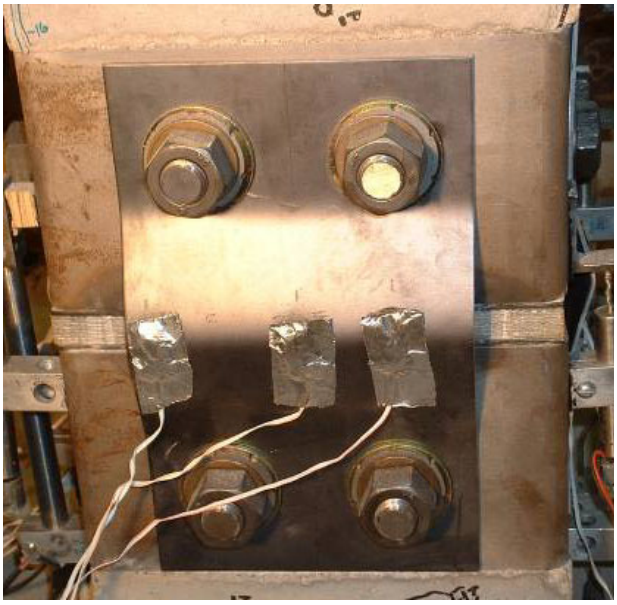

c.) East fuse plate buckling

d.) Northeast corner fuse plate buckling

Figure 130. Photographs of Column 5 – Cycle 24b.

a.) Northeast corner joint opening

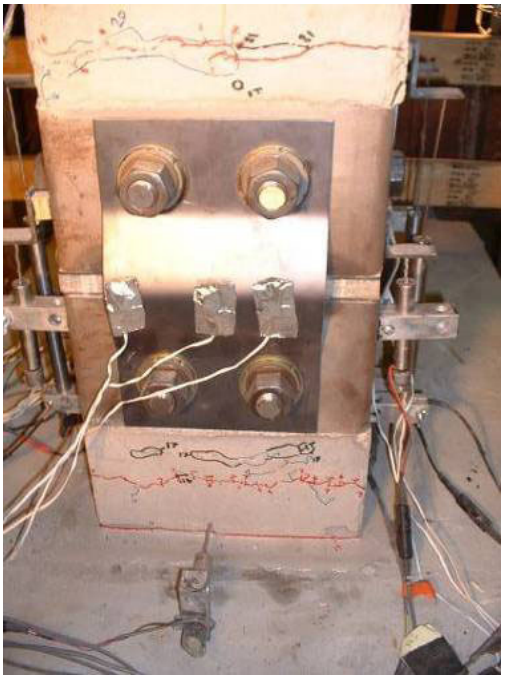

b.) East fuse plate buckling and segment damage

c.) West fuse plate buckling

Figure 131. Photographs of Column 5 – Cycle 26b.

a.) Differential buckling in north fuse plate buckling

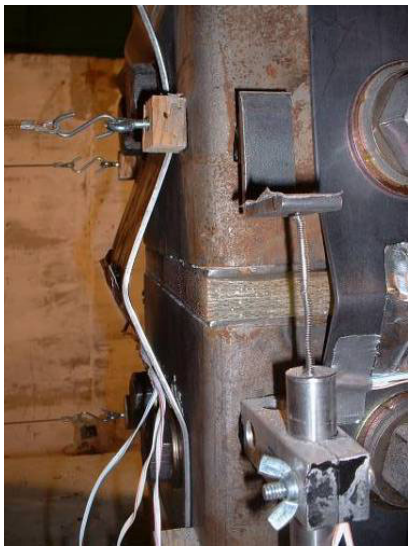

b.) West fuse plate buckling

c.) East joint opening

d.) East joint opening and segment damage

Figure 132. Photographs of Column 5 – Cycle 27b push half-cycle.

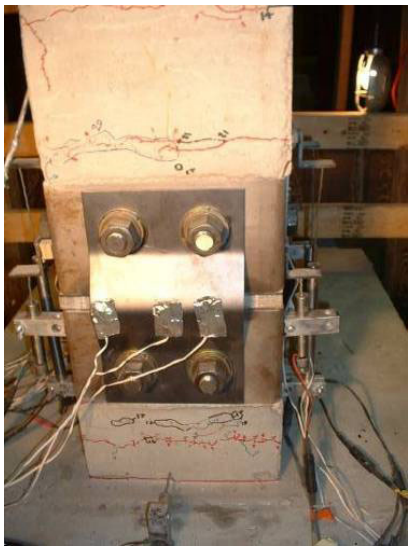

a.) East face under compression

b.) West joint opening

c.) Curling of west plate

Figure 133. Photographs of Column 5 – Cycle 27b pull half-cycle.

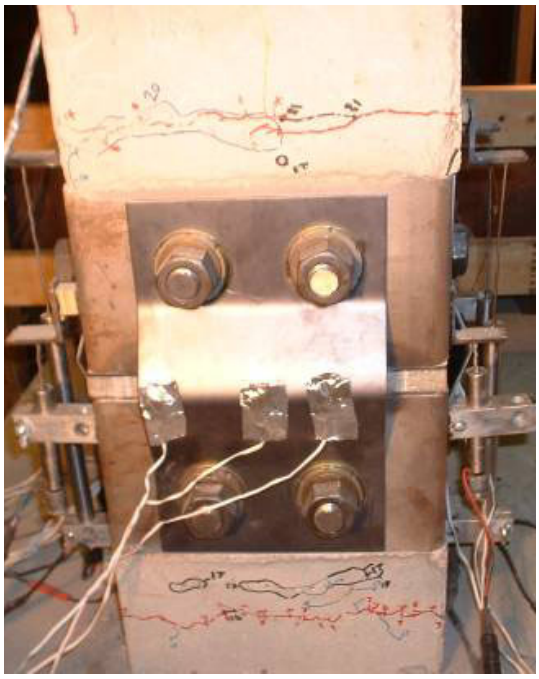

a.) East fuse plate buckling and column damage

b.) East fuse plate buckling

c.) Curling on top of the west plate

d.) Column deformation during push half-cycle

Figure 134. Photographs of Column 5 – Cycle 28b.

a.) East joint opening during push half-cycle

b.) West fuse plate buckling during push half-cycle

c.) East fuse plate buckling during pull half-cycle

Figure 135. Photographs of Column 5 – Cycle 29b.

a.) North fuse plate differential buckling

b.) West fuse plate buckling

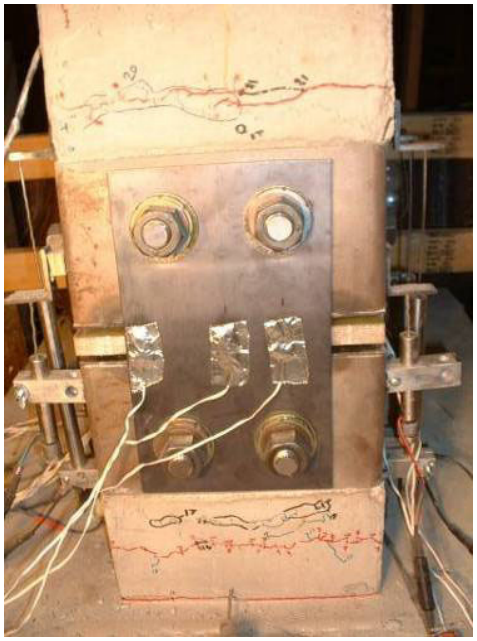

c.) East face damage and joint opening

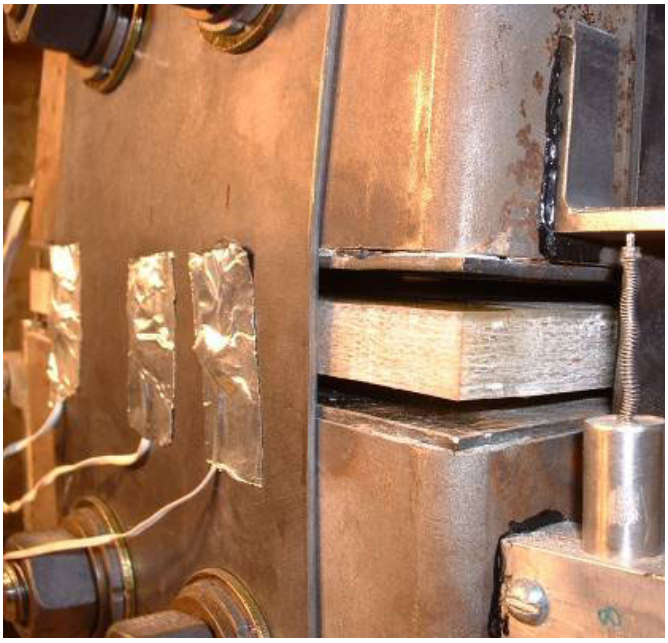

d.) East joint opening

Figure 136. Photographs of Column 5 – Cycle 30b push half-cycle.

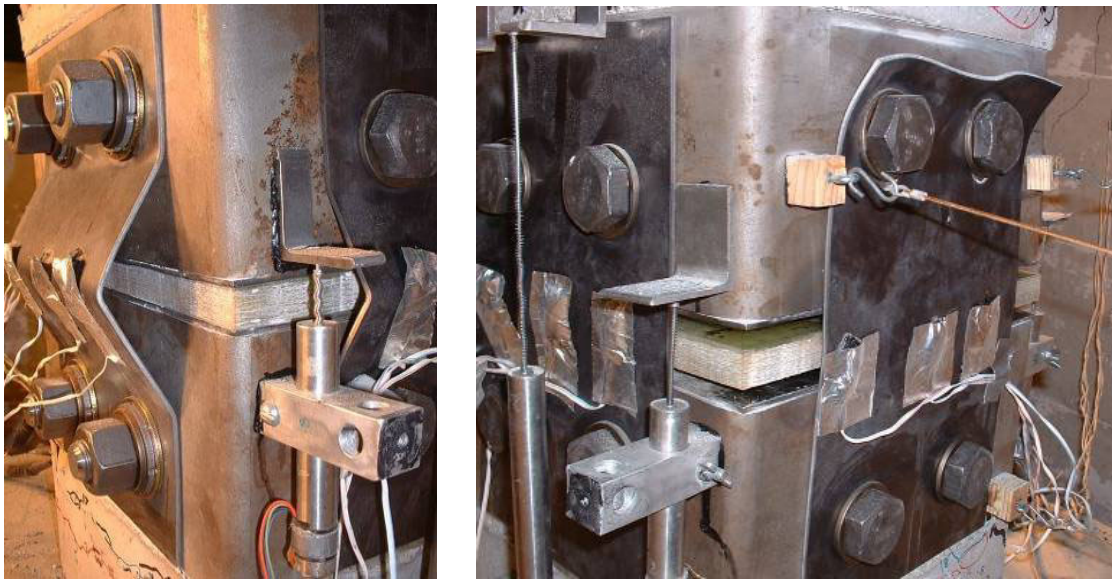

a.) East fuse plate buckling b.) West joint opening and bearing of west fuse plate on bolts

Figure 137. Photographs of Column 5 – Cycle 30b pull half-cycle.

a.) Residual fuse plate buckling b.) Residual curling on top of west plate

Figure 138. Photographs of Column 5 – After test.

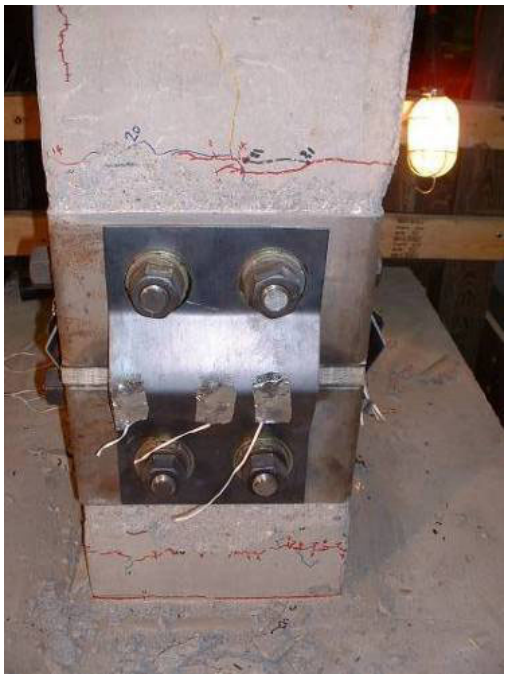

a.) East face after test

b.) North face after test

c.) West face after test

d.) South face after test

Figure 139. Photographs of Column 5 – Final damage after test.

After resolving the detailing issues identified in Columns 2–4, Column 5 performed as designed with the exception of the fuse plate slippage. The fuse plates at the column segment clearly exhibited tensile yielding and buckling. In addition, the joint section demonstrated large deformation capacity, which prevented the concrete segments from sustaining major damage (i.e., buckling of bonded reinforcement). By allowing a large amount of rotation to take place at the segment joint, less bending of the column segments occurred during large lateral displacements. Because the full stroke of the actuator was reached, greater damage such as fuse plate fracture, yielding of the post-tensioning, or crushing of concrete was not achieved.

Sandblasting of the faying surfaces at the slip-critical connection had been performed to increase the coefficient of static friction in the connection, and it was unclear whether or not the slippage or slightly lower lateral strength relative to the control column was caused by the actuator control incidents associated with the malfunctioning servo valve. The slippage of the fuse plates almost certainly caused the gradual decrease in lateral load at large lateral displacements. In future tests or field application, slippage could be readily addressed by increasing the clamping forces through the use of more or larger through-bolts. The large displacements achieved while maintaining high lateral loads relative to the control column, however, were considered a major improvement in performance. Repair by replacing fuse plates was also highly successful as evidenced by the nearly identical load-displacement performance of the repaired column to that of the column prior to repair.

6.7 Column 6 Results

Testing of Column 6 commenced and continued to a + 10.33 in. displacement on the positive (push) half-cycle and a - 10.00 in. displacement on the negative (pull) half-cycle, using the entire stroke of the actuator on the positive side of the displacement regimen. As discussed in Section 6.6, the difficulty of positioning the column with respect to the actuator limited the stroke of the actuator during the positive (push) half-cycle of testing to less than the actual stroke limit of the actuator of +12.00 in. Column 6 prior to testing is shown in Figure 140 and 141, and the incremental damage accrued over the imposed displacement regimen is illustrated in Figures 142-158. A small crack was first noted at the base of the east face on

Cycle 8a (displacement = +/- 0.5 in.). Cracking across the entire base of the column (see Figure 142a), as well as cracks 6 in. and 18 in. above the base of the column, was observed on Cycle 10a (displacement = +/- 1.0 in.) on the east face of the column. Cracking across the west face was noted at the base on Cycle 11a (displacement = +/- 1.0 in.) (see Figure 142b). Additional cracking of Column 6 was noted on subsequent cycles until replacement of the fuse plates took place (see Figure 143). Relative to Column 5, Column 6 had a narrower opening of the construction joint up to this point. On Cycle 16a (displacement = +/- 2.5 in.), buckling in the plates was barely detectable due to the shape recovery of the SMA material. However, this was the predetermined cycle to replace fuse plates, so testing was stopped and new SMA fuse plates were mounted on the column. Up to this point, a peak horizontal load of + 7.22 kips had been applied to the column.

The displacement regimen was then restarted with the second set of plates. The extent of cracking that took place during the entire “a” portion testing can be seen in Figure 145. Testing resumed without further cracking until Cycle 14b (displacement = +/- 2.0 in.), when several cracks extended, and a small amount of compression damage was noted on the west face of the column near the base. Compression damage on the northwest and southeast corners of the column increased above and below the collars for several cycles (see Figures 146-148). As previously discussed, this damage was minor and due to the collar bearing on the shallow face shell of concrete.

"Pinging" in the fuse plates was noted during Cycle 19b (displacement = +/- 3.5 in.), again indicating slippage between the fuse plates and through-bolts. Also during this cycle, the construction joint gap between column segments began to widen significantly. More "pinging" was heard from the fuse plates during Cycle 21b (displacement = +/- 5.0 in.), Cycle 22b (displacement = +/- 5.0 in.), and Cycle 23b (displacement = +/- 6.0 in.). After Cycle 23b, continuous "pinging" was heard in the fuse plates during the remaining cycles of the test. Compression damage continued to increase over the next few cycles, along with superficial, shallow (< 0.25 in. deep) spalling of the concrete around the collars (see Figures 151a, 151b, and 153). A decrease in lateral load was noted as the slippage in the fuse plates continued, as with previous tests.

The damage to Column 6 up to Cycle 26b can be seen in Figure 155. Fuse plate buckling and joint opening that took place during Cycle 28b is illustrated in Figure 156. On Cycle 29b, the south fuse plate fractured below the top left bolt and washer at a displacement of -5.22 in. (see Figure 157a). This fracture was likely caused by the small-radius bending of the lateral plates due to buckling on previous cycles. Testing was continued until the -9.0 in. displacement on Cycle 29b (see Figure 157b), when testing was terminated; the column began to tilt perpendicular to the axis of loading due to the fractured fuse plate, and it caused the load beam to impinge on the load frame (see Figure 158).

During the Column 6 test, a maximum positive horizontal load of + 10.13 kips was observed during Cycle 24b (displacement = +/- 7.0 in.). The maximum positive displacement of + 10.33 in. (also the actuator stroke limit during this test) was associated with a + 9.10 kip load. The largest negative horizontal load achieved during the negative half-cycle was - 10.47 kips on Cycle 23b. On Cycle 29b at - 9.0 in. displacement, despite the fractured lateral fuse plate, a horizontal load of - 7.38 kips was achieved. Quantitative lateral load versus displacement data for Column 6 are presented in Chapter 7.

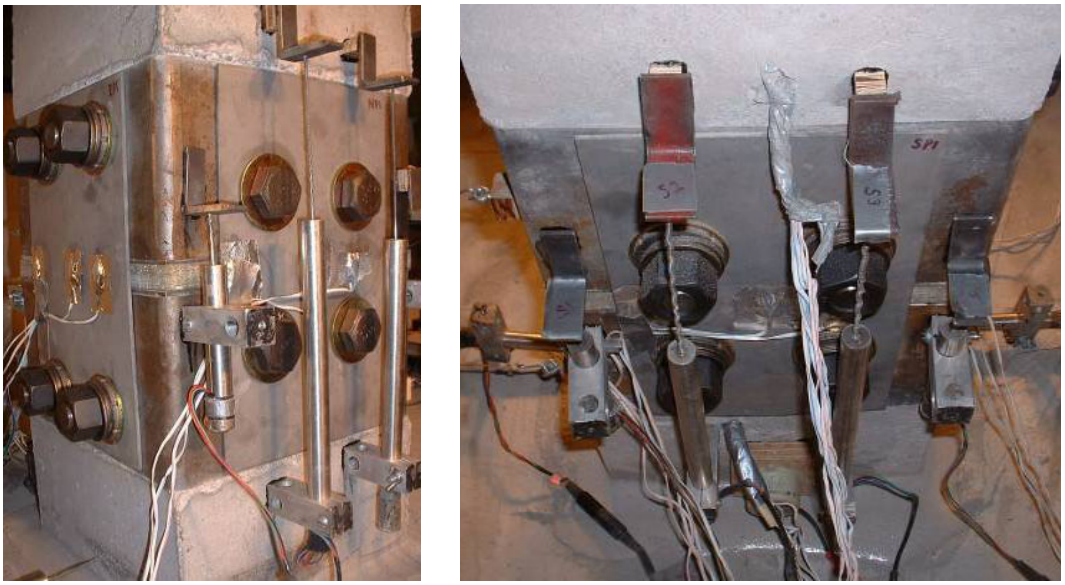

a.) Northeast corner **b.) South face**

Figure 140. Photographs of Column 6 – Segment joint prior to testing.

Figure 141. Photograph of Column 6 prior to testing.

a.) East face initial cracking **b.) West face initial cracking**

Figure 142. Photographs of Column 6 – Cycle 11a.

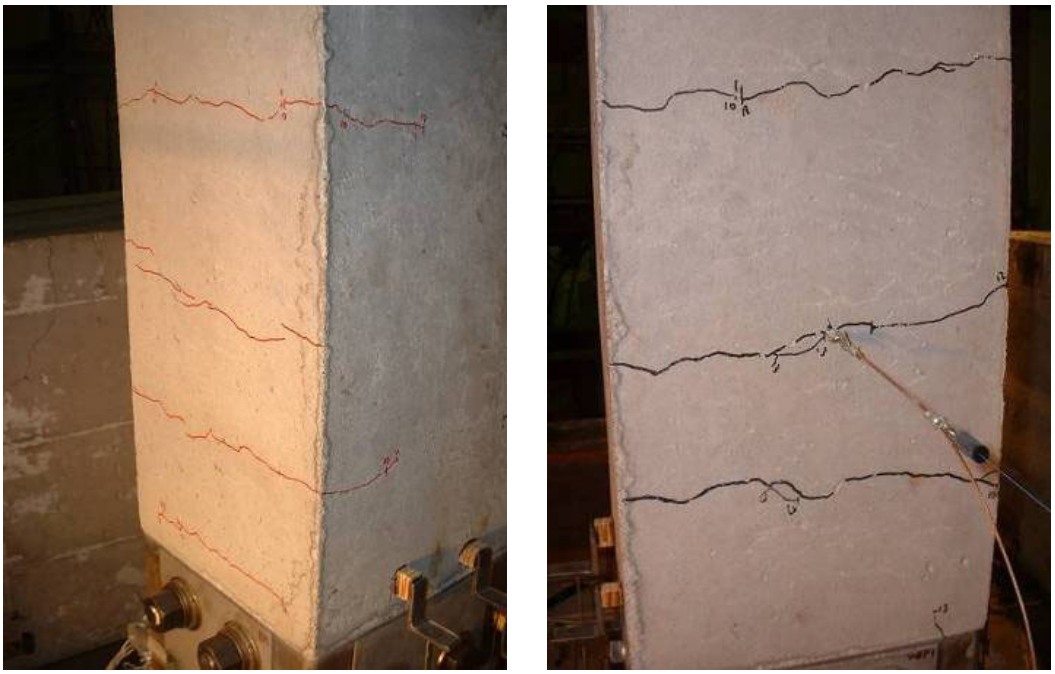

a.) East face of upper segment crack distribution b.) West face of upper segment crack distribution

Figure 143. Photographs of Column 6 – Cycle 13a.

a.) East face of upper segment crack distribution b.) West fuse plate initial buckling

Figure 144. Column 6 – Cycle 16a.

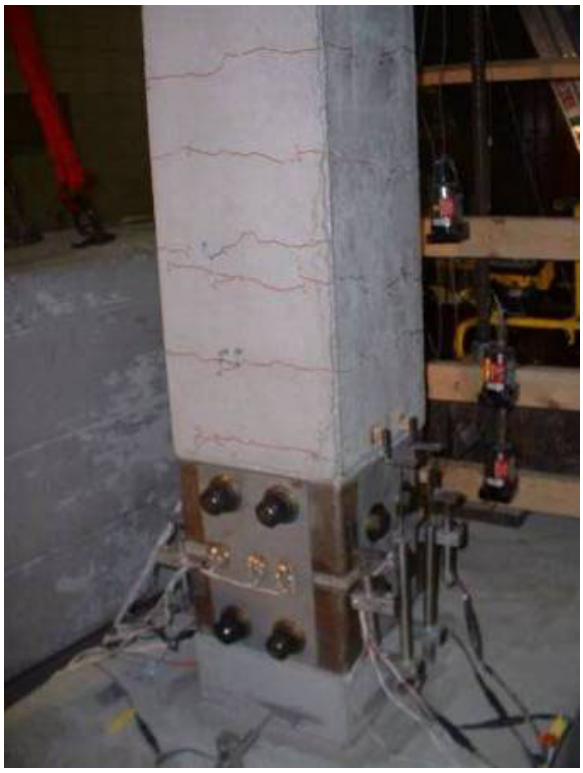

Figure 145. Photographs of Column 6 – Start of "b" portion of test.

a.) West face initial compression damage

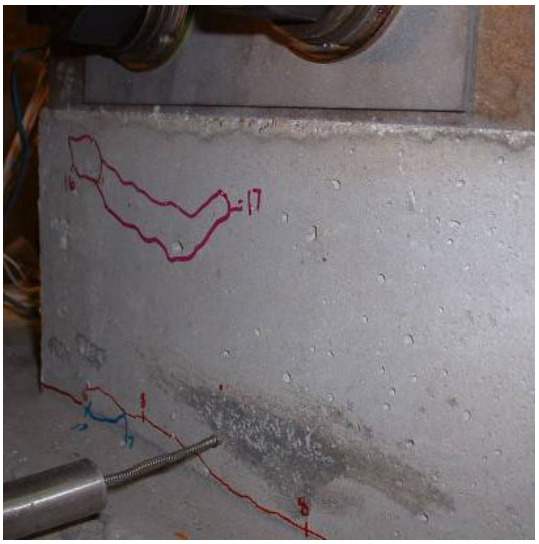

b.) East face initial compression damage

Figure 146. Photographs of Column 6 – Cycle 17b.

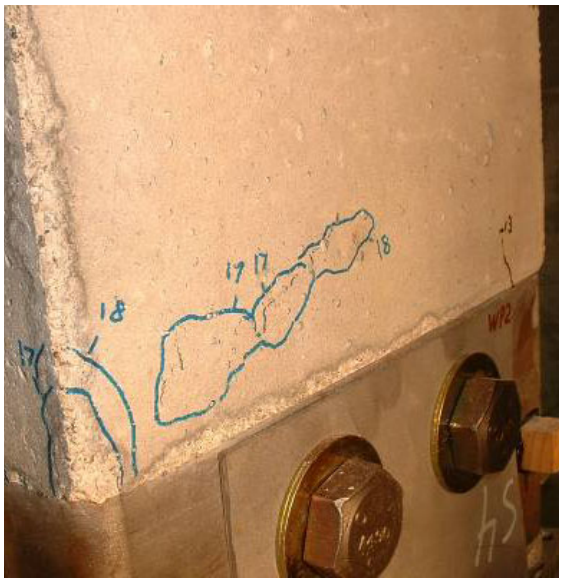

a.) Upper west column segment compression damage

b.) Northwest corner compression damage

Figure 147. Photographs of Column 6 – Cycle 18b.

a.) West fuse plate buckling

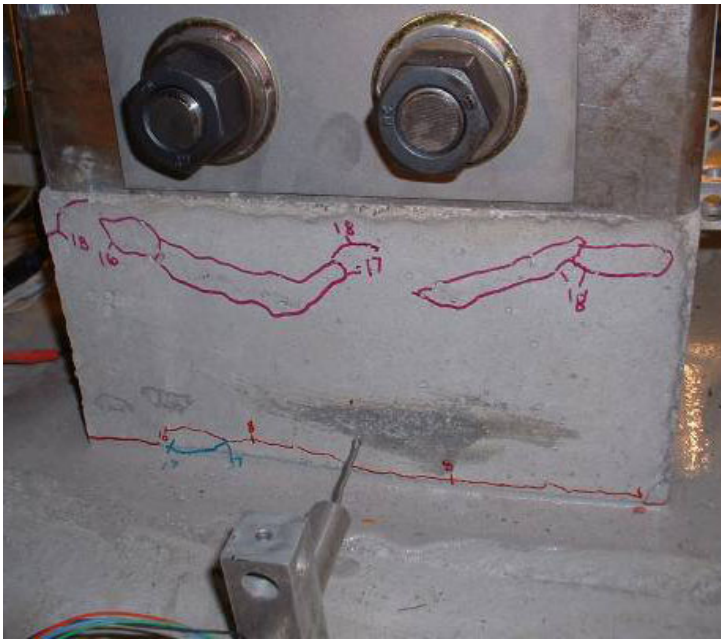

b.) East face compression damage

Figure 148. Photographs of Column 6 – Cycle 19b.

a.) West fuse plate buckling **b.) East fuse plate buckling**

Figure 149. Photographs of Column 6 – Cycle 20b.

Figure 150. Photographs of Column 6 – Cycle 21b, joint opening.

a.) Upper segment west face compression damage

b.) Lower segment west face compression damage

c.) Northwest corner joint opening

d.) West fuse plate buckling

Figure 151. Photographs of Column 6 – Cycle 23b, push half-cycle.

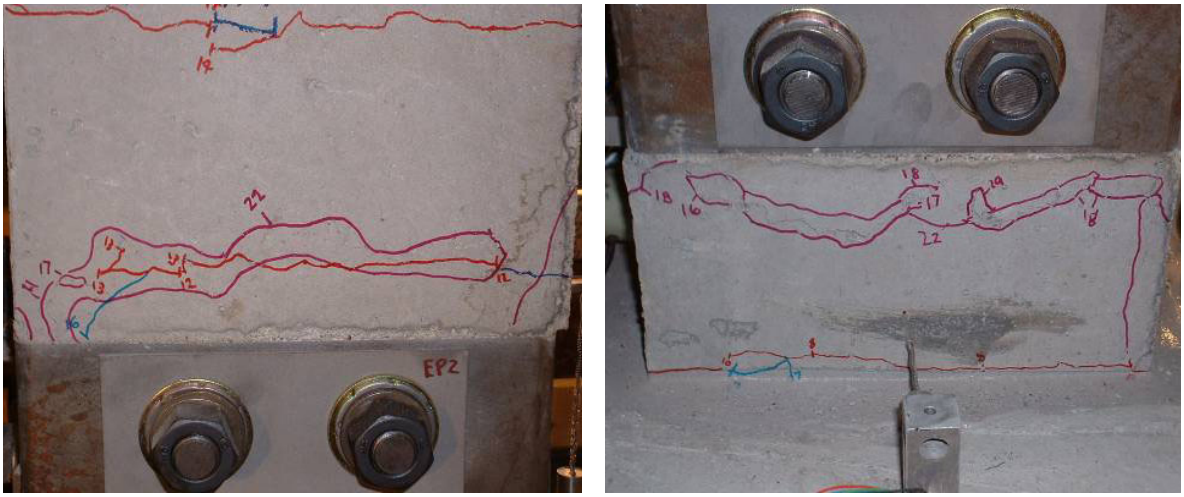

a.) East face of upper segment **b.) East face of lower segment**

Figure 152. Column 6 – Cycle 23b, pull half-cycle.

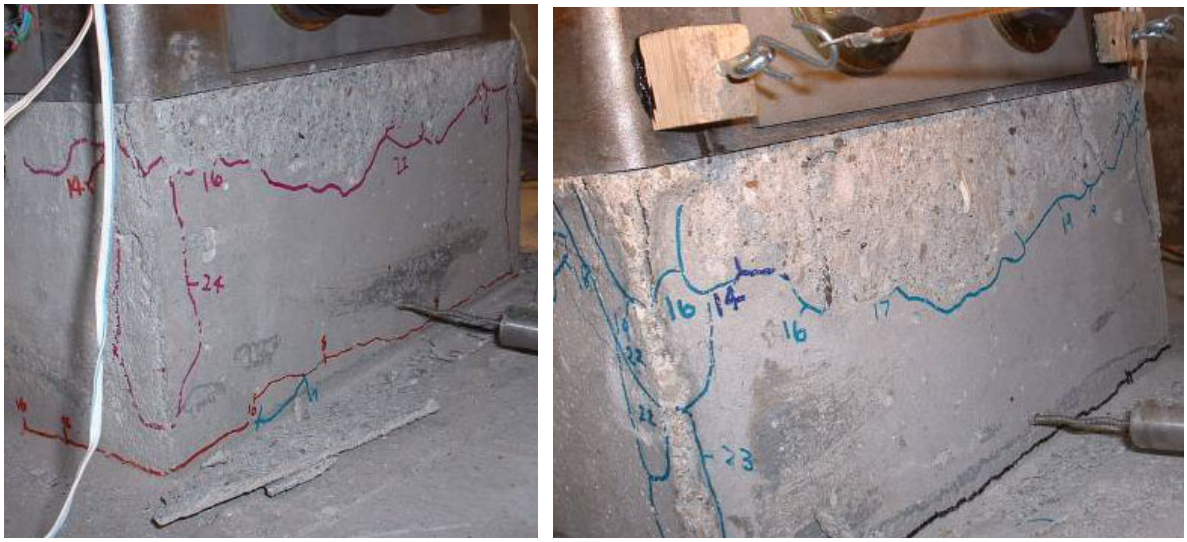

a.) Lower segment east face spalling **b.) Lower segment west face spalling**

Figure 153. Photographs of Column 6 – Cycle 26b.

Figure 154. Photograph of Column 6 – Cycle 26b, east joint opening.

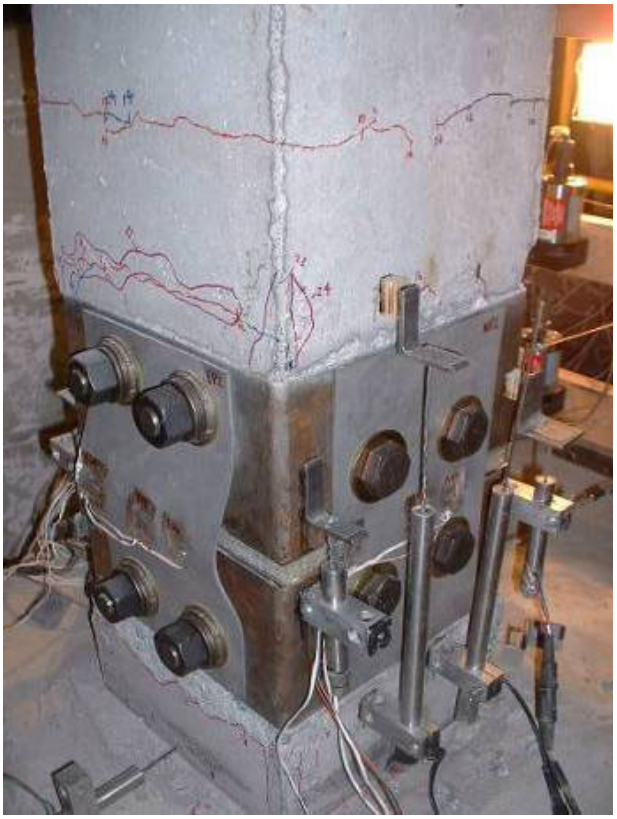

Figure 155. Photograph of Column 6 – Cycle 26b, column damage.

a.) West fuse plate buckling

b.) Northwest corner joint opening

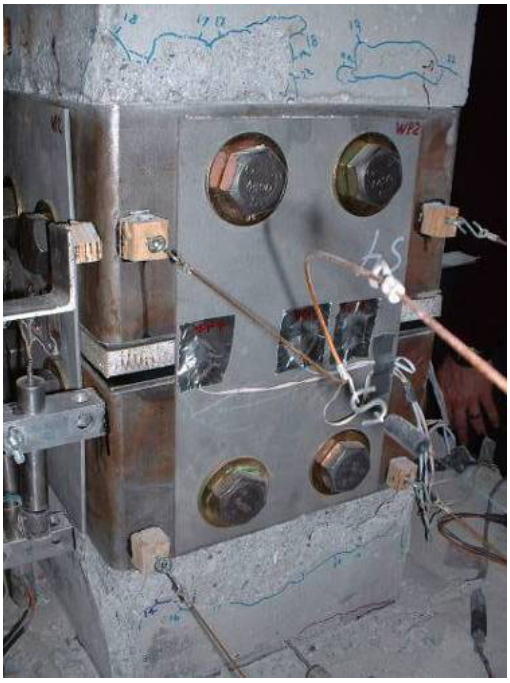

c.) West face under tension

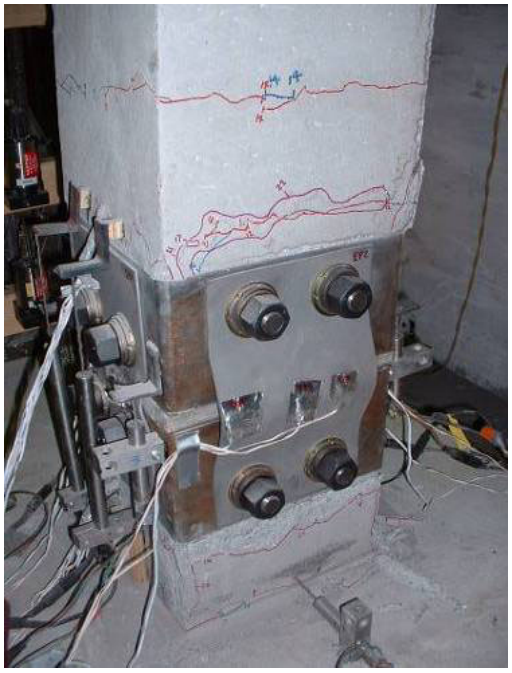

b.) East face under compression

Figure 156. Photographs of Column 6 – Cycle 28b.

a.) Initial fracture of south fuse plate at -5.22 in. displacement **b.) Fuse plate crack at -9.0 in. displacement**

Figure 157. Photographs of Column 6 – Cycle 29b fuse plate crack.

c.) Load beam impinging on load frame

Figure 158. Photographs of Column 6 – Cycle 29b.

Column 6 again demonstrated the ability of the segmented column system to sustain greater lateral deflections than the control column. It also demonstrated a higher lateral strength than Column 1. Material tests on the SMA (see Chapter 5) indicated higher strength than the A36 steel fuse plates used in Test 5, which lead to increased damage (cracking and spalling of concrete and yielding of internal reinforcement) in the precast column segments, as well as a higher lateral strength of the entire column. The greater damage to the concrete segments led, in turn, to higher residual displacements, despite the SMA's shape recovery property. It should be noted that this same effect could be achieved by using slightly larger A36 fuse plates.

Material tests indicated the SMA had lower ultimate strain capacity than the A36 steel, so fracture of the fuse was not surprising. It should be noted that fracture did not occur in one of the fuse plates on the extreme tension/compression faces of the column, but rather in one of the lateral fuse plates where lower radius bends due to buckling were imposed by the shorter gage length of the fuses on these lateral faces. The major advantage presented by the SMA plates aside from their greater resistance to corrosion is apparent after moderate lateral displacements. After 2.5 in. of lateral displacement, when the A36 plates had clearly yielded in tension and buckled in compression, the SMA plates appeared to be nearly undamaged. Thus a moderate-level loading event that would clearly require replacement of steel fuse plates may not cause enough damage to the SMA plates to warrant replacement.

7. QUANTITATIVE TEST RESULTS AND ANALYSES

Benchmarks referred to as performance indicators were used to quantitatively compare the behavior of each column. Emphasis was placed on comparisons between Column 1 (the control column) and Columns 5 and 6 with respect to these performance indicators. While the results from Columns 2, 3, and 4 were used to develop more effective structural details and identify effective materials for the bearing plates and fuse plates, meaningful comparisons were difficult to make due to the unforeseen mechanisms that developed leading to premature failures. The collar pull-off mechanism is discussed in Section 6.3, and the details developed to prevent its occurrence in Columns 5 and 6 are described in Chapter 4.

7.1 Notes from the tests of Columns 2, 3, and 4

While results from early displacement cycles of Columns 2, 3, and 4 gave some insight to the behavior of the proposed system, their usefulness once the failure mechanism developed at the collars was reduced. The following detailing requirements were developed as a result of these tests.

- Longitudinal bonded reinforcement must be anchored beyond *all* through-bolt ducts at the segment joints in a manner that prevents the bolts and collars from pulling off the end of the column. This can be effectively achieved by using U-shaped longitudinal bars that wrap around the bolt ducts or by using appropriately shaped end anchors positioned at the end of precast segments. These anchors may also be welded to the segment end plate to ensure positioning, but the weld is not a strict necessity.
- A steel plate welded to the end of the steel collars is effective in increasing confinement of the crucial segment ends. It is also a convenient means of producing a smooth, flat interface with the bearing plate to transfer loads between segments without stress concentrations.
- Fuse plates connected on all four faces of the column increase confinement of the segment ends and improve the performance of the column.

7.2 Performance Indicators

The performance indicators used to interpret and quantify the data collected for all six column tests are described as the following.

- *Lateral load capacity* — The mean of the greatest positive and greatest negative lateral forces applied to each column during the test is referred to as the lateral load capacity.
- *Initial lateral stiffness* — The initial lateral stiffness of each column was determined by computing the average slope of the load-displacement curve for all displacement cycles prior to initial cracking of the column.
- *Residual lateral stiffness* — The residual lateral stiffness was determined by computing the slope of the linear portion of the load-displacement curve for the largest displacement cycle prior to a distinct drop in lateral load capacity.
- *Energy dissipation* — The energy dissipated by the column over one displacement cycle was computed by calculating the area within the load-displacement curve for the cycle. These values could then be compared among columns for displacement cycles of the same magnitude or by summing the energy dissipation for all cycles.
- *Residual displacement* — After each half-cycle, the magnitude of lateral displacement at the top of the column when zero lateral load was applied was defined as the residual displacement.
- *Displacement at peak lateral load* — This parameter is defined as the displacement at the top of the column when lateral load capacity was achieved. It is useful in quantifying the column's ability to withstand deformation.
- *Longitudinal reinforcement strain* — Strain measured on the bonded longitudinal reinforcement in the column segments was indicative of the magnitude of damage to the column segments. If reinforcement strains do not exceed the yield strain of the reinforcement, the damage to the column segments will remain minor.

7.3 Lateral Load Displacement

The lateral load versus displacement graphs for each column are illustrated in Figures 159-170**.** These graphs give an effective quantitative indication of physical behavior and are used to directly compute several of the performance indicators. Two graphs are shown for each test. The first graph, designated with an "a", represents loading up to +/- 2.5 in. of lateral displacement. For the segmented columns, the fuse plates had yielded and buckled by this

stage and were replaced to repair the column. The second graph indicates the performance of the column after the fuse plates had been replaced. Although no attempt was made to repair the Column 1, two graphs are shown for this column for comparison purposes. The first graph is for cycles up to +/- 2.5 in. displacement and the second is for the entire test.

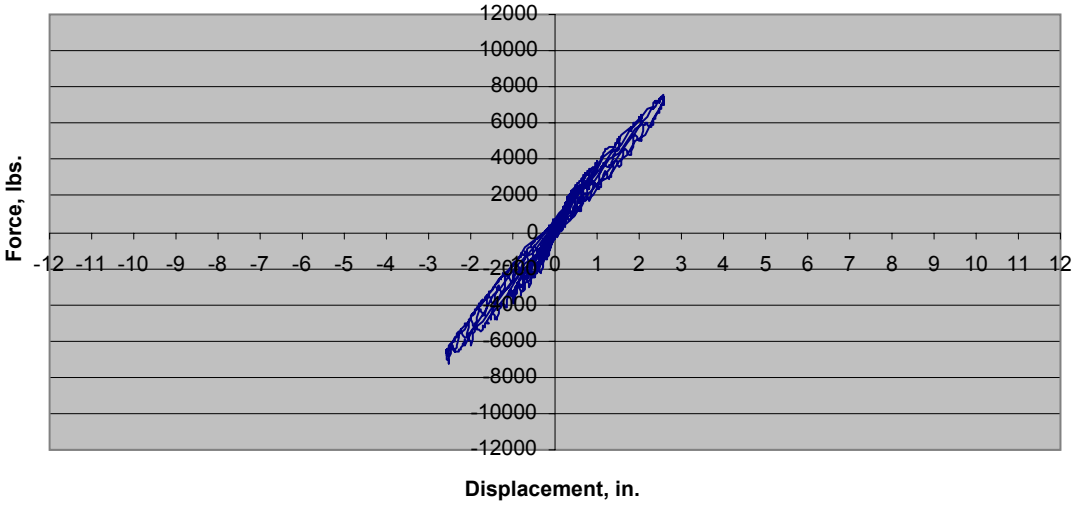

Figure 159. Test 1 load vs. displacement hysteresis through Cycle 16.

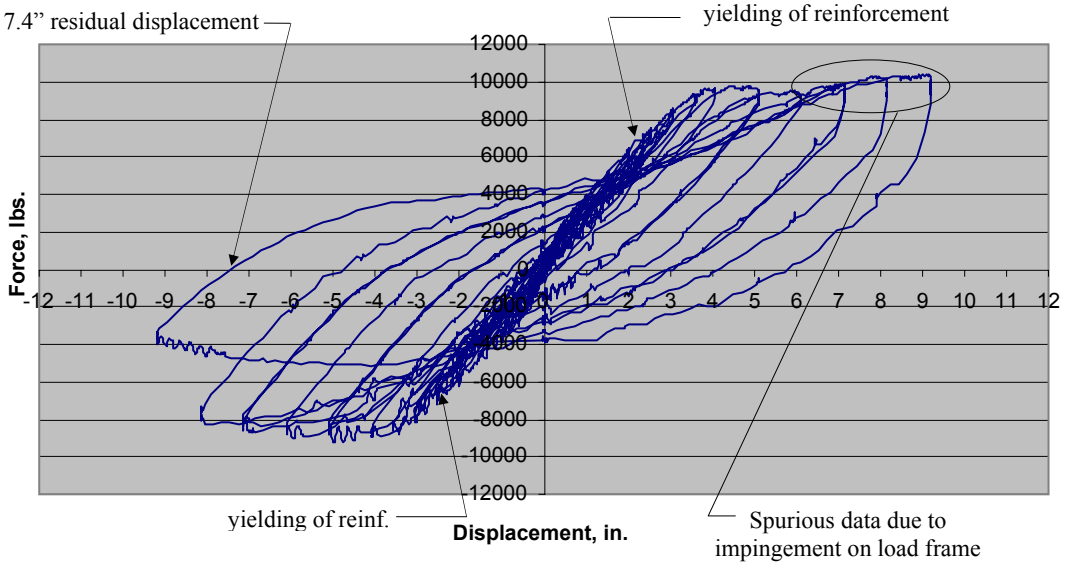

Figure 160. Test 1 load vs. displacement hysteresis.

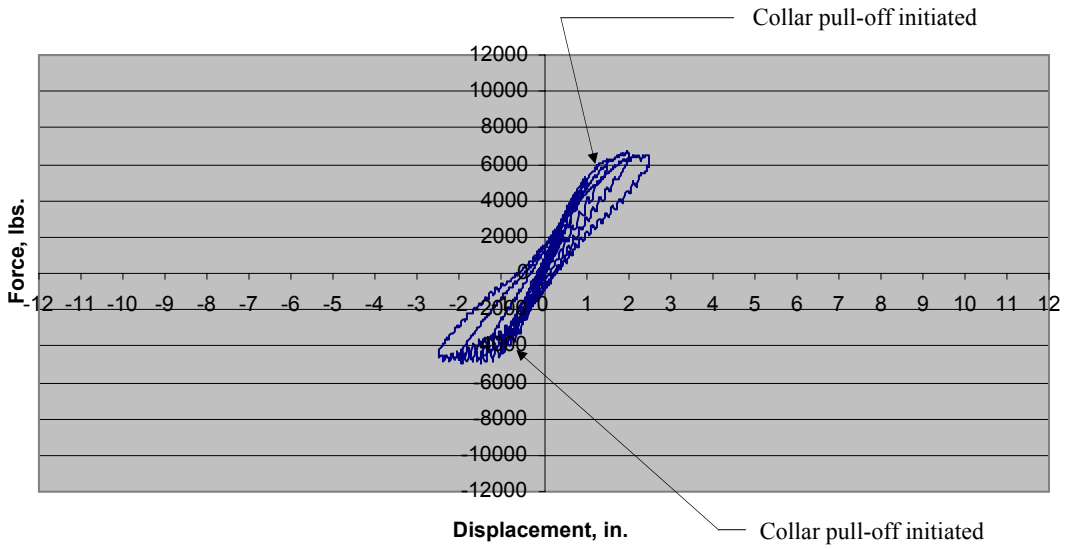

Figure 161. Test 2a load vs. displacement hysteresis.

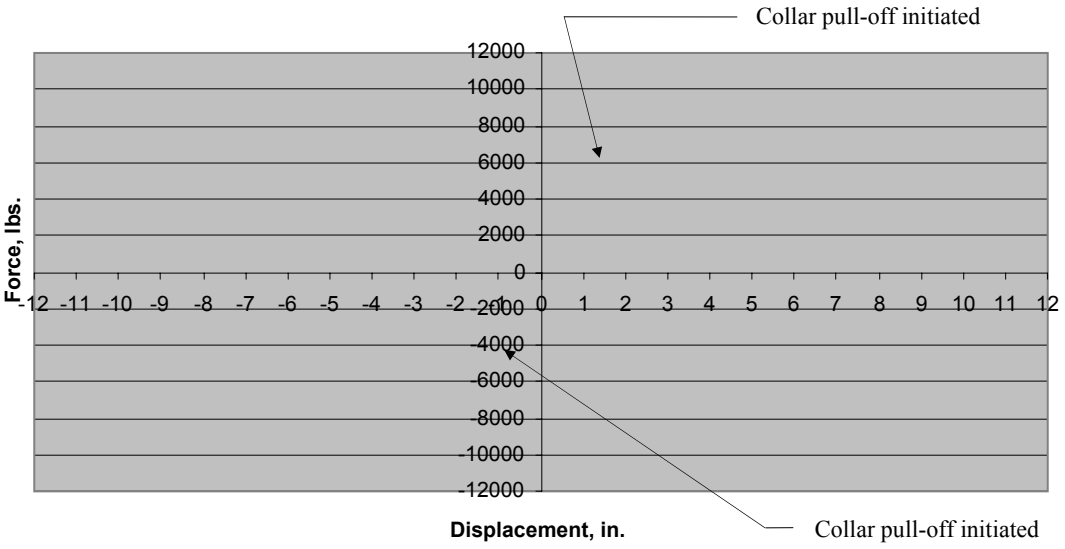

Figure 162. Test 2b load vs. displacement hysteresis.

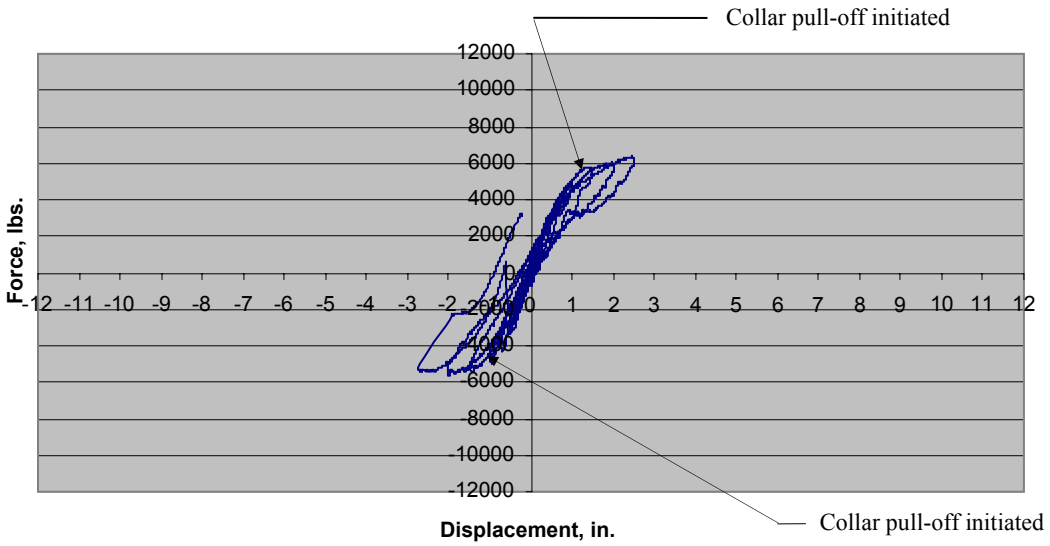

Figure 163. Test 3a load vs. displacement hysteresis.

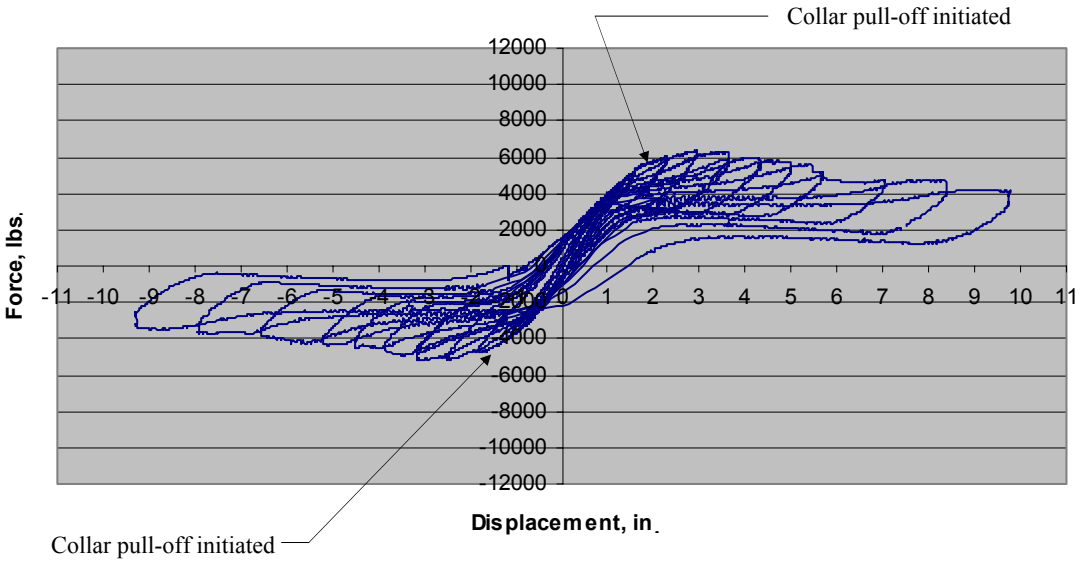

Figure 164. Test 3b load vs. displacement hysteresis.

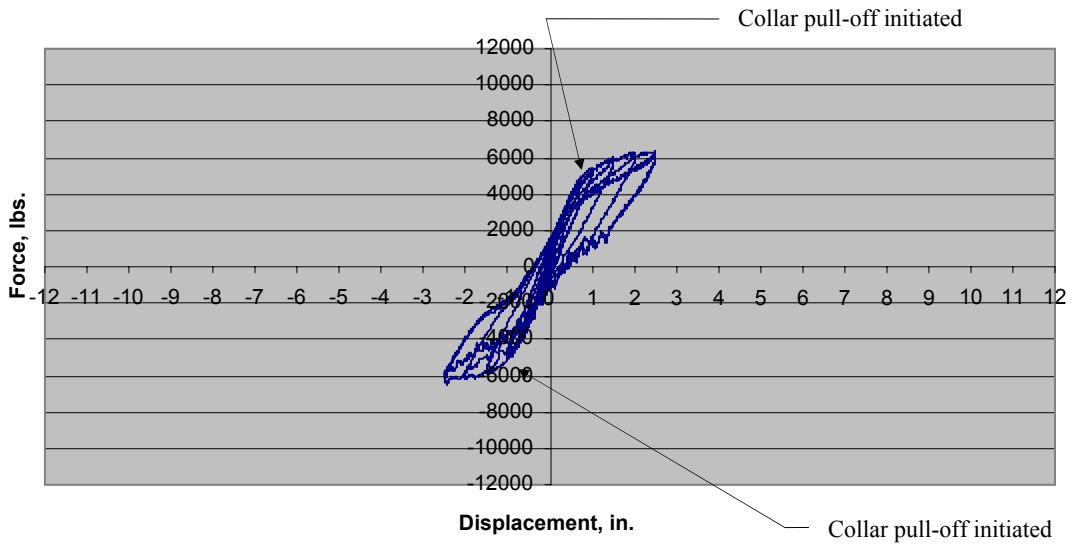

Figure 165. Test 4a load vs. displacement hysteresis.

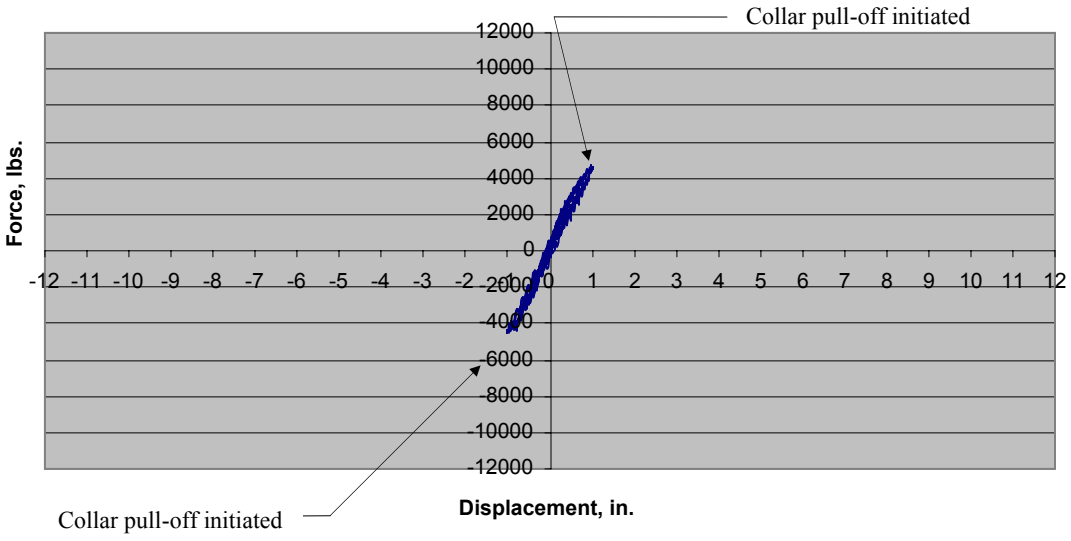

Figure 166. Test 4b load vs. displacement hysteresis.

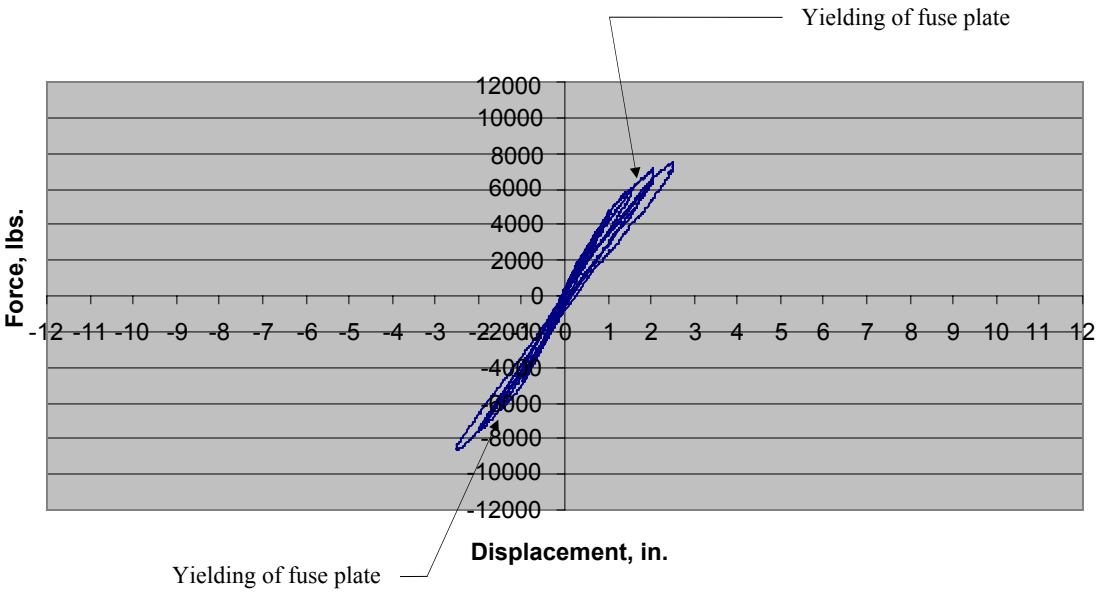

Figure 167. Test 5a load vs. displacement hysteresis.

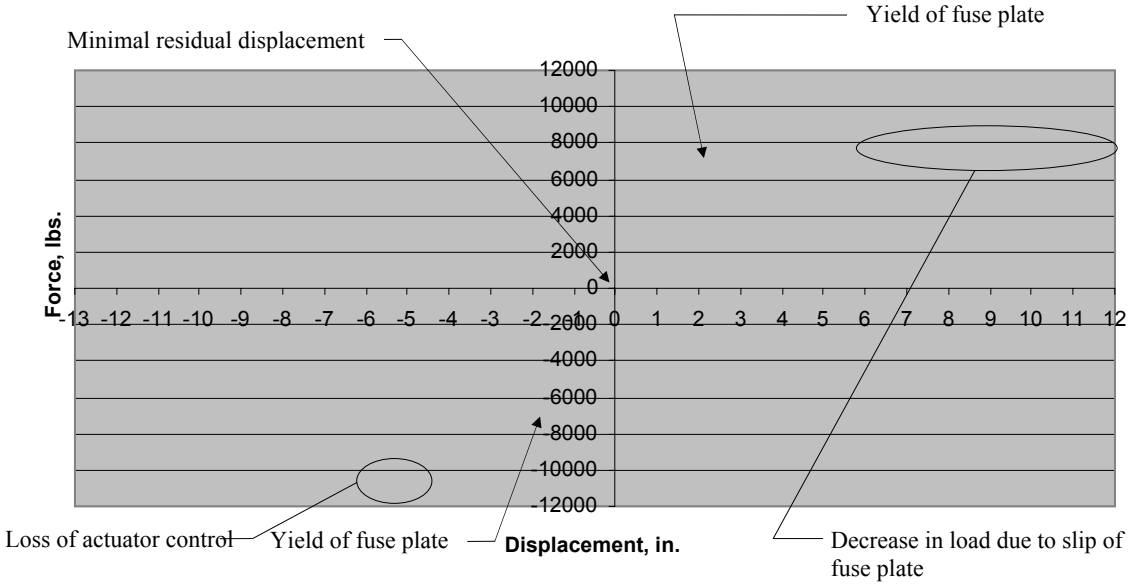

Figure 168. Test 5b load vs. displacement hysteresis.

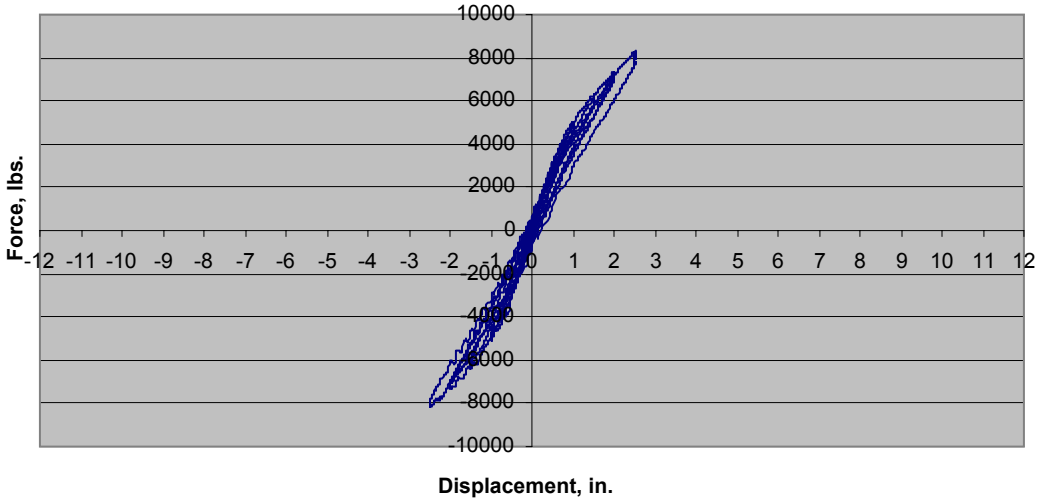

Figure 169. Test 6a load vs. displacement hysteresis.

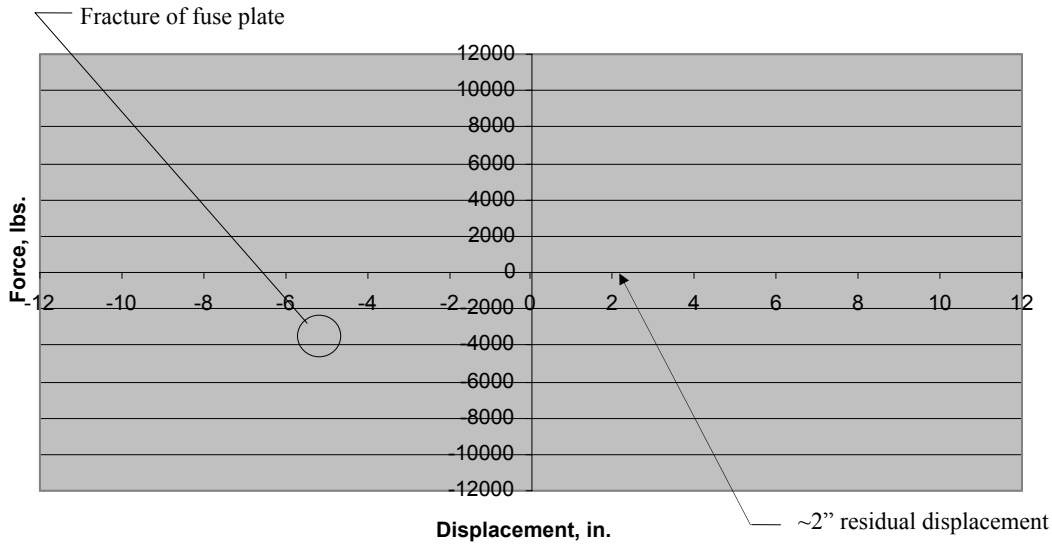

Figure 170. Test 6b load vs. displacement hysteresis.

7.4 Lateral Load Capacity and Displacement at Peak Lateral Load

7.4.1 Column 1

At a displacement of + 4.55 in., Column 1 resisted its maximum load of + 9.70 kips during the positive (push) half-cycle. Once this load was reached on Cycle 21, the maximum lateral loads sustained on subsequent cycles diminished significantly. Note that the load-displacement graph displays spurious values for the last four cycles on the positive (push) side of the graph, because the load beam impinged on the load frame as the column began to tilt to the south (see Figure 164). The expected result of the positive (push) portion of the hysteresis would be similar to the negative (pull) portion. Therefore, the negative portion of the hysteresis was considered representative of for both portions at displacements greater than + 6 in. (see Figures 159 and 160).

7.4.2 Columns 2-4

Results for Columns 2, 3, and 4 are not presented in Table 4 because their lateral load capacities were diminished due to the failure mechanism discussed previously. Lateral load versus lateral displacement hysteresis for each of these tests is shown in Figures 161-166.

7.4.3 Column 5

Column 5 resisted a maximum load of - 9.25 kips on Cycle 21b at a displacement of - 4.98 in. Unlike Column 1, Column 5 maintained at least 85% of its lateral load capacity throughout the largest displacements allowed by the actuator. The decrease in load was caused by slippage at the fuse plate connection; as the through-bolts began to bear on the bolt holes in the fuse plates, yielding of the fuse plates across the reduced section through the holes occurred instead of through the gross section at the centerline of the fuse plate, causing a reduction in moment capacity. The maximum displacement for this column was limited by the actuator, which reached maximum stroke at + 11.19 in. on the positive (push) side and - 12.00 in. on the negative (pull) side (see Figures 167 and 168).

7.4.4 Column 6

Column 6 sustained the largest loads of any of the columns tested. It resisted a maximum lateral load of - 10.48 kips on Cycle 23b at - 5.87 in. displacement on the negative (pull) half-cycle, while a + 10.13 kip load on the positive (push) half-cycle was achieved. Maximum loads on subsequent cycles for Column 6 remained at or above 90% in the positive direction and above 86% in the negative direction of the absolute maximum loads sustained during the test. Testing was stopped shortly after the fracture of the fuse plate on the south side of the column caused tilting perpendicular to the loading direction. Additionally, the full stroke of the actuator was achieved on the positive (push) portion of the loading regimen (see Figures 169 and 170).

Table 4. Lateral load capacity.

Column #	Lateral Load (kips)	Cycle #	Displacement, in.
1 (+)	9.7	21 (5 in.)	4.55
1 (-)	-9.2	21 (5 in.)	-4.99
1 (mean of absolute value of +/-)	9.45		
5 (+)	8.88	21 (5 in.)	4.91
5 (-)	-9.25	21 (5 in.)	-4.98
5 (mean of absolute value of +/-)	9.07		
6 (+)	10.13	24 (7 in.)	6.87
6 (-)	- 10.48	23 (7 in.)	- 5.87
6 (mean of absolute value of +/-)	10.31		

7.5 Initial Lateral Stiffness and Residual Lateral Stiffness

7.5.1 Column 1

Column 1 exhibited an initial lateral stiffness of 6,300 lbs/in. during its cycles prior to cracking. By Cycle 13 (+/- 1.5 in. lateral displacement), its lateral stiffness was reduced by nearly half of this initial value. On Cycle 26 (+/- 8 in. lateral displacement), the calculated stiffness was 710 lbs/in. This reduction was due to the large amount of damage near the base

of the column. As shown in Chapter 6, there was visual evidence that the longitudinal reinforcement experienced localized buckling 12 in. above the base of the column during later displacement cycles.

7.5.2 Columns 2-4

Columns 2, 3, and 4 exhibited initial lateral stiffnesses between 6,770 lbs/in. and 8,000 lbs/in. These values were largely unaffected by the collar pull-off mechanism that later developed during the tests, since the column behavior at small displacements was dominated by the effect of the post-tensioning. The largest initial lateral stiffness value, which was exhibited by Column 4, was additionally influenced by the retrofit angles that were added at the base of the column. The lateral stiffness values of all three of these columns remained well above that of the control column. After the replacement of the plates, even with the collar pull-off mechanism partially developed, the stiffness was over 80% of the initial stiffness and approximately the same as the control column's initial stiffness. Throughout the remainder of each of these tests, the stiffness values of these columns remained greater than that of Column 1.

7.5.3 Column 5

Column 5 exhibited an initial lateral stiffness of approximately 6,660 lbs/in and remained above 5,000 lbs/in. until Cycle 14a (+/- 2 in. displacement). Comparatively, the control column remained above 5,000 lbs/in. until Cycle 8 at a +/- 0.5 in. displacement. After the replacement of fuse plates, the lateral stiffness of Column 5 was 4,750 lbs/in. (~71% of initial). The stiffness gradually dropped over the duration of the Test b to 2,110 lbs/in. at +/- 12 in. displacement.

It should be noted that part of the reduction in stiffness during testing of Column 5 was due to the slippage in the connection between the fuse plates and the steel collars. Furthermore, once buckling had occurred in the fuse plates, the lateral stiffness of the column was reduced on subsequent cycles because the force required to straighten the fuse plate after buckling was much less than when the fuse plate was in direct tension. This behavior is further evident in the load-displacement relationship (see Figure 168). A marked increase in stiffness is

apparent at larger displacements when the buckled fuse plate is straightened and begins to experience direct tension.

7.5.4 Column 6

Column 6 exhibited an initial lateral stiffness of 6,600 lbs/in. Its lateral stiffness remained above 6,000 lbs/in. until it reached 1 in. displacement. Immediately after the fuse plates were replaced, a stiffness of 5,380 lbs/in. (81% of initial lateral stiffness) was computed for the column. The column's stiffness remained over 4,000 lbs/in. until the +/- 2.5 in. displacement cycle when its lateral stiffness began to degrade more severely. At the maximum displacement, Column 6 exhibited a lateral stiffness of 1,010 lbs/in.

The mild degradation of lateral stiffness relative to the other jointed columns displayed by Column 6 until Cycle 16a (displacement = +/- 2.5 in.) displacement cycle was largely due to the SMA fuse plates. Since the degree of buckling in these fuse plates was minor, the fuse plates straightened much earlier on each cycle when loading was reversed. Also, the higher yield strength of the SMA plates caused more extensive concrete cracking and higher stresses in bonded reinforcement in Column 6 than in Column 5.

As illustrated in Figure 171, the initial lateral stiffness values of Columns 5 and 6 for displacement cycles out to +/- 2.5 in. were both notably higher than those of Column 1. Furthermore, the stiffness values of these columns had smaller reductions in stiffnesses than Column 1 on each subsequent cycle during Test a. Comparing stiffness values presented in Figure 172 for Test b shows that Column 5 had the highest residual lateral stiffness values during larger displacement cycles. The stiffness values of Column 6 at larger displacements, while lower than those achieved by Column 5, were still significantly higher than the stiffness values of Column 1. Additional column stiffness data are presented in Table 5.

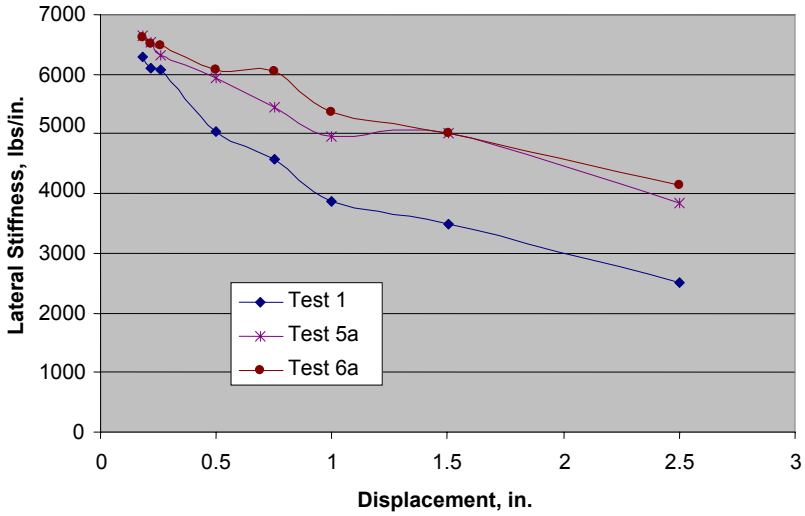

Figure 171. Test "a" lateral stiffness comparisons between Columns 1, 5, and 6.

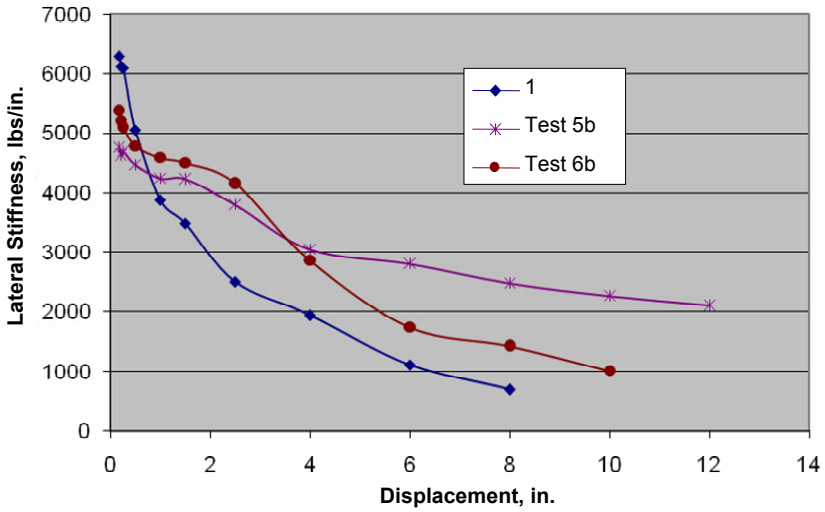

Figure 172. Test "b" lateral stiffness comparisons between Columns 1, 5, and 6.

Table 5. Lateral stiffness.

Test cycle	Displacement, in.	Test 1	Test 2	Test 3	Test 4	Test 5	Test 6
original fuse plates in place							
2a to 3a	0.18	6290	6770	7720	8000	5490	6620
3a to 4a	0.22	6100	6230	7470	7950	5680	6520
4a to 5a	0.26	6090	6530	7310	7810	5610	6500
7a to 8a	0.50	5050	6030	6600	7160	5180	6080
9a to 10a	0.75	4580	5750	6400	7070	5320	6060
10a to 11a	1.00	3880	5130	5560	6320	5120	5370
12a to 13a	1.50	3490	4670	5010	5540	5010	5010
15a to 16a	2.50	2500	3250	3770	3110	3830	4140
after fuse plate replacement							
2b to 3b	0.18	6290	5580	N/A	6460	4760	5380
3b to 4b	0.22	6110	5390	N/A	6230	4630	5220
4b to 5b	0.26	6090	5190	N/A	6150	4690	5100
7b to 8b	0.50	5050	4720	N/A	5700	4460	4780
10b to 11b	1.00	3880	4340	5550	5300	4240	4580
12b to 13b	1.50	3490	4130	5300	5090	4230	4500
15b to 16b	2.50	2500	2660	3980	3290	3800	4160
19b to 20b	4.00	1950	2320	3090	2580	3050	2858
22b to 23b	6.00	1120	1330	2890	1530	2810	1750
25b to 26b	8.00	710				2480	1430
27b to 28b	10.00					2270	1010
29b to 30b	12.00					2110	
**Note:	Test 1a results are given in the b cycles for comparison purposes Results are in units of lbs./in.						

7.6 Energy Dissipation

Dissipation of hysteretic energy provides an indication of a structure's ability to withstand a dynamic load and to dampen vibration. In typical reinforced concrete structures, the primary mechanism for energy dissipation is through yielding of bonded reinforcement which leads to large residual deformations. Structures that behave elastically until failure raise concerns of resonant vibrations and brittle failure modes. Thus, there would appear to be a tradeoff between energy dissipation and residual deformation. Comparisons of load vs. displacement behavior among Columns 1, 5 and 6 reveal this inverse relationship between energy dissipation and residual displacements. It should be noted that Column 5, while exhibiting small residual deformations, was able to dissipate a significant amount of hysteretic energy through yielding of its fuse plates.

7.6.1 Column 1

Relative to the other test columns, Column 1 exhibited significantly more hysteretic energy dissipation. Once the bonded bars in the column began to yield and major cracking and spalling of the concrete were observed, this amount increased significantly. Through Cycle 27b 795,540 in.-lbs. of hysteretic energy was dissipated. As previously discussed, this ability to dissipate energy was achieved primarily through yielding of bonded reinforcement leading to the relatively large residual deformations observed for Column 1. Note that the calculated energy dissipation for Cycles 24b-27b were corrected for the spuriously high lateral loads recorded on the positive (push) half-cycles caused by the impingement of the load beam against the lateral load frame.

7.6.2 Columns 2-4

Columns 2, 3, and 4 exhibited larger amounts of energy dissipation than the control column during the few cycles prior to the +/- 2.5 in. cycle in Test a. This can be attributed to yielding of the fuse plates. Damage accrued through the collar pull-off mechanism also contributed to energy dissipation on these cycles for the first three jointed columns.

7.6.3 Column 5

Column 5 exhibited less hysteretic energy dissipation than Columns 1 and 6. Up to fuse plate replacement, Column 5 had dissipated 15,060 in.-lbs., approximately 52% of that dissipated by Column 1 over the same displacement regimen. After the fuse plates were replaced, energy dissipated by Column 5 was 27% that of the Column 1 through Cycle 27b since yielding of the bonded reinforcement within the segments was prevented. As designed, yielding occurred only in the fuse plates experiencing direct tension. The energy dissipation capacity for jointed columns could be increased by using multiple joints without sacrificing the small residual displacements observed.

7.6.2 Column 6

Because the higher yield strength of the SMA fuse plates relative to the A36 fuse plates, which allowed limited yielding of bonded reinforcement within the Column 5 segments,

Column 6 exhibited greater amounts of energy dissipation than Column 5. Even so, these amounts were still significantly less than those achieved in Column 1. Prior to replacement of the fuse plates, Column 6 dissipated 19,640 in.-lbs, 68% that dissipated by the control column. After plate replacement, Column 6 dissipated 35% of the energy dissipated by Column 1 through Cycle 27b.

Energy dissipation data for Columns 1, 5, and 6 are presented in Table 6, while a comparison between the three columns' energy dissipation is illustrated by Figure 173. As shown by this table, Columns 5 and 6 both dissipated over half the amount of energy Column 1 dissipated up to the +/- 2.5 in. displacement cycle. After that, however, Column 1 dissipated an increasingly larger amount of energy than the segmented columns. There are a number of possible means of increasing the energy dissipation capacity of the jointed system, such as developing details to prohibit buckling of the fuse plates when loaded in compression. One of the most promising possibilities, which would likely not sacrifice the small residual deformations achieved, would be to employ multiple joints to allow additional fuse plates to yield. This requires additional investigation since such was beyond the scope of this study.

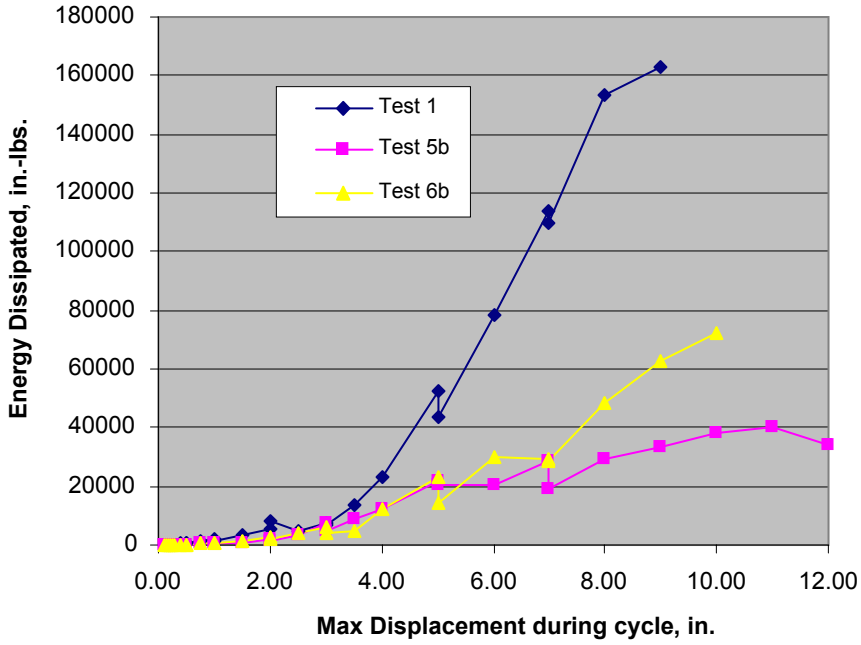

Figure 173. Test "b" energy dissipation comparisons between Columns 1, 5, and 6.

Table 6. Energy dissipation.

Test cycle	Displacement, in.	Test 1	Test 2	Test 3	Test 4	Test 5	Test 6
original fuse plates in place							
1a	0.10		30	30	50	30	20
2a	0.14		40	40	40	50	40
3a	0.18		60	30	60	60	50
4a	0.22		80	50	80	70	60
5a	0.26		120	70	110	100	70
6a	0.30		130	120	150	120	100
7a	0.40		240	280	320	170	170
8a	0.50		360	480	490	240	270
9a	0.50		330	350	350	220	260
10a	0.75		1090	1140	1410	400	1030
11a	1.00		1660	1890	2730	560	1500
12a	1.00		1190	1270	2360	450	1030
13a	1.50		4140	3930	5810	2300	2950
14a	2.00		7330	6120	8930	3490	4060
15a	2.00		10490	8870	11660	2180	2400
16a	2.50			9560	9440	4620	5630
After Replacement of Plates							
1b	0.10	50	30	N/A	0	30	20
2b	0.14	70	40	N/A	50	50	40
3b	0.18	100	60	N/A	60	70	60
4b	0.22	150	80	N/A	50	90	70
5b	0.26	230	100	N/A	120	90	90
6b	0.30	250	120	N/A	100	120	110
7b	0.40	510	190	N/A	190	130	190
8b	0.50	850	290	360	N/A	250	270
9b	0.50	510	310	N/A	220	240	250
10b	0.75	1530	690	760	700	430	450
11b	1.00	1790	1240	1380	1360	670	680
12b	1.00	1160	1140	N/A	1120	610	640
13b	1.50	3340	3380	3640	4070	980	1310
14b	2.00	5790	6950	5960	6610	1870	2850
15b	2.00	7880	10240	8900	10550	1160	1910
16b	2.50	4690	9060	7230	7440	3460	4110
17b	3.00	7820	12910	10000	12530	7340	6400
18b	3.00	6580	11230	N/A	7600	4870	4310
19b	3.50	13850	14470	12400	N/A	8820	4720
20b	4.00	23450	17290	13340	18440	12030	12390
21b	5.00	52490	25330	17580	28260	21930	22970
22b	5.00	43590	31540	22740	25750	20290	14050
23b	6.00	78200		31430	40130	20130	30250
24b	7.00	113810				28520	29380
25b	7.00	110070				19200	28480
26b	8.00	153710				29130	48440
27b	9.00	163070				33720	62840
28b	10.00					38480	72490
29b	11.00					39900	
30b	12.00					33820	
**Note:	Units are in in.-lbs.						

7.7 Residual Displacement

7.7.1 Column 1

The residual displacements exhibited by Column 1 remained relatively small (<0.8 in.) through Cycle 20 (+/- 4.0 in.). A significant increase up to an average of 1.48 in. residual displacement was observed during Cycle 21 (+/- 5.0 in.). As greater lateral displacements were imposed, residual displacements accrued rapidly. On the final cycle, Column 1 exhibited residual displacements of + 5.78 in. on the positive (push) half-cycle and - 7.40 in. on the negative (pull) half-cycle. These values were 64% and 82% respectively of the maximum displacements of +/- 9.0 in.

7.7.2 Columns 2-4

Columns 2, 3, and 4 experienced small initial residual displacements. However, once the collar pull-off mechanism initiated, the residual displacements increased rapidly. After this mechanism began to control the behavior of these columns, the data were no longer useful for comparisons among other columns. Therefore, results for these tests are excluded from Table 7.

7.7.3 Column 5

Column 5 exhibited negligible residual displacements through Cycle 16a when the fuse plates were replaced. During the test's “b” cycles, the residual displacements remained less than 0.22 in. on average of both the positive and negative half-cycles. Associated with these smaller residual displacements was a more pronounced opening of the construction joint during larger displacement cycles, as well as a reduction in column cracking relative to the other columns tested. Such small residual displacements indicated that the column remained nearly elastic with minimal damage to the column segments.

7.7.4 Column 6

Column 6 experienced residual displacements less than 0.2 in. prior to fuse plate replacement. After the fuse plates were replaced, residual displacements remained negligible

through Cycle 15b (+/- 2.0 in.). These residual displacements increased steadily as cycling continued, and at the maximum displacement of +/- 10 in., they reached an average value of 1.91 in. between the positive and negative half-cycles (See Table 7).

The relative magnitudes of the mean residual displacements for each displacement cycle are graphed in Figure 174. It can be seen that, prior to fuse plate replacement at a displacement of 2.5 in., Column 1 exhibited slightly higher residual displacements than Columns 5 and 6. However, the relative displacement gap between the control column and the segmented columns grew significantly after the 3 in. displacement cycle.

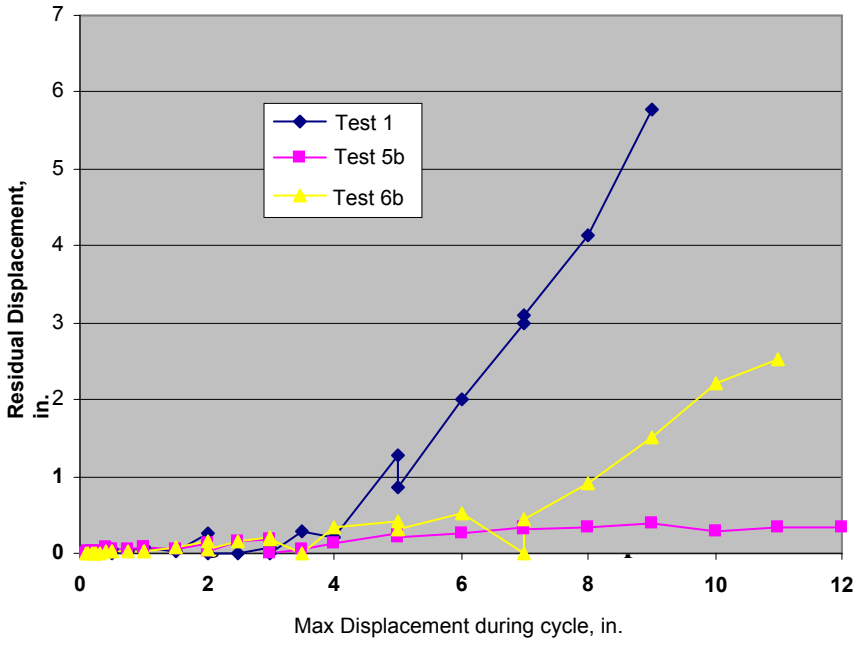

Figure 174. Test "b" residual displacements.

Table 7. Residual displacements.

Test cycle	Displacement, in.	Test 1 (+)	Test 1 (-)	Test 5 (+)	Test 5 (-)	Test 6 (+)	Test 6 (-)
original fuse plates in place							
1a	0.10			0.06	-0.08	0.00	-0.02
2a	0.14			-0.05	-0.08	0.01	-0.02
3a	0.18			-0.06	-0.08	0.00	-0.02
4a	0.22			-0.04	-0.08	0.01	-0.02
5a	0.26			-0.05	0.00	0.07	-0.02
6a	0.30			-0.04	-0.09	0.01	-0.01
7a	0.40			-0.04	-0.10	0.01	-0.03
8a	0.50			-0.04	-0.09	0.01	-0.04
9a	0.50			-0.03	-0.09	0.02	-0.04
10a	0.75			-0.03	-0.09	0.07	-0.06
11a	1.00			-0.02	-0.08	0.07	-0.09
12a	1.00			-0.04	-0.08	0.06	-0.07
13a	1.50			0.05	-0.13	0.13	-0.13
14a	2.00			0.09	-0.09	0.15	-0.16
15a	2.00			0.12	-0.06	0.08	0.11
16a	2.50			0.21	-0.08	0.20	-0.12
after replacement of fuse plates							
1b	0.10	0.03	0.01	0.00	0.00	-0.01	-0.03
2b	0.14	0.02	0.00	0.02	-0.02	-0.01	-0.03
3b	0.18	0.02	0.00	0.04	-0.02	0.01	-0.02
4b	0.22	0.01	0.00	0.04	0.00	0.01	-0.01
5b	0.26	0.01	-0.01	0.00	-0.02	0.00	-0.04
6b	0.30	0.01	-0.02	0.03	0.00	0.01	-0.04
7b	0.40	0.03	-0.04	0.08	0.00	0.02	-0.03
8b	0.50	0.05	-0.05	0.04	-0.03	0.03	-0.04
9b	0.50	0.01	-0.04	0.05	-0.02	0.03	-0.01
10b	0.75	0.02	-0.09	0.05	0.00	0.02	-0.03
11b	1.00	0.09	-0.12	0.07	0.00	0.04	-0.04
12b	1.00	0.09	-0.09	0.08	-0.02	0.03	-0.02
13b	1.50	0.03	-0.20	0.05	-0.02	0.07	-0.06
14b	2.00	0.27	-0.23	0.12	0.02	0.15	-0.04
15b	2.00	0.01	-0.28	0.04	0.00	0.06	-0.09
16b	2.50	0.00	-0.25	0.15	0.06	0.16	-0.06
17b	3.00	0.09	-0.34	0.18	0.06	0.21	-0.17
18b	3.00	0.00	0.32	N/A	N/A	0.19	-0.12
19b	3.50	0.29	-0.47	0.05	-0.17	N/A	-0.20
20b	4.00	0.22	-0.78	0.13	-0.17	0.33	-0.16
21b	5.00	1.27	-1.68	0.25	0.03	0.42	-0.38
22b	5.00	0.87	-1.62	0.22	-0.02	0.30	-0.30
23b	6.00	2.00	-2.58	0.27	-0.07	0.51	-0.51
24b	7.00	2.98	-3.69	0.34	-0.05	N/A	-0.86
25b	7.00	3.10	-3.77	0.31	0.01	0.44	-0.75
26b	8.00	4.14	-4.78	0.35	0.05	0.90	-1.20
27b	9.00	5.78	-7.40	0.38	0.06	1.51	-1.34
28b	10.00			0.29	-0.09	2.21	-1.62
29b	11.00			0.33	-0.04	2.52	-0.90
30b	12.00			0.33	-0.01		
Note:	(+) and (-) denotes displacements after positive and negative half-cycles						

7.8 Longitudinal Reinforcement Strain

Longitudinal reinforcement strain data helped quantify damage sustained by the column segments throughout the tests. A strain of approximately 2,500 microstrain was associated with yielding of the bonded reinforcement used in the column segments. Once this strain level was reached in the bars, permanent deformation of the bars was assumed to occur. For strains less than the yield threshold, crack widths in the concrete segments were expected to remain small upon unloading and the column was considered to remain effectively elastic. As stated in Chapter 4, strain gages were mounted on the four corner reinforcing bars for Columns 1–4, while all six longitudinal bars had gages attached for Columns 5 and 6. Representative strain data from tests of Columns 1, 5, and 6 are presented in Figures 175-184. Strain data from tests of Columns 2-4 are not presented because the premature failure mode discussed previously limited the usefulness of this data for comparison with that recorded from Columns 1, 5, and 6. In the following figures, strain data are presented in separate graphs for the “a” and “b” portions of the Column 5 and 6 tests. The data for Column 1 are also presented in two separate graphs for comparison purposes. Data in the first of these (Figure 179) were recorded through the +/- 2.5 in. displacement cycle and compare with the “a” portion of the Column 5 and 6 tests while data in the second of these (Figure 180) were recorded for the entire test and compare with the “b” portion of the Column 5 and 6 tests.

7.8.1 Column 1

Strain gages in Column 1 were located at the base section of the column at the point of maximum moment. The data in Figure 175 indicate that the reinforcement yielded in tension on the +/- 2.5 in. displacement cycle. The data shown for the entire test in Figure 176 indicate tensile strains in the bar above 12,000 microstrain. As displacement cycles increased in magnitude, the strain leveled off at reduced levels due most likely to the formation of a plastic hinge above the gage location.

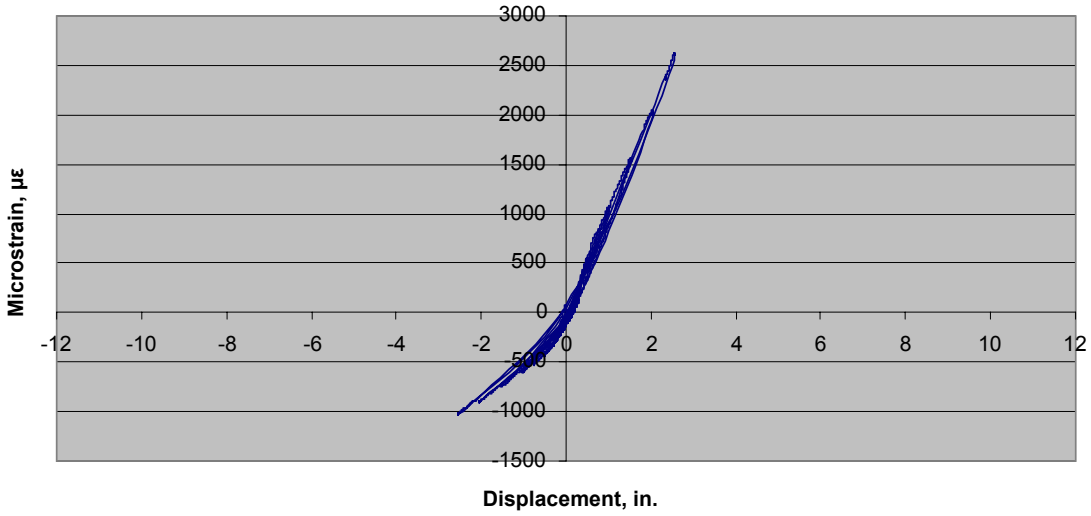

Figure 175. Column 1 longitudinal reinforcement strain through 2.5 in. displacement cycle.

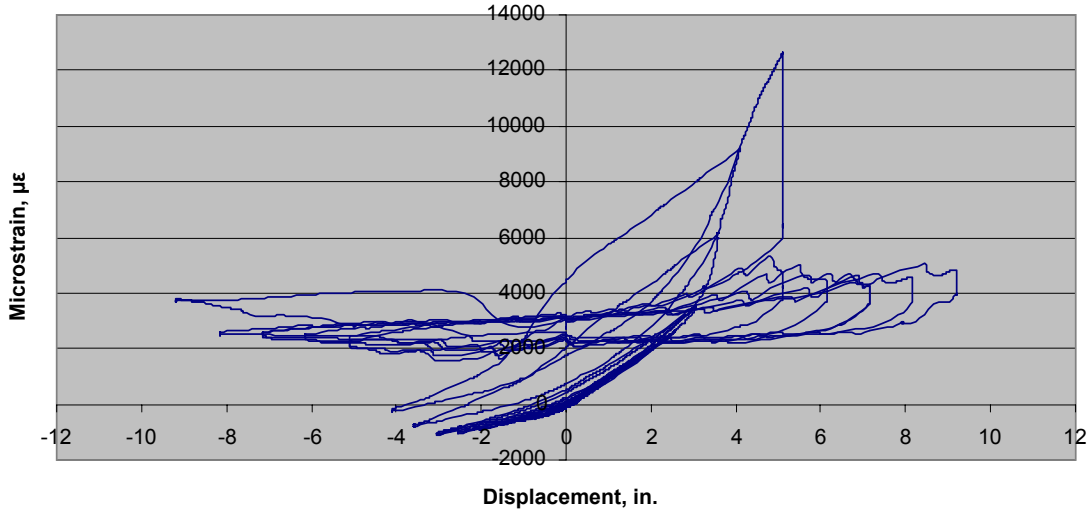

Figure 176. Column 1 longitudinal reinforcement strain for the entire test.

7.8.2 Column 5

Strain gages in Column 5 were located at the base section of the column on all six longitudinal reinforcing bars, as well as one ft. above the construction joint on all six longitudinal reinforcing bars. The strain data presented in Figures 177-180 were measured on the southwest reinforcing bars in the lower column segment and on the upper segment. The data from the "a" portion of testing (Figures 177 and 179) indicate that the bonded

reinforcement in both column segments remained below yield strain prior to replacement of the fuse plates. The data from the "b" portion of testing (Figures 178 and 180) indicate that the reinforcement approached or just exceeded yield strain at large displacements. The small strains recorded at zero displacement for all cycles indicate little permanent deformation of the column segments.

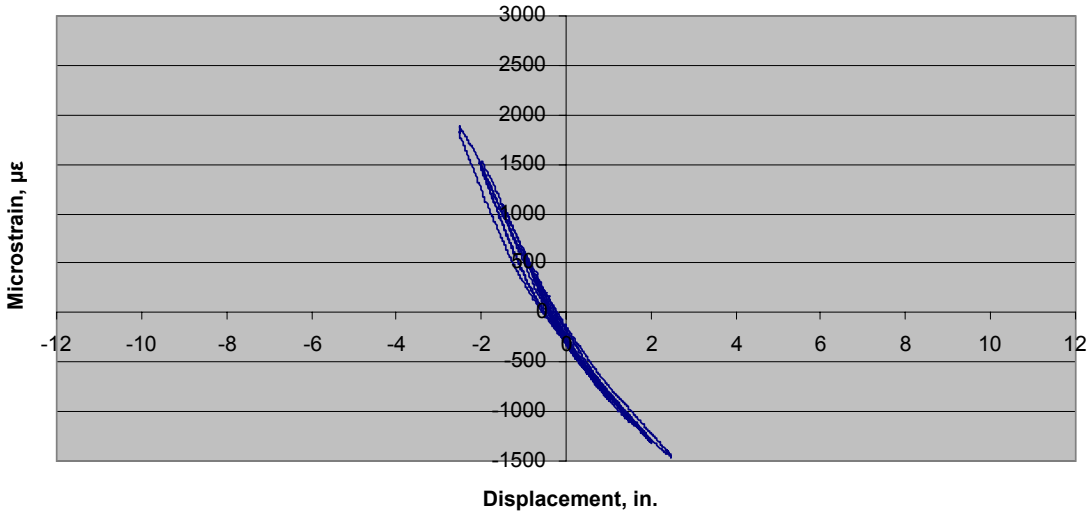

Figure 177. Column 5a lower segment longitudinal reinforcement strain.

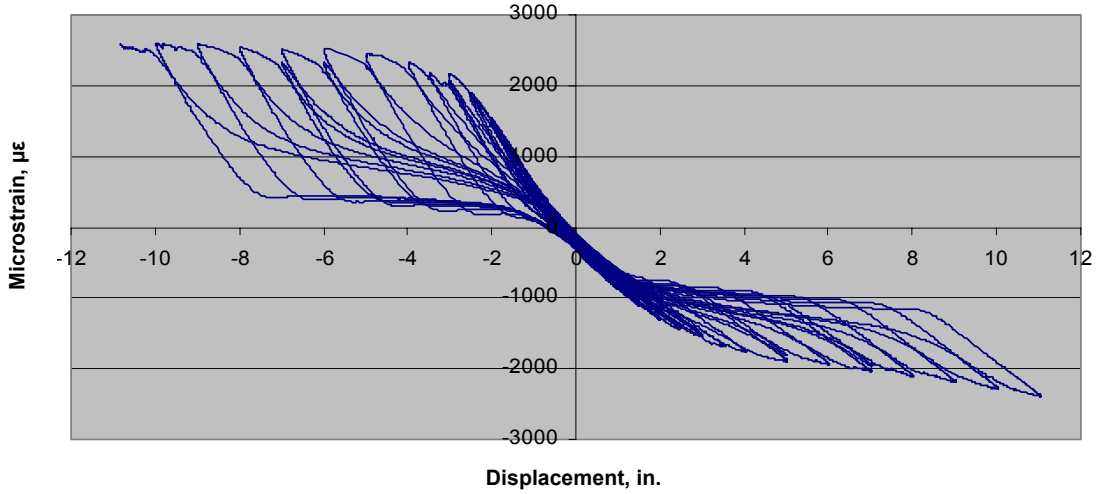

Figure 178. Column 5b lower segment longitudinal reinforcement strain.

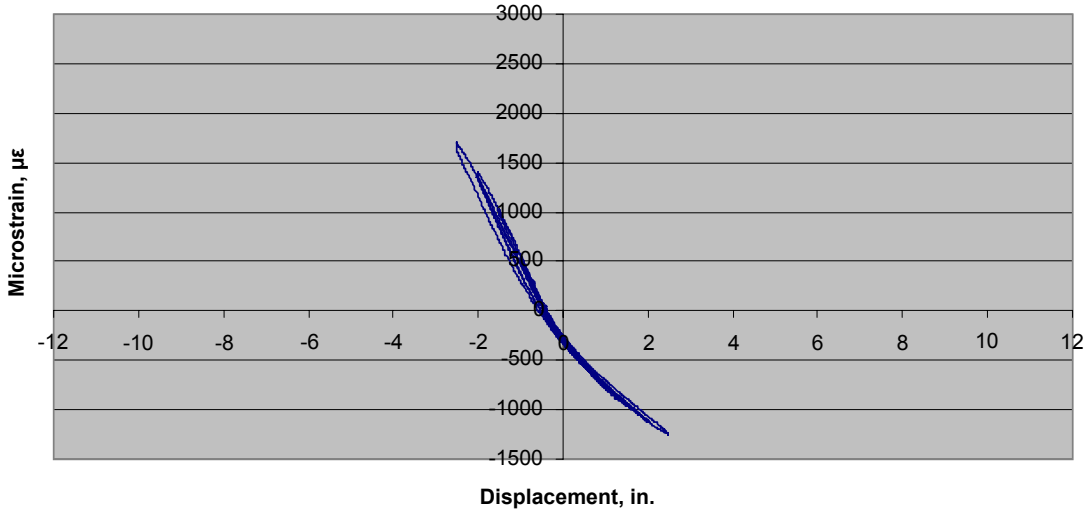

Figure 179. Column 5a upper segment longitudinal reinforcement strain.

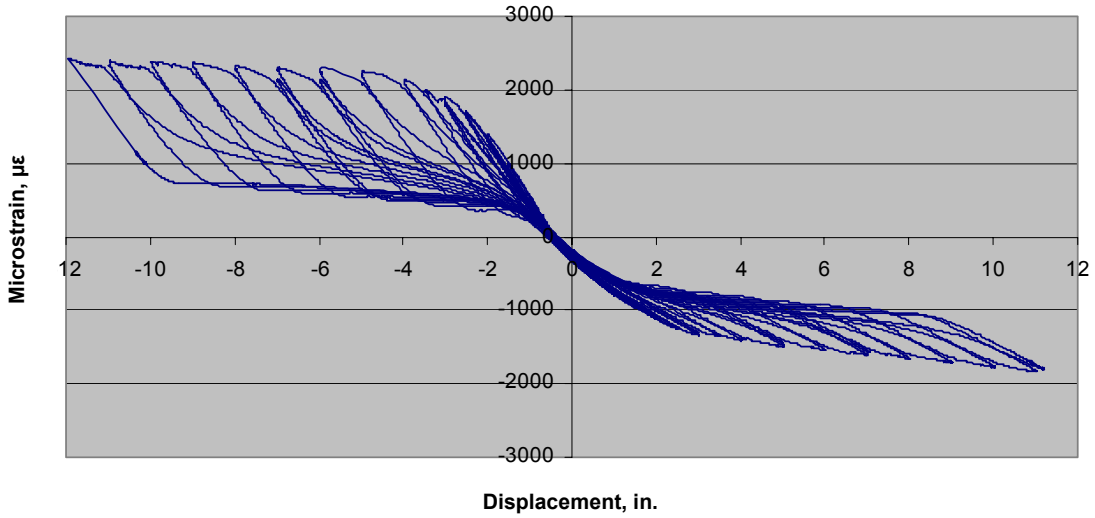

Figure 180. Column 5b upper longitudinal reinforcement strain.

7.8.3 Column 6

As in Column 5, strain gages in Column 6 were located at the base section of the column on all six longitudinal reinforcing bars, as well as one ft. above the construction joint on all six reinforcing bars. The strain data presented in Figures 181-184 were measured on the northeast reinforcing bars in the lower segment and the upper segment. The data from the "a" portion of testing (Figures 181 and 183) indicate that the reinforcement in the upper segment remained well below yield strain while the bottom column gages recorded strains

approaching yield prior to fuse plate replacement. The data from the "b" portion of testing (Figures 182 and 184) indicate that the reinforcement in the bottom column segment reached maximum tensile strain in excess of 8,000 microstrain (Figure 182), while the top column reinforcement strains reached 4,000 microstrain in tension (Figure 184). These values help to explain the increased damage and residual displacements experienced by Column 6.

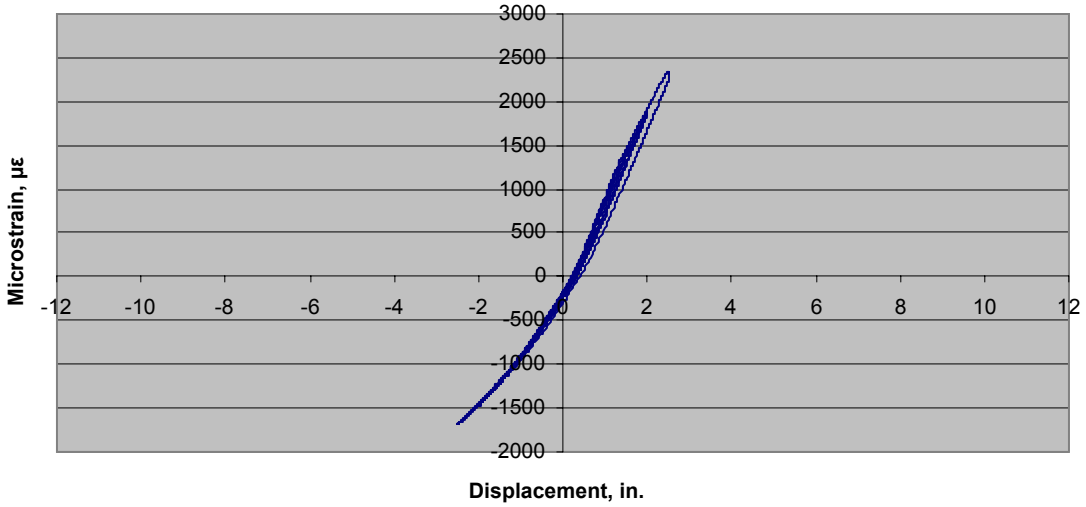

Figure 181. Column 6a lower segment longitudinal reinforcement strain.

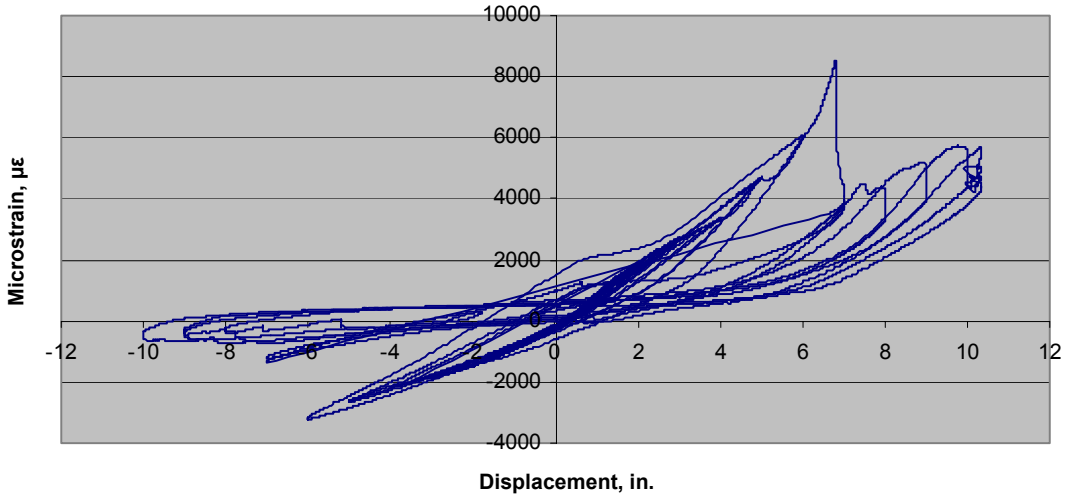

Figure 182. Column 6b lower column longitudinal reinforcement strain.

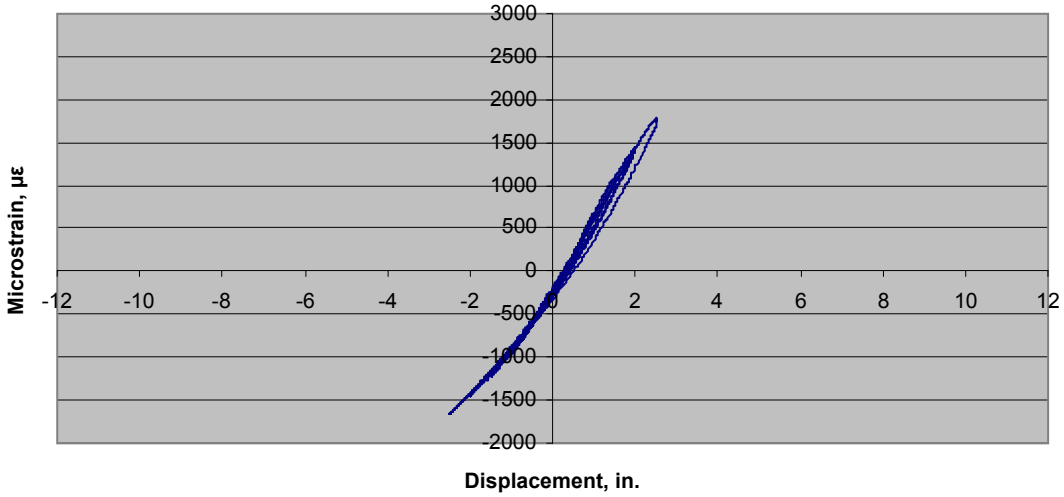

Figure 183. Column 6a upper segment longitudinal reinforcement strain.

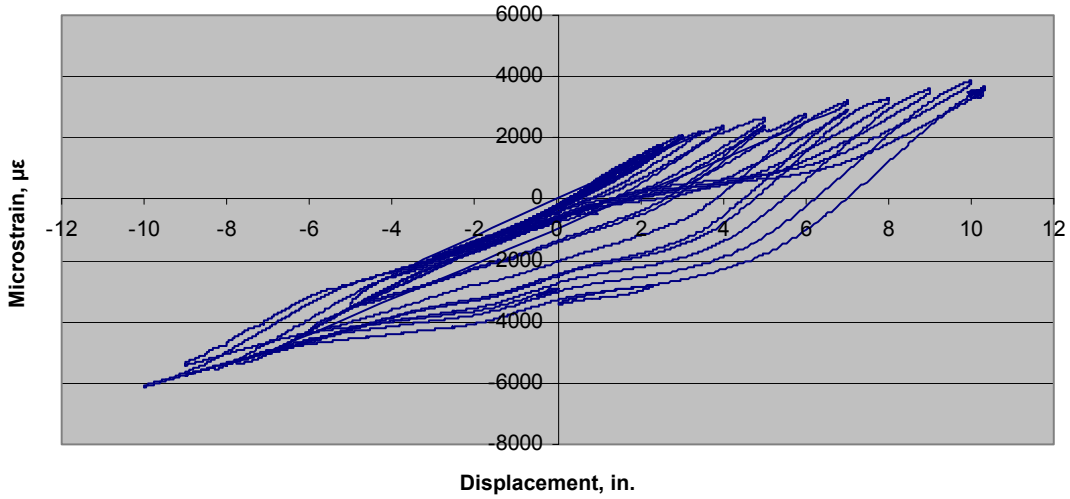

Figure 184. Column 6b upper segment longitudinal reinforcement strain.

7.9 Foundation Connection Results

While no gages were used to monitor strains in the bonded reinforcement in the foundation blocks, visual inspection revealed no cracking in the foundation concrete or in the epoxy grout at the socket connections to the columns. Additionally, rotation of the columns at the socket connection was negligible indicating effective base fixity as designed.

7.10 Analytical Predictions of Behavior

7.10.1 Outline of analytical procedure

To predict the behavior of the columns and aid in design, software using Microsoft Excel Visual Basic was developed to perform a push-over analysis for the unjointed Column 1 and the segmented columns that were tested. This software explores a simplified approach that employs traditional reinforced concrete (R/C) analysis techniques and assumptions. It is adaptable for different column sizes, materials, and reinforcement details and could be used as a design aid for subsequent laboratory tests and field applications.

In the first stage of the routine the software performs an analysis of an axially loaded, reinforced concrete cantilever that computes material stresses, strains, and lateral deflection of a typical R/C column with increasing lateral load increments. The software assumes that the user defined dead load remains constant and vertical as the column is displaced laterally while a second-order P-□ analysis for each incremental lateral load is performed. In this approach, an iterative procedure is carried out to account for the P-□ effect until the routine converges on a solution for lateral displacement within a predefined tolerance.

The second stage of the analysis deals with a jointed column with unbonded post-tensioning. Stresses and strains are computed for the construction joint materials including the fuse plates and bearing plates in order to estimate the rotation that will occur at the segment joint. The subsequent deflection of the jointed column due to the rotation at the segment joint is added to the deflection calculated for a monolithic reinforced cantilever column using the same incremental loading scheme as applied in the first stage. These two components of lateral deflection of the column are illustrated in Figure 185. A third component of deflection arising from rotation at the foundation of the column was measured and determined to be negligible for the laboratory experiments in this investigation and thus was subsequently neglected in the analysis. The total lateral deflection is then used to compute the change in post-tensioning force due to the deformation of the column. It should be noted that considerable computational complexity is created with the addition of unbonded post-tensioning because the traditional assumption of strain compatibility across a section is not valid. To calculate the effect of the unbonded post-tensioning, the deformation of the entire

member must be considered. Program logic is illustrated more formally in the flowchart shown in Figure 186.

a.) Column deflection due to column bending **b.) Column deflection due to joint rotation**

Figure 185. Components of lateral deflection of a jointed column.

7.10.2 Analysis of an unjointed column

Two distinct phases of analysis are performed as the unjointed, R/C cantilever column model is subjected to vertical loading plus increasing lateral loads. In the first phase, lateral deflections are computed up to the point that the bonded longitudinal reinforcement yields in tension. In the second phase, the nominal moment capacity of the column and the associated lateral deflections are computed. Deflections corresponding to lateral loads between the points of yielding and nominal moment capacity are then back-calculated using simple linear interpolation. Assumptions for the unjointed cantilever stage of the analysis include the following.

- The effective moment of inertia, I_{eff}, as defined in Equation (2) is used for the entire column.
- Idealized elastic-plastic stress-strain behavior is assumed for the longitudinal reinforcement.
- The modulus of rupture is used to approximate tensile strength of the concrete.
- Linear strain distribution is assumed at all sections.
- Strain compatibility of concrete and bonded reinforcement is assumed at all sections.
- Concrete stress versus strain relationship remains linear up to a stress level of $0.5 \cdot f'_c$.

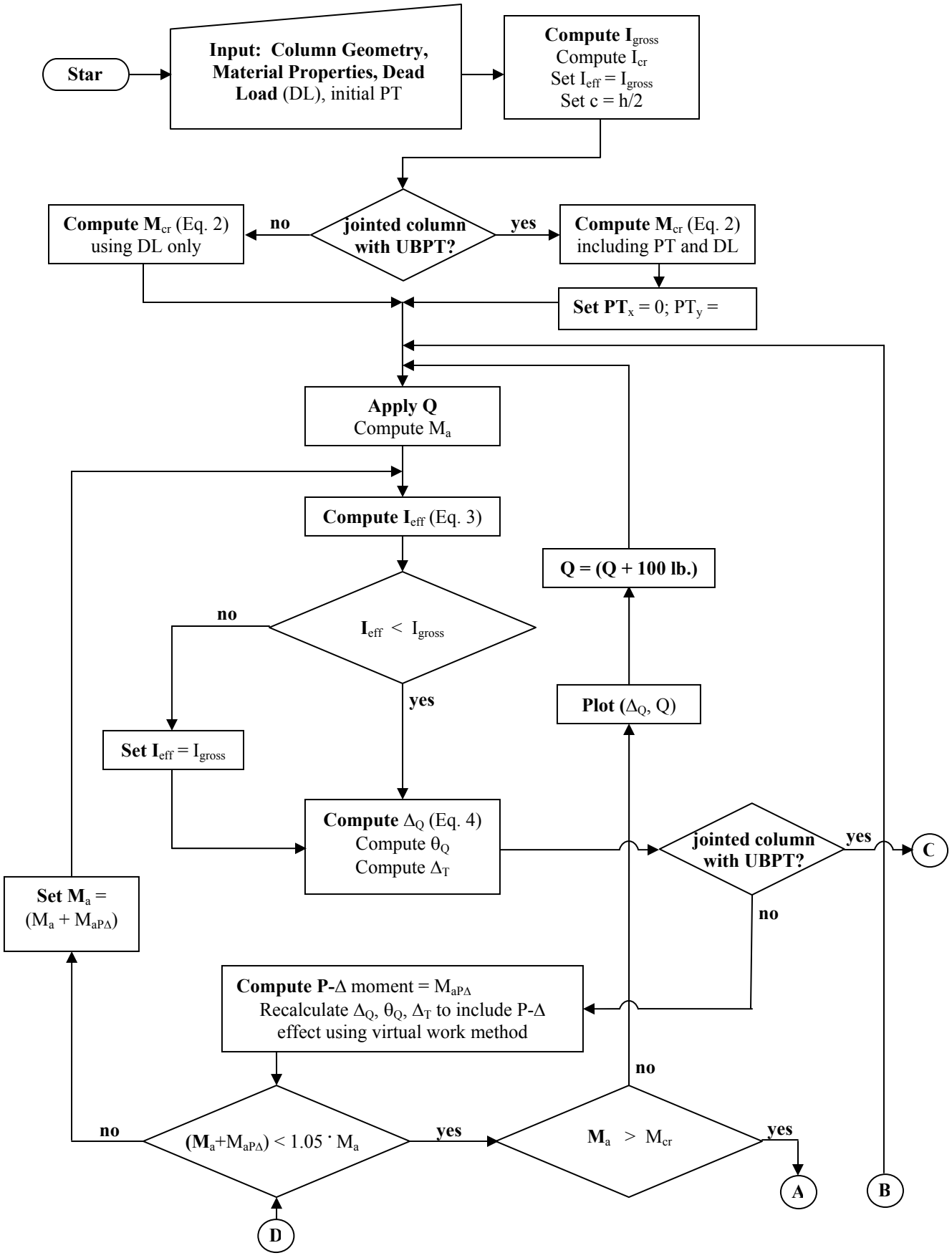

Figure 186. Excel visual basic flowchart.

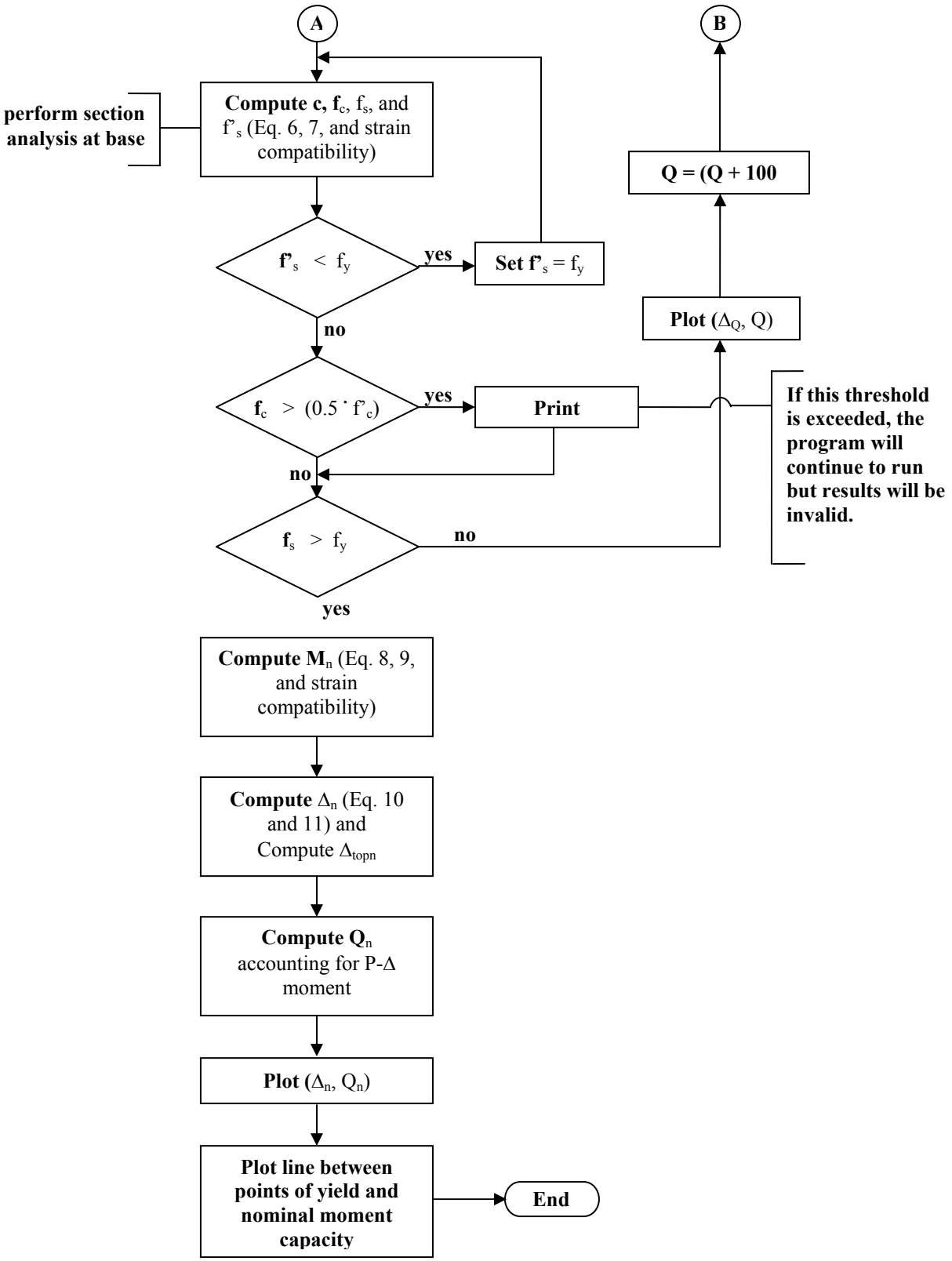

Figure 186 continued. Excel visual basic flowchart.

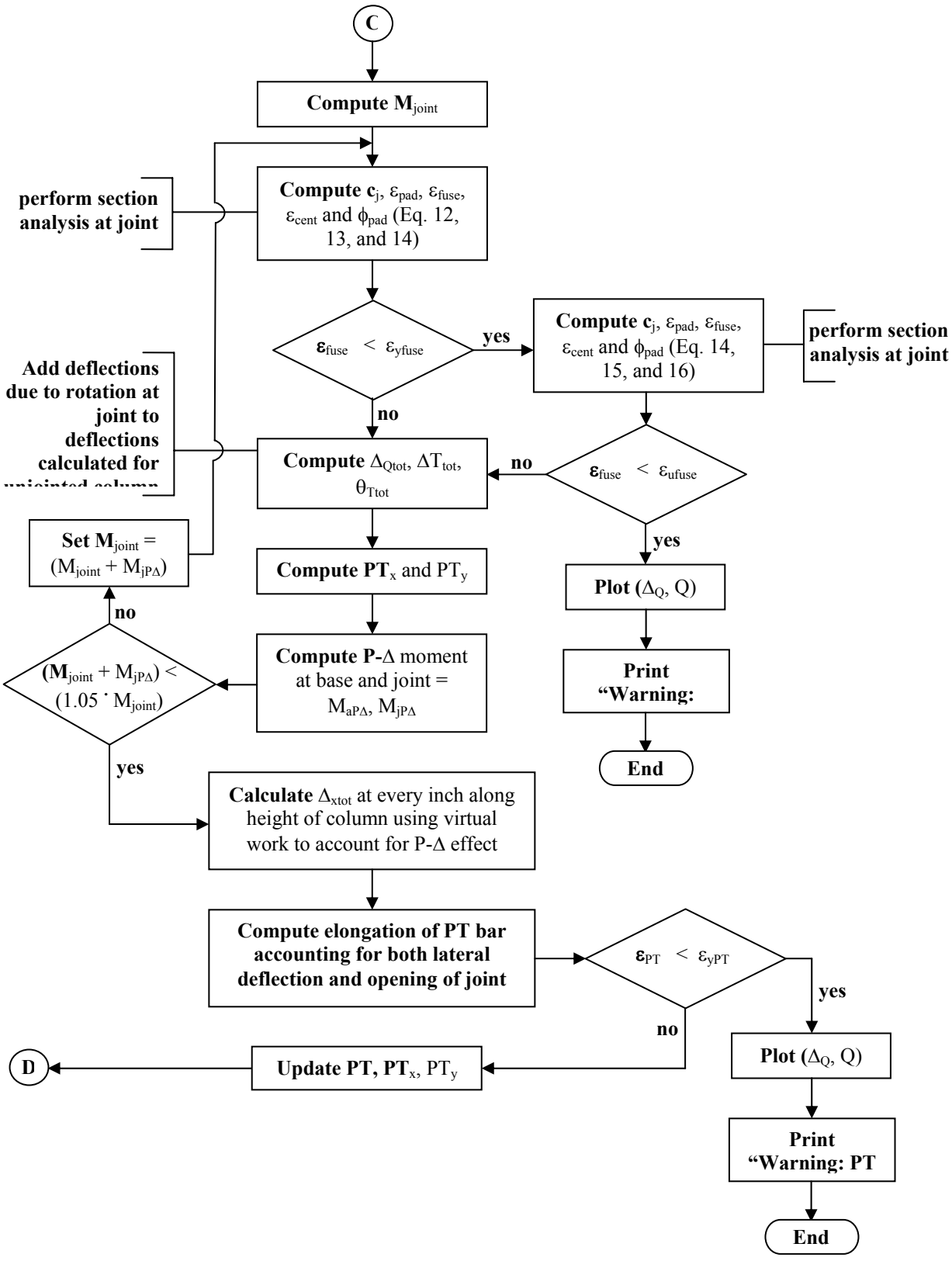

Figure 186 continued. Excel visual basic flowchart.

7.10.2.1 Analysis prior to tensile yielding of bonded reinforcement

Prior to initial lateral loading, the column is assumed to be uncracked and to behave elastically. The lateral deflection of the column below the point of lateral load application may be expressed by the differential equation (Equation (1)) and is illustrated in the free body diagram in Figure 187. This equation is solved using an iterative procedure for each incremental lateral load (applied in 100 lb. increments). In this phase, the cracking moment of the axially loaded cantilever is computed using Equation (2). For each lateral load increment, lateral deflection due only to the applied lateral force is computed at the point of lateral loading using Equation (4). Deflection at the top of the column (Δ_T) is also computed for each load increment. Once these deflections are calculated, the program calculates the additional lateral deflection due to the P-Δ effect using the virtual work method until the total lateral deflections for a given lateral load increment converge to constant values.

$$E_c \cdot I_{eff} \cdot \left(\frac{d^2 v}{dz^2} \right) + (DL) \cdot (v) = -Qz \qquad (1)$$

where,

DL = dead load

E_c = modulus of elasticity of the concrete

I_{eff} = effective moment of inertia of the column cross-section

v = distance from the point of vertical load to a general deflected section of the column

Q = lateral load applied by actuator

z = distance from the point of lateral load to a general section at z

During this phase, the effective moment of inertia of the column, I_{eff} (Equation (3)), is used to calculate lateral deflections. This empirical relationship was developed by Branson (1977) and is found in the American Concrete Institute Building Code (ACI 318, 2005). The authors realize that when the applied loads cause distributed cracking, the moment of inertia will vary along the length of the column.

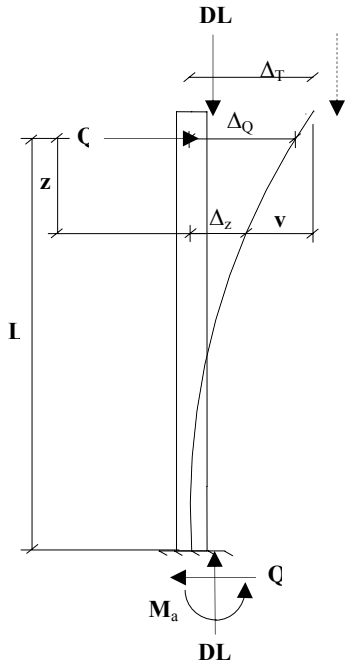

Figure 187. Free body diagram of R/C cantilever with an axial load.

The use of I_{eff} as an approximate means of computing deflections in reinforced concrete members has been found to correspond to within +/- 5% of more exact methods employing variable moments of inertia for laterally loaded cantilevers (Wang, 1998). Although axial load was neglected in this comparison presented by Wang, the use of the constant I_{eff} for a given set of lateral and axial loads was adopted for its simplicity and common recognition among practitioners. Note that prior to reaching the cracking moment, Equation (3) conservatively sets I_{eff} equal to the gross moment of inertia of the column section.

$$M_{cr} = \frac{(f_r + f_{ax}) \cdot I_{eff}}{c} \qquad (2)$$

where,

M_{cr} = cracking moment

f_r = modulus of rupture of the concrete, $f_r = 7.5 \cdot \sqrt{f'_c}$

f_{ax} = stress on column cross section due to axial loads

c = neutral axis location

I_{eff} = effective moment of inertia of the column cross-section

$$I_{eff} = \left(\frac{M_{cr}}{M_a}\right)^3 \cdot I_{gross} + \left[1 - \left(\frac{M_{cr}}{M_a}\right)^3\right] \cdot I_{cr} \quad (3)$$

where,

M_a = total moment at the base of the column

I_{gross} = gross moment of inertia of the column cross-section

I_{cr} = cracked moment of inertia of the column cross-section

$$\Delta_Q = \frac{QL^3}{3 \cdot E_c \cdot I_{eff}} \quad (4)$$

where,

Δ_Q = lateral displacement of the column at the actuator elevation

Q = lateral load applied in a given increment

L = vertical distance, in inches, between the base of the column and the centerline of the actuator head

E_c = modulus of elasticity of the concrete

I_{eff} = effective moment of inertia of the column cross-section

It should be noted that an additional component of deflection due to the rotation of the tested column specimens with imperfect base fixity may have been present. Laboratory measurements indicated that such rotations were sufficiently small to be within the range of uncertainty of the instrumentation used and thus were assumed to be zero (i.e., fixed end condition).

At each incremental lateral load step, a sectional analysis is performed at the base section of the cantilever to compute material stresses, strains, and neutral axis location. The section analysis is based on vertical force equilibrium (Equations (5) and (6)), moment equilibrium (Equation (7)), and strain compatibility of concrete and the bonded, longitudinal reinforcement. The stress and strain relationships for this analysis, once the cracking moment is exceeded, are illustrated in Figure 188.

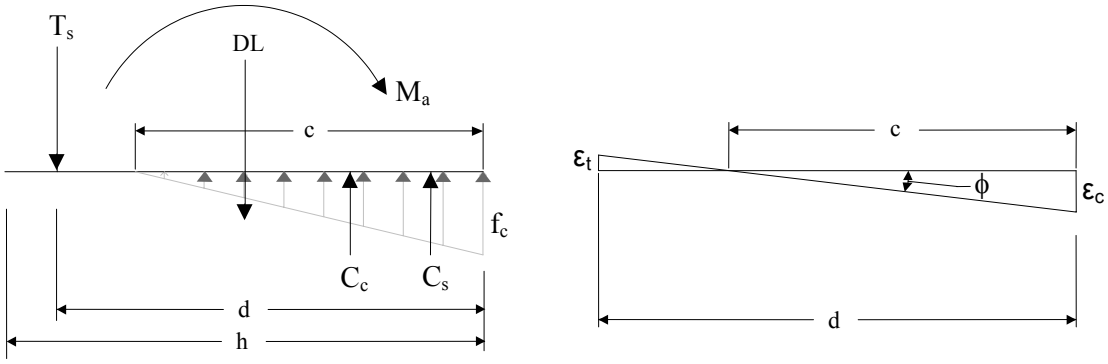

a.) Stress diagram **b.) Strain diagram**

Figure 188. Stress, strain diagrams of R/C column (Column 1) for displacements up to yield moment.

where,

ε_t = strain in tension reinforcement

ε_c = strain in concrete on compression face of the column

Vertical force equilibrium requires

$$DL = C_c + C_s - T_s \tag{5}$$

where,

DL = dead load

C_c = compressive resultant in the concrete

C_s = compressive force in the longitudinal reinforcement

T_s = tensile force in the longitudinal reinforcement

This becomes

$$DL = \frac{f_c \cdot b \cdot c}{2} + A'_s \cdot f'_s - A_s \cdot f_s \tag{6}$$

where,

f_c = compressive stress in concrete < $0.5 \cdot f'_c$

b = width of column (perpendicular to lateral load)

c = location of the neutral axis

A'_s = area of reinforcement in compression

f'_s = stress of reinforcement in compression

A_s = area of reinforcement in tension

f_s = stress of reinforcement in tension

Moment equilibrium about the plastic centroid of the section requires

$$M_a = \frac{f_c \cdot b \cdot c}{2} \cdot \left(\frac{h}{2} - \frac{c}{3}\right) + A'_s \cdot f'_s \cdot \left(\frac{h}{2} - d'\right) - A_s \cdot f_s \cdot \left(d - \frac{h}{2}\right) \quad (7)$$

where,

M_a = total external moment at the base of the column including the P-□ moment

h = height of column cross-section

d’ = distance from compression face of column to center of reinforcement in compression

d = distance from compression face of column to center of reinforcement in tension

This procedure continues as lateral loads are incremented until the computed stress in the tensile reinforcement reaches its yield value. Thus, the values of yield moment, M_y, lateral load required to cause yielding in the tension steel, Q_y, the associated lateral deflection, Δ_y, and the associated sectional rotation, □$_y$, are computed. At each load increment, compressive stresses in the reinforcement are limited to a maximum value equal to the yield stress of the reinforcement. Compressive stresses in the concrete are checked to ensure that they remain below $0.5 \cdot f'_c$ so that the assumption of a linear stress distribution prior to tensile yielding is valid.

7.10.2.2 Analysis after yielding of tensile reinforcement

During this phase of the analysis, the nominal moment capacity of the base section of the column is calculated using a constant concrete stress distribution and linear strain relationships as illustrated in Figure 189.

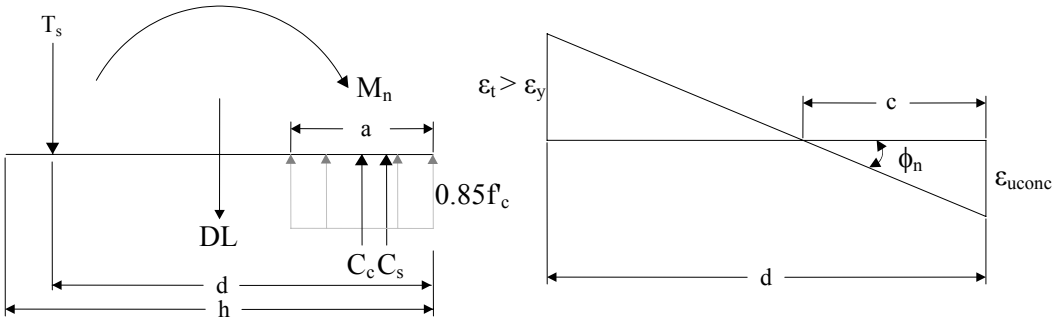

a.) Stress diagram for ultimate strength analysis **b.) Strain diagram for ultimate strength analysis**

Figure 189. Stress and strain diagrams of reinforced concrete column at nominal moment capacity.

The solution for nominal moment capacity, M_n is based on vertical force equilibrium, moment equilibrium, and strain compatibility. As in the previous phase of the analysis, Equation (8) is derived from vertical force equilibrium, and Equation (9) is derived from moment equilibrium.

$$DL = .85f'_c \cdot a \cdot b + A'_s \cdot f'_s - A_s \cdot f_y \tag{8}$$

$$M_n = 0.85 \cdot f'_c \cdot a \cdot b \cdot \left(\frac{h}{2} - \frac{a}{2}\right) + A'_s \cdot f'_s \cdot \left(\frac{h}{2} - d'\right) + A_s \cdot f_y \cdot \left(d - \frac{h}{2}\right) \tag{9}$$

where,

f_y = yield stress of tensile reinforcement

$\square_y$ = yield strain of tensile reinforcement

To calculate the corresponding lateral deflection, $\square_n$, when the nominal moment capacity is reached, the rotation of the base section, $\square_n$, is computed from the strain diagram shown in Figure 189b. Once the longitudinal steel yields, it is assumed that a plastic hinge develops with a length of "d" at the base of the column, where "d" is the distance to the tension reinforcement from the extreme compression fiber. Once the plastic hinge forms, it is assumed that all remaining deformations take place as rotation at the plastic hinge. The nominal rotation capacity, $\square_n$, is computed when the extreme compression fiber reaches ε_{uconc}. ε_{uconc} for this analysis is assumed to be 0.004 in./in., because relatively high confinement is provided in the region near the base section by the socket connection to the foundation.

Once the strain profile of the base section at nominal moment capacity is established, the nominal rotation capacity, ϕ_n, is computed using Equation (10).

$$\phi_n = \arctan\left(\frac{\varepsilon_{uconc}}{c}\right) \quad (10)$$

where,

ϕ_n = rotation at nominal moment capacity

ε_{uconc} = ultimate concrete compressive strain

Using the moment area method, the nominal deflection capacity of the column, Δ_n, at the point of lateral loading is found by Equation (11).

$$\Delta_n = \Delta_y + (\phi_n - \phi_y) \cdot d \cdot (L - \frac{d}{2}) \quad (11)$$

where,

Δ_n = nominal deflection of the column at the lateral loading point when nominal moment capacity is reached

Δ_y = lateral deflection at which tensile yielding of bonded reinforcement occurs

d = distance to the tension reinforcement from the extreme compression face

L = vertical distance, in inches, between the base of the column and the centerline of the actuator head

After accounting for the P-Δ moment as described previously, the nominal lateral load capacity, Q_n, is computed. Lateral loads and the corresponding deflections between the point of first tensile yielding and nominal lateral load capacity are then back calculated using simple linear interpolation.

7.10.3 Analysis of a jointed column with unbonded post-tensioning

In addition to the deflection of an unjointed reinforced column, columns with a segment joint have another deflection component due to the rotation at the relatively compliant construction joint as illustrated schematically in Figure 185b. Furthermore, the effects of the unbonded post-tensioning must be taken into account for the jointed columns. To predict the lateral force versus deflection behavior of the jointed columns, an additional section analysis is performed at the construction joint. Due to the small relative thickness of the joint, a single

cross section at the center of the bearing plate is analyzed to determine rotation at this joint. Here an additional incremental procedure for the member is performed to account for changes in post-tensioning force as the column deflects laterally.

Similar to the analysis of an unjointed column, two phases of analysis are required: one phase prior to yielding of the tension fuse plate and another phase after the tension fuse plate yields. The following additional assumptions are associated with the section analysis of the construction joint.

- The force in the compression fuse plate is neglected because the fuse plate will buckle before sustaining significant compressive forces.
- A linear strain distribution is assumed in the bearing plate material.
- A linear stress distribution is assumed in the bearing plate material. Since the bearing plate used in each test had at least twice the compressive strength of the surrounding concrete, the compressive stress in the plate will be limited to less than half its compressive strength and thus should remain approximately linear.
- Due to the relatively short length of the fuse plates, the tension fuse plate is treated as if bonded to the concrete and thus is subjected to strain compatibility with the concrete. Forces in the fuse plates are conservatively assumed to act at the extreme fiber of the column cross section.
- An idealized elastic-plastic stress-strain curve is used for the fuse plate in tension.
- The stress and strain diagrams shown in Figure 189 are used at the construction joint to determine the rotation at the joint section.
- The contribution of the side fuse plates are conservatively neglected.

7.10.3.1 Analysis prior to yielding of tension fuse plate

Again, force and moment equilibrium in conjunction with the assumed linear stress-strain relationships formulate the basis used in the approach to develop the lateral load vs. deflection, stress, and strain relationships of the segmented columns. These relationships are given in Equations (12)-(14). Since the fuse plates and the bearing plate material for this portion of the analysis are in their linear-elastic ranges, linear stress and strain relationships

are used. In the experiments, bolts connecting the fuse plates were not fully tensioned until after the post-tensioning force was applied, so the fuse plates were assumed to have zero strain at the start of the tests. As illustrated in Figure 190, the compressive strain in the bearing plate is related to the tensile strain in the fuse plate by a constant value. This constant is the initial compressive strain in the bearing plate due to the column dead load and the initial post-tensioning force (Equation (14)). Because the post-tensioning bar does not remain vertical as the column deflects, the post-tensioning force applied at the top of the column is resolved into its horizontal and vertical components, PT_x and PT_y, respectively.

$$PT_y + DL = \frac{1}{2} \cdot \varepsilon_{pad} \cdot E_{pad} \cdot c_j \cdot b - A_{fuse} \cdot E_{fuse} \cdot \varepsilon_{fuse} \tag{12}$$

where,

PT_y = vertical force applied to column by post-tensioning

E_{pad} = modulus of elasticity of bearing plate

ε_{pad} = strain at edge of bearing plate

A_{fuse} = cross-sectional area of fuse plate

E_{fuse} = modulus of elasticity of fuse plate

ε_{fuse} = strain in tension fuse plate

b = width of column (perpendicular to lateral load)

c_j = location of the neutral axis at the joint

$$M_{joint} = \frac{1}{2} \cdot \varepsilon_{pad} \cdot E_{pad} \cdot c_j \cdot b \cdot \left(\frac{h}{2} - \frac{c_j}{3} \right) - A_{fuse} \cdot E_{fuse} \cdot \varepsilon_{fuse} \cdot \frac{h}{2} \tag{13}$$

$$\varepsilon_{fuse} = \varepsilon_{ax} + \frac{\varepsilon_{pad} (h - c_j)}{c_j} \tag{14}$$

where,

ε_{ax}= initial strain at construction joint caused by DL+PT force

h = height of column cross-section

M_{joint} = external moment at joint section including P-□ moment

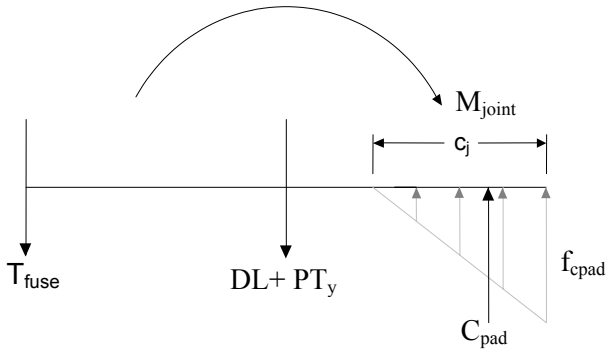

a.) Stress diagram at segment joint

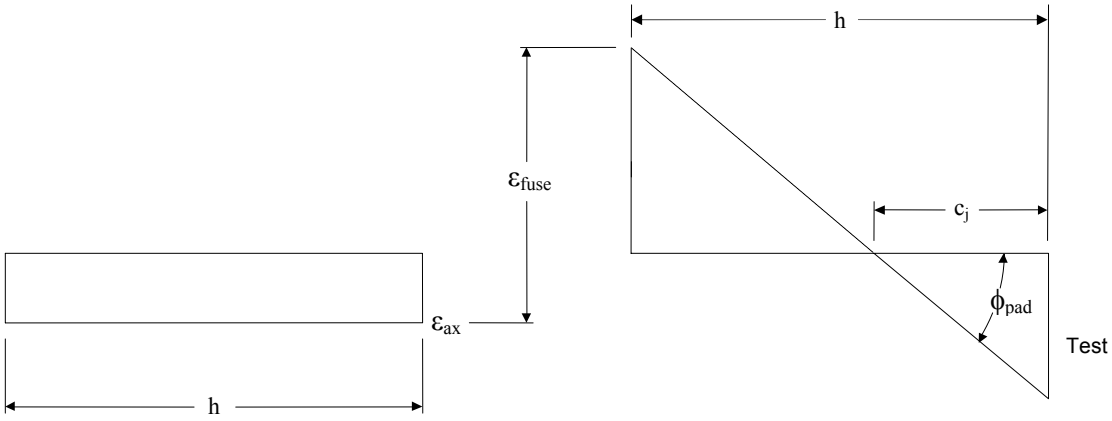

b.) Strain condition at segment joint with axial load only

c.) Strain condition at segment joint with lateral + axial loads

Figure 190. Stress and strain diagrams at segment joint.

Equations (12)-(14) are used to compute c_j, which is then used to determine the rotation at the joint and the component of lateral deflection due to that rotation (see Figure 185b) for a given lateral load increment. P-□ moments are computed with the same iterative procedure described for the unjointed column. At each lateral load increment, a check is performed to ensure the tensile strain in the fuse plate does not exceed the yield strain of the material. This procedure continues for increasing increments of lateral load until yield strain in the fuse plate is reached.

7.10.3.2 Analysis after yielding of fuse plates

Once the fuse plate has yielded in tension, it is assumed to remain in a constant state of stress. The value of c_j is calculated from Equation (14) coupled with the following equations representing force and moment equilibrium (Equations (15) and (16)).

$$PT_y + DL = \frac{1}{2} \cdot \varepsilon_{pad} \cdot E_{pad} \cdot c_j \cdot b - A_{fuse} \cdot f_{fuse_y} \quad (15)$$

$$M_{joint} = \frac{1}{2} \cdot \varepsilon_{pad} \cdot E_{pad} \cdot c_j \cdot b \cdot \left(\frac{h}{2} - \frac{c_j}{3} \right) - A_{fuse} \cdot f_{fuse_y} \cdot \frac{h}{2} \quad (16)$$

where,

f_{fuse_y} = yield strength of fuse plate

Note that the term M_{joint} includes the P-□ moment computed for the lateral load increment. The rotation at the joint and the resulting lateral deflections due to the joint rotation can then be determined. The total lateral deflection of the column is computed by adding the deflection of the unjointed column to the deflection due to the rotation at the relatively compliant construction joint. Once the total lateral deflection is computed, the program cycles until the total P-□ moment converges on a stable value. The ultimate state rotation at the joint is reached when the strain in the tension fuse plate reaches its ultimate strain, when the post-tensioning bar yields, or when the concrete at the base of the column reaches its ultimate compressive strain.

7.10.3.3 Unbonded post-tensioning analysis

To calculate the stresses induced in the unbonded post-tensioning, deflections are calculated incrementally at every inch from the base of the column to the top. Between each increment, linear interpolation is used to determine the elongation in the post-tensioning bar. The elongations computed for each 1 inch increment of height are summed to determine the total elongation of the post-tensioning bar.

An additional component of elongation is added to the post-tensioning bar when the construction joint is included in the analysis. As a gap at the construction joint opens, the post-tensioning bar elongates a corresponding amount. The additional component of

elongation of the post-tensioning bar is determined by computing the opening of the gap at the center of the column.

Once the total elongation is computed for the bar, a linear stress-strain relationship is used to determine the stress reached in the post-tensioning bar. A check is then performed to ensure the stress in the post-tensioning bar does not exceed its yield stress of 120 ksi. The effect of the post-tensioning change is computed within each of the loops for each lateral load increment, so Equations (12)-(16) are updated continuously to correlate post-tensioning force with lateral displacement.

7.11 Analytical Predictions

This analytical procedure was used with the applied loads, material properties, and geometry of the columns tested in this study to compare the theoretical behavior with behavior measured in the laboratory. Comparisons of the theoretical and measured lateral load versus lateral deflection for Columns 1 and 5 are presented in Table 8. Such comparisons are not shown for Columns 2-4 since these specimens failed prematurely through a mechanism that the program did not consider. Neither are comparisons presented for Column 6 because the nonlinear stress versus strain response of the SMA fuse plates was not accounted for in the analytical procedure.

Analytical predictions for Column 1 matched the test results closely with the exception that the program underpredicted the ultimate lateral load by 15%. If the yield stress of the bonded reinforcement were actually greater than the specified minimum of 60 ksi, this discrepancy could be reduced significantly.

Predictions for Column 5 were not as precise. Predicted values for the jointed column were particularly dependent on deflection calculations required to predict behavior of the unbonded post-tensioning. Deflection estimates for any concrete members are difficult due to variations in moment of inertia caused by cracking patterns as well as to high sensitivity to estimates of the concrete's modulus of elasticity. This analysis is also sensitive to stress and strain distributions computed at the construction joint.

Results are encouraging, but additional test data would be beneficial in further calibration and refinement of the program. Slippage of the fuse plates also obscured the quantitative data

collected from the jointed columns because tension in the fuse plates could not be directly related to lateral displacement of the columns. Thus, the displacement at maximum lateral loads, $\square_n$, may have been lower than expected due to this phenomenon.

Table 8. Comparison of theoretical results to experimental results.

Column 1 (control column)

Results	Q_{cr}	Δ_{cr}	Q_y	Δ_y	Q_n	Δ_n
Theoretical	1500	0.39	7800	3.99	8060	4.45
Experimental	1600	0.4	7070	3.70	9450	4.80

Column 5 (segmented column with A36 fuse plates)

Results	Q_{cr}	Δ_{cr}	Q_y	Δ_y	Q_n	Δ_n
Theoretical	2200	0.63	10500	6.04	11040	6.37
Experimental	2000	0.50	8800	4.5	9070	4.95

Q is the lateral load in pounds and Δ is the deflection in inches.

8. CONCLUSIONS

8.1 Summary

Six concrete columns were constructed and tested in laboratory experiments that were conducted to investigate the feasibility of a precast bridge pier column system. The columns were evaluated for constructability, structural performance, and effectiveness of repair. Each column was subjected to constant vertical dead loads and a regimen of cyclic, quasi-static lateral loads. After sustaining significant lateral displacements, the jointed columns were repaired by replacing the structural fuses at the segment joint. The columns were then retested to failure to investigate the effectiveness of the repair.

To represent the behavior of a conventional reinforced concrete column and provide a basis for comparison, Column 1 was cast as a single R/C column. Columns 2-4 failed prematurely due to a detailing issue. Few results could be quantified, but several valuable detailing improvements were recognized from these tests. Columns 5 and 6 were then tested and compared with the control column using performance indicators. The results of the structural performance of the columns are presented in Chapter 7.

8.2 Construction Aspects

Several details for expediting construction of the proposed system proved to be effective from both labor and structural performance perspectives.

- Use of a prefabricated bearing plate at segment joints may reduce on-site labor by eliminating grouting procedures at segment joints.
- Socket connections to the foundation were quick, clean, and robust, and simplified positioning and alignment of the precast columns.
- The fuse plate connections at segment joints ensured alignment and eliminated the need for temporary bracing during erection.
- Steel encasement of column segment ends protected concrete corners during handling and erection. These steel collars also provided a flat, smooth surface for joining the segments and eliminated the need for match casting.
- Because the post-tensioning was designed to be unbonded, no grouting of ducts was required after post-tensioning.

- Concrete segments can be cast horizontally, eliminating the need for pumping, scaffolding, or tall lifting equipment for handling.
- Repairing the columns by replacing damaged fuse plates was effective and required minimal labor (~1 man-hour).

8.3 Structural Detailing

Testing identified both effective and unsatisfactory details in the jointed columns. Specific detailing requirements identified include the following.

- The longitudinal bonded reinforcement must be anchored below *all* through-bolt ducts at the segment joints in a manner to prevent the bolts and collars from "pulling off" the end of the column. This is effectively achieved by using U-shaped bars that wrap around the bolt ducts or by using appropriately shaped end anchors positioned at the end of the precast segment. These anchors can even be welded to the segment end plate to ensure positioning, but the weld is not structurally required.
- A steel plate welded to the end of the steel collars is effective in increasing confinement of the crucial segment ends and is also a convenient means of producing a smooth, flat interface with the bearing plate.
- Fuse plates connected on all four faces of the column provide additional confinement of the segment ends and improve the performance of the column.
- The glass fiber reinforced polymer (GFRP) appeared to be the most effective material for the bearing plate, showing no evidence of bulging, splitting or other damage. Furthermore, this material is durable and easily laid up flat and cut to the required dimensions. Its strength and elastic modulus matched well with requirements for the desired system performance.
- A36 steel performed satisfactorily for the fuse plates. A36 is readily available in a wide variety of plate thickness, is relatively inexpensive, and has a high ultimate elongation.
- The advantages demonstrated by SMA fuse plates could be achieved more cost-effectively by other means such as higher strength steel plates. In addition, the relatively low strain capacity presents a risk of fracture as occurred in Column 6.

- Bolted slip-critical connections designed and tensioned to AISC standards for steel-to-steel connections may not maintain clamping force when bearing on concrete. Slip of the fuse plates adversely affected structural performance of the jointed columns. More research on this effect is recommended.

8.4 Structural Behavior Aspects

The proposed segmented columns compared favorably in many respects to the control column, which was a conventional reinforced concrete column.

- Similar or greater lateral strength can be achieved with the jointed column relative to the conventional column.
- Both initial and (especially) residual lateral stiffnesses were greater for the jointed column system than for the conventional column.
- The jointed columns had greater lateral deformation capacity than the conventional column. The jointed system sustained their maximum loads to larger lateral displacements and experienced a more gradual decrease in load capacity when displaced beyond ultimate loads when compared to the conventional column. Column 5, in fact, developed no obvious failure mechanism even when displaced to the maximum stroke of the actuator (10% drift).
- The jointed system dissipated far less hysteretic energy than the conventional columns.
- The self-centering capability of the jointed system was demonstrated. Residual deformations could be nearly eliminated. This property could allow a bridge subjected to an extreme lateral load to remain in service until repair is performed.

8.5 Repair Aspects

One major advantage of the proposed system is the possibility for rapid, cost-effective repair if damaged by an extreme load event. Repairs to jointed columns when subjected to design level loads were highly effective. Some loss of lateral stiffness was observed, but no evidence of reduction in lateral strength was apparent. Columns behaved similarly after repair as they did initially. With fuse plates proportioned to yield prior to longitudinal

reinforcement, damage to precast column segments can be minimized as demonstrated in Column 5. Cracks in the concrete remain small and close to the point of being difficult to identify with the naked eye due to the combined post-tensioning force and dead loads. Buckled plates offer clear evidence for maintenance engineers or technicians that replacement is required.

9. RECOMMENDED RESEARCH

Based on research completed to date, the proposed segmented column system is a feasible alternative to conventional pier systems. Additional research is recommended to verify these findings and address the following items.

- Slippage of the bolted fuse plates occurred during all of the segmented column tests. Although the initial clamping force in the bolts was verified with direct tension indicating washers, the friction between the fuse plates and column segments was inadequate to prevent slip at large displacements. Factors that may have contributed to this occurrence include strain hardening of the fuse plates, inelastic deformation of the concrete within the steel collars leading to a reduction of clamping force, and prying forces generated by the buckling of the fuse plates leading to inelastic elongation of the bolts. Eliminating slippage of this friction connection would improve the structural performance of the columns.
- Column 5 and 6 dissipated approximately ¼ and ½ of the total energy dissipated by Column 1, respectively. Increasing the energy dissipation capacity of the jointed columns could improve the global performance of a structure subjected to dynamic loads. Possible means of achieving this goal without sacrificing small residual displacements could be provided through the use of multiple joints or through the use of advanced, nonlinear elastic materials for post-tensioning.
- Systems with multiple joints could provide opportunities to more precisely tailor structural response and optimize cost savings. Multiple joints placed at strategic locations could provide improvements in ductility, energy dissipation, redundancy, and safety.
- Alternative materials and details for both the continuous elastic elements and structural fuses could increase the effectiveness of the system. For example, the use of unbonded composite strips on the external faces of the column might reduce post-tensioning demands and increase deformation capacity.
- Corrosion protection for all components of the system is crucial. Corrosion and environmental exposure should be systematically considered in material selection,

detailing, and coating selection. Cathodic protection systems might also be effectively employed to protect exposed metallic components such as fuse plates.

- Connection details and procedures for attaching pier caps to columns should to be investigated with respect to both constructability and structural performance. A connection similar to the foundation socket used at the base of the column may prove effective.
- Design specifications and procedures should calibrated and formalized to advance this technology from the laboratory to general practice.
- Standardization of the structural elements could streamline precast operations and make the proposed system more cost-effective. An inventory of standard components could significantly reduce lead times for design, construction and repair as well as reduce fabrication costs.

10. REFERNCES

Billington, S. L., Barnes, R. W., Breen, J. E. 2001. "Alternate substructure systems for standard highway bridges." *J. Bridge Eng.*, 6(2), 87-94.

Billington, S. L., Yoon, J.K. 2004. "Cyclic response of unbounded posttensioned precast columns with ductile fiber-reinforced concrete." *J. Bridge Eng.*, 9(4), 353-363.

Branson, Dan E. *Deformation of Concrete Structures*. New York: McGraw-Hill, 1977.

Hieber, D.G., J.M. Wacker, M.O. Eberhard, and J.F. Stanton. *State-of-the-Art Report on Precast Concrete Systems for Rapid Construction of Bridges*. Washington State Department of Transportation Technical Report # WA-RD 594.1, Mar. 2005.

Ikeda, S. (1998). "Seismic behavior of reinforced concrete columns and improvement by vertical prestressing." *Challenges for Concrete in the Next Millennium, Proc., XIIIth FIP Congress*, D. Stoelhorst and G. P. L. den Boer, eds, Vol. 1, Balkema Rotterdam, The Netherlands, 879-884.

Ito, T., Yamaguchi, T., and Ikeda, S. (1997). "Seismic performance of concrete piers prestressed in vertical direction." *Proc., Japan Concrete Institute*, 19(2), 1197-1202 (in Japanese).

Kwan, W.-P., Billington, S.L. "Unbonded posttensioning concrete bridge piers. I: Monotonic and cyclic analysis." *J. Bridge Eng.*, 8(2), 92-101.

Rouse, J. M. 2003. Behavior of bridge pier columns with ductile fiber reinforced hinge regions and vertical, unbonded posttensioning. PhD Thesis, Cornell University.

Stephan, B., Restrepo, J., Seible, F. 2003. Seismic behavior of bridge columns built incorporating MMFX steel. Final report. University of California, San Diego.

Wang, Chu-Kia, Salmon, Charles G. *Reinforced Concrete Design, Sixth Edition*. United States of America: Addison Wesley Educational Publishers, Inc, 1998.

ACKNOWLEDGEMENTS

Funding for this investigation was provided by the Iowa Department of Transportation Highway Division and the Iowa Highway Research Board. The authors are also grateful to Sika, USA, Polymer Pipe Technology, LLC, Fyfe Company, LLC, and Dayton Superior for their generous donations of both materials and advice. The authors also deeply appreciate keen insight and support of the technical advisory committee consisting of Dean Bierwagen of the Iowa Department of Transportation, Mark Nahra of Delaware County, Tom Schoellen of Butler County, and Kim Triggs of Godbersen-Smith Construction Company. Furthermore, the authors are thankful to Doug Wood at the Iowa State University Research Laboratory for helping with many construction, setup, and testing aspects of the project, student assistants Mike Siedsma, Xuhao Wang, and Bin Tong for their assistance with laboratory work, and Casey Faber for his programming support and laboratory assistance.

BIOGRAPHICAL SKETCH

Mark Christopher Currie was born September 14, 1984, in Ida Grove, Iowa. He received his Bachelor of Science in Civil Engineering from Iowa State University in 2007 and the Master of Science in Civil Engineering from Iowa State University in 2009. He served as a Research Assistant in the Civil, Construction, and Environmental Engineering Department at Iowa State University.